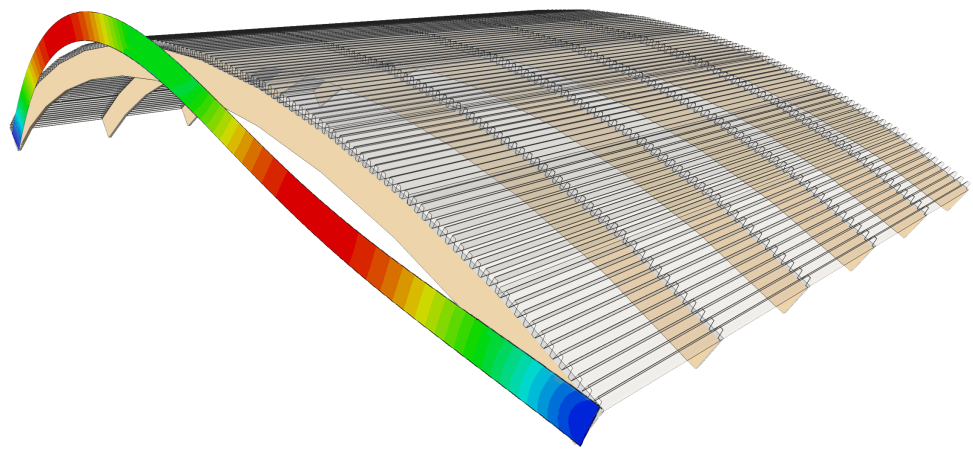




**LUND**  
UNIVERSITY



# VERIFICATION OF BUCKLING ANALYSIS FOR GLULAM ARCHES

BJÖRN ANDERSSON and GUSTAF LARSSON

Structural  
Mechanics

*Master's Dissertation*



DEPARTMENT OF CONSTRUCTION SCIENCES  
**DIVISION OF STRUCTURAL MECHANICS**

ISRN LUTVDG/TVSM--14/5195--SE (1-154) | ISSN 0281-6679

MASTER'S DISSERTATION

# VERIFICATION OF BUCKLING ANALYSIS FOR GLULAM ARCHES

**BJÖRN ANDERSSON and GUSTAF LARSSON**

Supervisors: Professor **PER JOHAN GUSTAFSSON**; Div. of Structural Mechanics, LTH, Lund  
and **TORD ISAKSSON**, PhD, Skanska Teknik.

Examiner: **KENT PERSSON**, PhD, Div. of Structural Mechanics, LTH, Lund.

Copyright © 2014 Division of Structural Mechanics  
Faculty of Engineering (LTH), Lund University, Sweden.

Printed by Media-Tryck LU, Lund, Sweden, June 2014 (*PI*).

**For information, address:**

Div. of Structural Mechanics, LTH, Lund University, Box 118, SE-221 00 Lund, Sweden.

Homepage: <http://www.byggmek.lth.se>





## Abstract

An arch structure offers an effective load carrying system for large span structures. Environmental and economical considerations makes glulam a good material of choice for the arch members. However, asymmetric loading of an arch cause bending moment that implies use of deep and narrow arch cross-sections. Such slender section shape increases the risk of instability.

The purpose of this master's thesis is to gain knowledge of instability phenomena of timber arches. Identification and evaluation of influencing variables by non-linear numerical analysis are compared to the rules for structural design used in EU: Eurocode.

Eurocode considers instability of straight beams and columns with respect to boundary conditions and cross-section properties, while initial imperfections are considered only implicitly. For instability of curved members no analytical approach is provided in the code, thus some numerical method is needed.

In structural design the load carrying capacity of arches is commonly evaluated by finite element (FE) method. Typically used today is linear instability FE analysis. However, this thesis also includes non-linear FE analysis which considers large deformations with redistribution of stresses and a material fail criterion.

Our findings conclude that the linear analysis overestimates the critical load due to instability typically by 20-40% for a parabolic arch. The analysis further indicates that the lateral arch support setup is a fundamental design aspect for the buckling behaviour for which both extrados and intrados lateral support is needed to obtain an effective structure.

The variations in timber material properties and the influence of moisture and long duration of loading are effectively regarded in Eurocode using reduction coefficients. Non-linear FE calculations with respect to influence of moisture and load duration indicated reasonably good agreement with Eurocode. Reduction of material strength due to moisture and load duration effects does not affect the critical load as much as the corresponding reduction of material stiffness. Moisture induced stiffness reduction can give 20% reduction of critical load.

The difficulty in Eurocode is to determine a feasible capacity reduction with respect to the risk of instability for an arch. The authors conclude that structural design of a parabolic arch should be conducted using critical loads from a non-linear FE analysis to be implemented in the Eurocode design calculations.

### Keywords:

GLULAM, ARCH, INSTABILITY, BUCKLING, FEM, NON-LINEAR, EUROCODE, LATERAL SUPPORT



## Sammanfattning

Vid konstruktioner med längre spännvidder, såsom vid hallbyggnader, utgör en bågkonstruktion ett effektivt bärande system. Limträ är då ett bra materialval sett ur ekonomisk och miljöperspektiv. Osymmetriska lastfall orsakar böjmoment varvid ett slant tvärsnitt ofta eftersträvas vilket dock innebär en ökad risk för instabilitetsproblem.

Syftet med detta examensarbete är att erhålla djupare kunskap om instabilitet av limträbågar. Identifiering och utvärdering av ingående parametrars inverkan på brottlasten utförs och jämförs med den gemensamma byggnormen i EU: Eurokod.

Eurokod beaktar instabilitet av raka balkar och pelare med hänsyn till definierade randvillkor och tvärsnittsmått medan initiala imperfektioner enbart behandlas implicit. För instabilitet av krökta element erhålls inga analytiska bärförmågeberäkningar varför en numerisk metod behövs.

Genom att använda finita elementmetoden (FEM) kan limträbågens bärförmåga beräknas. Vid denna typ av FEM-beräkningar används vanligtvis linjär knäckningsanalys. Den här rapporten behandlar dock även olinjär analys vilken tar hänsyn till stora deformationer med omfördelning av spänning samt kriterium för materialbrott.

Vid jämförelse med olinjär analys överskattar linjär FEM analys bärförmågan med avseende på instabilitet med hela 20-40% för en parabolisk båge. Studien visar även att stagnation ut ur planet har stor inverkan på den kritiska instabilitetslasten. För en effektiv konstruktion krävs stagnationspunkter både i ovan- och underkant.

Variationen av materialparametrar hos trä orsakade av fukthalt och långtidslaster behandlas effektivt i Eurokod genom reduktionskoefficienter. Parameterstudier utförda i de olinjära FEM-analyserna påvisar en relativt bra överensstämmelse med Eurokod. Reduktion av hållfasthetsvärden på grund av fuktkvot och långtidslaster påverkar inte bärförmågan i lika stor utsträckning som motsvarande reduktion av styvhetssegenskaperna. Vid hög fukthalt kan styvhetsreduktionen orsaka en reduktion av bärförmågan på ca 20%.

Svårigheten i Eurokod är att bestämma en rimlig reduktion av bärförmågan med avseende på instabilitet av ett bågsegment. Författarna drar slutsatsen att en limträbåge bör utformas i enlighet med Eurokod genom att implementera kritisk last beräknad i en olinjär FEM-modell.

### Nyckelord:

LIMTRÄ, BÅGE, INSTABILITET, KNÄCKNING, VIPPNING, FEM, OLINJÄR, EUROKOD, STAGNING

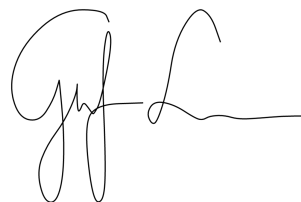


This master's dissertation concludes our five year civil engineering master program at Lund University. It will be a time remembered by the academic quarter, a weak economy and a ginormous amount of enthusiasm which have shaped our personalities for a lifetime. The dissertation has been conducted in collaboration with Skanska AB and we would like to thank Jens Erik Jørgensen and all colleagues for a great time at the Malmö office. A special thanks to our supervisors Prof. Per Johan Gustafsson and Ph.D. Tord Isaksson for all their support and guidance. We would also like to thank Ph.D. Kent Persson and the rest of the Division of Structural Mechanics at Lund University. Finally we would like to thank our family and friends. Without you nothing would have been possible.

LUND, MAY 2014



BJÖRN ANDERSSON



GUSTAF LARSSON



## List of Notations and Abbreviations

$A$	Cross-sectional area	$m^2$
$C_{ijkl}$	Elastic flexibility tensor	–
$D_{ijkl}$	Elastic stiffness tensor	–
$E$	Modulus of elasticity	$Pa$
$f$	Arch rise	$m$
$f_c$	Compression strength	$Pa$
$f_d$	Design strength	$Pa$
$f_k$	Characteristic strength	$Pa$
$f_m$	Bending moment strength	$Pa$
$f_t$	Tension strength	$Pa$
$f_v$	Shear strength	$Pa$
$G$	Shear modulus	$Pa$
$h$	Cross-sectional height	$m$
$I$	Moment of inertia	$m^4$
$J$	Torsion constant	$m^4$
$k$	Linear spring constant	$N/m$
$k_{crit}$	Reduction coefficient w.r.t. torsional buckling	–
$k_{def}$	Deformation coefficient	–
$k_{mod}$	Material modification coefficient	–
$k_c$	Reduction coefficient w.r.t. buckling	–
$k_l$	Non-linear stress distribution coefficient	–
$k_r$	Internal stress coefficient due to curvature	–
$L$	Length	$m$
$L_e$	Effective length	$m$
$m$	Mass	$kg$
$M$	Bending moment	$Nm$
$M_{cr}$	Critical bending moment regarding instability	$Nm$
$N$	Normal force	$N$
$P$	Axial point load	$N$
$P_{cr}$	Critical axial point load regarding instability	$N$
$q$	Lateral distributed load	$N/m$
$Q$	Lateral point load	$N$
$s$	Snow load	$N/m^2$
$S$	Static moment of area	$m^3$
$u$	Moisture content	–
$V$	Shear force	$N$
$w$	Cross-sectional width	$m$
$W$	Elastic section modulus	$m^3$

---

$\beta$	Euler effective length factor	—
$\gamma_4$	Parabolic arch buckling factor	—
$\gamma_M$	Material property deviation constant	—
$\epsilon$	Strain	—
$\lambda$	Slenderness ratio	—
$\nu$	Poisson's ratio	—
$\sigma$	Stress	<i>Pa</i>
$\sigma_c$	Compression stress	<i>Pa</i>
$\sigma_m$	Bending stress	<i>Pa</i>
$\sigma_t$	Tension stress	<i>Pa</i>
$\sigma_{crit}$	Critical stress regarding instability	<i>Pa</i>
$\sigma_{t,90}$	Tension stress perpendicular to grain	<i>Pa</i>
$\tau$	Shear stress	<i>Pa</i>

<i>DOF</i>	Degrees of freedom
<i>DOL</i>	Duration of load
<i>EC</i>	Eurocode
<i>FE</i>	Finite element
<i>FEM</i>	Finite element method
<i>FSP</i>	Fibre saturation point
<i>Glulam</i>	Glued laminated timber
<i>IP</i>	In-plane
<i>MOE</i>	Modulus of elasticity
<i>MPC</i>	Multi-point constraint
<i>MSTRS</i>	Maximum stress failure theory
<i>OP</i>	Out-of-plane
<i>UDL</i>	Uniformly distributed load



# Contents

<b>1</b>	<b>Introduction</b>	<b>11</b>
1.1	Background . . . . .	11
1.2	Objective and Method . . . . .	12
1.3	Limitations . . . . .	12
1.4	Report Outline . . . . .	13
<b>2</b>	<b>Wood and Timber</b>	<b>15</b>
2.1	Material Structure of Wood . . . . .	15
2.2	Natural Characteristics of Wood . . . . .	16
2.3	Physical Properties of Wood . . . . .	17
2.3.1	Wood and Moisture . . . . .	17
2.3.2	Density . . . . .	18
2.3.3	Distorsion of Timber . . . . .	18
2.4	Mechanical Properties of Wood and Timber . . . . .	19
2.4.1	Strength and Stiffness of Wood . . . . .	19
2.4.2	Strength Grading . . . . .	20
2.4.3	Influence of Moisture . . . . .	21

2.4.4	Influence of Temperature . . . . .	22
2.4.5	Influence of Size . . . . .	22
2.4.6	Influence of Time . . . . .	23
2.5	Short- and Long-term Deformations of Timber Structures . . . . .	23
2.5.1	Elastic Deformations . . . . .	24
2.5.2	Viscoelastic Deformations . . . . .	24
2.5.3	Mechano-sorptive Deformations . . . . .	25
2.6	Linear Elastic Behaviour . . . . .	26
2.6.1	Orthotropy . . . . .	26
2.6.2	Transverse Isotropy . . . . .	29
2.6.3	Timber as an Orthotropic Elastic Material . . . . .	29
<b>3</b>	<b>Glulam and Glulam Arches</b>	<b>31</b>
3.1	Glulam . . . . .	31
3.2	Arches . . . . .	33
3.3	Glulam Arches . . . . .	34
3.3.1	Crown and Abutment . . . . .	34
3.3.2	Lateral Support . . . . .	35
3.3.3	Global Lateral Stability . . . . .	37
3.3.4	Additional Stresses in Arches . . . . .	38

---

<b>4</b>	<b>Instability Phenomenon</b>	<b>41</b>
4.1	Order of Theory . . . . .	42
4.2	Buckling . . . . .	42
4.2.1	Buckling of Columns . . . . .	43
4.2.2	Buckling of Beam-columns . . . . .	44
4.2.3	Buckling of Arches . . . . .	45
4.3	Lateral Torsional Buckling . . . . .	46
4.3.1	Lateral Torsional Buckling of Beams . . . . .	46
4.3.2	Lateral Torsional Buckling of Arches . . . . .	48
<b>5</b>	<b>Arch Structure Studied</b>	<b>49</b>
5.1	Geometry . . . . .	49
5.2	Material . . . . .	52
5.3	Design Loads . . . . .	52
5.3.1	Permanent Load . . . . .	52
5.3.2	Snow Load . . . . .	53
5.3.3	Wind Load . . . . .	54
5.3.4	Load Combination . . . . .	54
5.4	Internal and Reaction Forces . . . . .	56
5.4.1	Uniformly Distributed Load . . . . .	56
5.4.2	Triangular Distributed Load . . . . .	57

---

<b>6</b>	<b>Design According to Eurocode</b>	<b>59</b>
6.1	Design Forces . . . . .	60
6.2	Modification Factors . . . . .	60
6.2.1	Modification Factor $k_{mod}$ . . . . .	60
6.2.2	Deformation Factor $k_{def}$ . . . . .	61
6.3	Influence of Curvature . . . . .	61
6.4	Normal Force Capacity with regard of Instability . . . . .	63
6.5	Bending Moment Capacity with regard of Instability . . . . .	64
6.6	Shear Strength . . . . .	65
6.7	Total Load Bearing Capacity . . . . .	66
6.7.1	Compressed Edge Restrained from Lateral Buckling . . . . .	66
6.7.2	Compressed Edge Unrestrained from Lateral Buckling . . . . .	66
6.8	Eurocode Verification Summary . . . . .	67
<b>7</b>	<b>Finite Element Method and Abaqus</b>	<b>69</b>
7.1	Finite Element Method . . . . .	69
7.2	Linear Elastic Buckling Analysis . . . . .	72
7.3	Non-linear Buckling Analysis . . . . .	72
7.4	Element Types . . . . .	74
7.4.1	Characterising Elements . . . . .	74
7.4.2	3D Solid Element . . . . .	75
7.4.3	3D Shell Element . . . . .	75
7.4.4	3D Beam Element . . . . .	76
7.5	Abaqus . . . . .	76

---

<b>8 Arch FE Model Studied</b>	<b>79</b>
8.1 Introduction . . . . .	79
8.2 Straight Member Approximation . . . . .	80
8.3 Material Model . . . . .	81
8.3.1 Linear Elastic Material Model . . . . .	81
8.3.2 Failure Criterion . . . . .	82
8.4 Boundary Conditions . . . . .	84
8.4.1 Hinges . . . . .	84
8.4.2 Lateral Support . . . . .	85
8.5 Loads . . . . .	86
8.5.1 Uniform Load Distribution . . . . .	87
8.5.2 Asymmetric Triangular Load Distribution . . . . .	87
8.6 Elements and Mesh . . . . .	88
8.7 Verification of Model . . . . .	89
8.7.1 Multi-point Constraints . . . . .	90
8.7.2 Failure Stress Criterion . . . . .	90
8.7.3 Springs . . . . .	91
8.8 Method of Analysis using Abaqus . . . . .	92
8.8.1 Linear Buckling Analysis . . . . .	92
8.8.2 Non-linear Buckling Analysis . . . . .	93
8.8.3 Abaqus Nomenclature . . . . .	95

---

<b>9</b>	<b>Arch FE Analysis and Discussion</b>	<b>97</b>
9.1	Lateral Support . . . . .	97
9.2	Geometry . . . . .	100
9.2.1	Slenderness . . . . .	100
9.2.2	Arch Rise . . . . .	102
9.3	Instability with respect to Imperfections . . . . .	104
9.3.1	In-plane Imperfections . . . . .	105
9.3.2	Out-of-plane Imperfections . . . . .	108
9.3.3	Linear Combination of Imperfection Modes . . . . .	110
9.3.4	Imperfections Conclusions . . . . .	111
9.4	Long Term Deformations . . . . .	113
9.4.1	Reduction of MOE . . . . .	113
9.4.2	Reduction of Failure Strength . . . . .	114
9.5	Moisture . . . . .	115
<b>10</b>	<b>Comparison between FE Analysis and Eurocode</b>	<b>119</b>
10.1	Parametric Comparison . . . . .	119
10.1.1	Influence of Initial Imperfections . . . . .	119
10.1.2	Influence of Cross-section Dimensions . . . . .	120
10.1.3	Influence of Time Effects . . . . .	122
10.1.4	Influence of Moisture Content . . . . .	123
10.2	Critical FE Load versus Design Load . . . . .	124
<b>11</b>	<b>Conclusion</b>	<b>127</b>

<b>12 Suggestions for Further Research</b>	<b>129</b>
<b>A Loads</b>	<b>I</b>
A.1 Permanent Load . . . . .	I
A.2 Snow Load . . . . .	II
A.3 Wind Load . . . . .	III
A.4 Load Combination . . . . .	V
<b>B Internal Forces and Reactions</b>	<b>IX</b>
B.1 Uniformly Distributed Load . . . . .	IX
B.2 Triangular Distributed Load . . . . .	X
<b>C Design According to Eurocode 5</b>	<b>XIII</b>
C.1 Geometric Properties . . . . .	XIII
C.2 Material Properties . . . . .	XIV
C.3 Partial Factors . . . . .	XIV
C.4 Actions . . . . .	XV
C.5 Modification Factors . . . . .	XVII
C.6 Stresses in Apex . . . . .	XIX
C.7 Compression Strength . . . . .	XX
C.8 Bending Strength . . . . .	XXI
C.9 Shear Strength . . . . .	XXII
C.10 Combined Stress Condition . . . . .	XXII
<b>D FE Analysis Support Calculations</b>	<b>XXV</b>
D.1 Stiffness of Extrados Lateral Support . . . . .	XXV
D.2 Stiffness of Intrados Lateral Support . . . . .	XXVII





# Chapter 1

## Introduction

### 1.1 Background

During the winter of 2010 a considerable number of roof structures failed in Sweden. In the report [Boverket, 2010] it was concluded by The Swedish National Board of Housing, Building and Planning that the snow loads that led to the collapse was not likely greater than the loads specified in the standards. It was rather weaknesses in the structure, such as poor design with regard to instability, which resulted in the failure.

Cross-sectional optimization of structural elements is a natural part of environmental friendly construction and economical gain. Since a high cross-section is more effective for bending moment the optimization often leads to increasingly slender structural elements. Slender element are however more prone to structural instability, such as buckling. Hence it is vital that the instability phenomenon is properly addressed in the design process.

To increase the capacity of slender elements limited by instability, lateral bracing is often introduced in the structural system. By limiting lateral movements of the main element critical loads can be increased significantly. Not only does the structural system affect the critical load, but since wood is a complex material also time and moisture affects the critical loads.

Buckling are, for straight members, well investigated both experimentally and theoretically. However, curved elements such as arches are not well defined theoretically and the analysis is normally conducted using computer analysis. The computer analysis is conventionally conducted using finite element method (FEM) with linear analysis, which is not a consistently conservative approach.

Glulam represents today an alternative to concrete and steel structures. The use of engineered wood products produces significant technological benefits such as high level of industrialization, prefabrication and erection process besides the possibility to reduce the carbon footprint. The natural characteristics and properties of wood do however imply some difficulties in the design process, of which some will be analysed in this thesis.

## 1.2 Objective and Method

The objective of this master's dissertation is to gain knowledge of the instability phenomenon of timber arches. Identification and evaluation of influencing variables are to be compared to the technical rules for structural design within the European Union: Eurocode. Furthermore, linear analysis will be compared to non-linear in order to determine the accuracy of conventional linear FEM analyses.

Instability analyses will be conducted on a reference model for a range of varying parameters such as geometries, imperfections, lateral support, moisture and time effects using the commercial FEM-software Abaqus. The dissertation will be concluded by a comparison between the results of a non-linear model and the corresponding parameters in Eurocode.

## 1.3 Limitations

The following limitations apply to the study presented in this master's dissertation.

- All arches are 3-hinged parabolic glulam arches.
- A specific arch model is used as a reference in the simulations.
- Linear elastic rectilinear transversely isotropic material properties are assumed.
- No local material defects are modelled, e.g. knots.
- All analyses are conducted on arch structural level with interaction between other parts of the structure modelled only by springs.
- Only load models from Eurocode.
- Dead loads are considered as uniformly distributed load along the horizontal axis.
- No load eccentricity.
- No mechano-sorptive effects are modelled.
- No moisture movements are included, i.e. swelling and shrinkage.

## 1.4 Report Outline

<i>Ch.1</i>	<i>Introduction</i>	Background and purpose of the thesis.
<i>Ch.2</i>	<i>Wood and Timber</i>	Theory of material properties for wood and timber. Reduction of material model.
<i>Ch.3</i>	<i>Glulam and Glulam Arches</i>	Short introduction to glulam and arches. Common structural details for glulam arches are presented.
<i>Ch.4</i>	<i>Instability Phenomenon</i>	Theory of structural stability. Buckling and lateral torsional buckling of beams and arches.
<i>Ch.5</i>	<i>Arch Structure Studied</i>	Reference arch structure for the thesis is presented. Geometry, material and loads are defined.
<i>Ch.6</i>	<i>Design According to Eurocode</i>	Short introduction to Eurocode. Design verification with applied modification factors and combined stress state.
<i>Ch.7</i>	<i>Finite Element Method and Abaqus</i>	Theory of Finite Element Method. A review of different element types and the commercial FE analysis software Abaqus.
<i>Ch.8</i>	<i>Arch FE Model Studied</i>	FE arch model presented with model assumptions. Verification of different functions and a short description concerning method of analysis.
<i>Ch.9</i>	<i>Arch FE Analysis and Discussion</i>	Parametric study of arch structure presented with results and discussion.
<i>Ch.10</i>	<i>Comparison between FE Analysis and Eurocode</i>	Comparison of parametric study and Eurocode modification factors.
<i>Ch.11</i>	<i>Conclusion</i>	Conclusions from the performed study.
<i>Ch.12</i>	<i>Suggestions for Further Research</i>	Suggestions for further research.



# Chapter 2

## Wood and Timber

Wood is created by trees optimised for the conditions trees are exposed to. More and less prominent features of the tree can be explained by natural selection. For example, wind loads are minimized using a round stem and branches are maximizing the effective area for photosynthesis. Of the less prominent features there is also toxic chemicals in the centre of the tree in to prevent insect infestation.

Timber is a collective term for harvested wood which has been manufactured into wood products, such as boards and planks. In this chapter, material properties of softwood will be presented since its use is dominating in engineering. Softwood is wood from angiosperm trees (most evergreen trees) and, despite what the name suggests, is not necessarily softer than hardwood.

### 2.1 Material Structure of Wood

Wood is an organic composite built up mainly of cellulose, hemicellulose and lignin. The most common cell type in softwood is tube-shaped fibres with an approximate length of 2-4mm which is called the tracheid. The fibre wall consists of four layers with varying micro fibre direction, P and S1-S3, surrounding the central cell cavity used for transportation of liquids, see Figure 2.1 [Johansson, 2011].

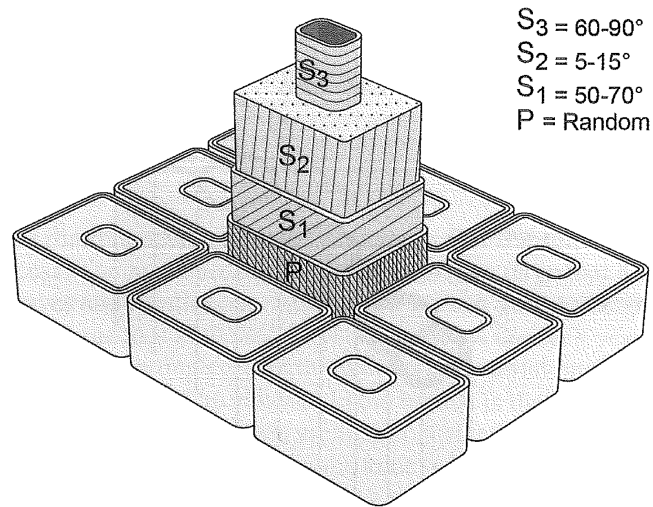


Figure 2.1: Structure of the most common cell type in softwood, called tracheid. The individual micro fibre direction of the fibre wall layers is illustrated [Johansson, 2011].

Whereas hardwood consists of a great variety of cell types, 90% of the softwood tissue is made up from tracheids [Bodig and Jayne, 1982]. Depending on the time of year the cell is formed, cell structure varies causing thick lighter coloured band and thinner dark coloured band to occur in a wood cross-section. The lighter coloured earlywood is formed in spring time with larger cell cavities and thinner cell walls to facilitate transport of liquids during the growth period. The thinner dark band is latewood which is formed during summer and fall. Not only is the need of liquid transport less, greater strength is needed due to increased wind and snow loads. Hence the darker colour is due to thicker cell walls [Johansson, 2011]. As expected, the ratio of earlywood and latewood highly influences the mechanical properties of wood.

The only wood cells having capacity of cell division, i.e. are truly alive, are the outermost cells close to the bark. This region is called cambium.

## 2.2 Natural Characteristics of Wood

In engineering a number of wood characteristics can be considered as defects of which some are described in this section.

To support needles branches are used to increase the effective area of the tree. The branches are gradually embedded in the stem as the tree grows causing an irregularity, a knot. Even though the branch and stem is of the same material and the tissue systems are interconnected, the fibre orientation is distorted and the mechanical properties of sawn timber are impaired [Bodig and Jayne, 1982].

Around the trunk of the tree wood fibres tends to grow in a spiral. The most accepted explanation to this phenomenon is that it creates more flexibility in the young stem which resist a brittle failure do to wind and snow loads. The spiral grain angle often reaches a maximum of 3-4 degrees within the first ten annual growth rings [Johansson, 2011]. Similarly to the knots, as the fibre direction is incoherent mechanical properties are effected.

During the first 5-20 years of growth juvenile wood is formed near the pith. It is characterised by a progressive increase in cell dimensions and changes in cell pattern arrangement as well as cell characteristics. The consequences include 10-15% lower density and 15-30% lower strength [Johansson, 2011].

## 2.3 Physical Properties of Wood

### 2.3.1 Wood and Moisture

Water content has large influence on the properties of wood. The moisture content is dependent on the relative humidity in the surrounding air which is bound to the cell walls. Once the cell walls are saturated cell cavity starts to fill up.

Moisture content or moisture ratio defines the amount of water in wood and is defined by

$$u = \frac{m_u - m_{dry}}{m_{dry}} \quad (2.1)$$

where

- $u$  moisture content ratio
- $m_u$  wood mass at moisture content  $u$
- $m_{dry}$  dry wood mass

Several material properties of wood is independent of the water level in the cavity, hence the concept of fibre saturation point (FSP) is introduced. FSP is a cut-off point in the moisture variation of wood properties, such as swelling, due to moisture content. For softwoods grown in Europe the FSP is often between a moisture content of 27-33% [Johansson, 2011].

### 2.3.2 Density

Almost all mechanical properties of wood is correlated to density. Density  $\rho$  is defined by the ratio between mass and volume. As expected, density is moisture dependent since both mass and volume is dependent of the moisture content. The most commonly used definition in timber engineering is density at 12% moisture content,  $\rho_{12}$ , which is used in all standard tests for wood strength. The normal density ( $\rho_{12}$ ) for softwood grown in the Nordic countries are 300-600  $kg/m^3$  [Dinwoodie, 2000].

### 2.3.3 Distorsion of Timber

Varying shrinkage within a timber element can cause geometrical distortions. Four types of distortions are illustrated in Figure 2.2.

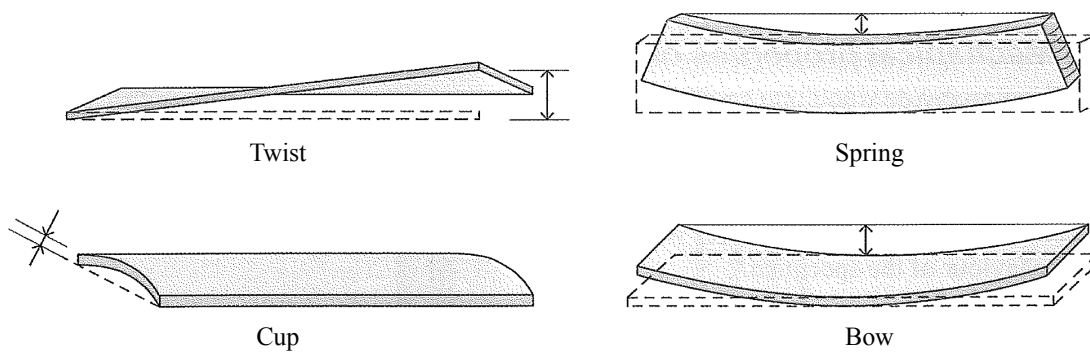


Figure 2.2: Timber distortion modes. Source: Johansson [2011].

For studs used in the building industry, largest problems are due to twist [Johansson, 2011]. Twist occurs due to the combined effect of annual ring orientation, spiral grain orientation and shrinkage. Shrinkage perpendicular to the actual fibre direction, according to the spiral grain orientation, is large combined with the circular shape of the annual rings causes each annual ring to twist and consequently the entire board.

The extent of distortion of sawn timber can be influenced by different sawing patterns and drying regimes.



## 2.4 Mechanical Properties of Wood and Timber

The mechanical properties depends not only of the characteristics of wood fibre, but also of natural characteristics such as knots, spiral grain angle and presence of juvenile wood. Thus wood is usually divided into wood and timber. Wood is then referring to the clear specimen of only straight wood fibres without anomalies, while timber is highly dependent of the natural characteristics which to a great extent determines the properties and behaviour of the specimen.

### 2.4.1 Strength and Stiffness of Wood

Wood is an anisotropic material due to the non-uniform orientation of the fibres. For example, the fibre orientation causes higher compression strength parallel to the stem than perpendicular. Consequently it is important to define the stresses for different directions, which is found in Figure 2.3.

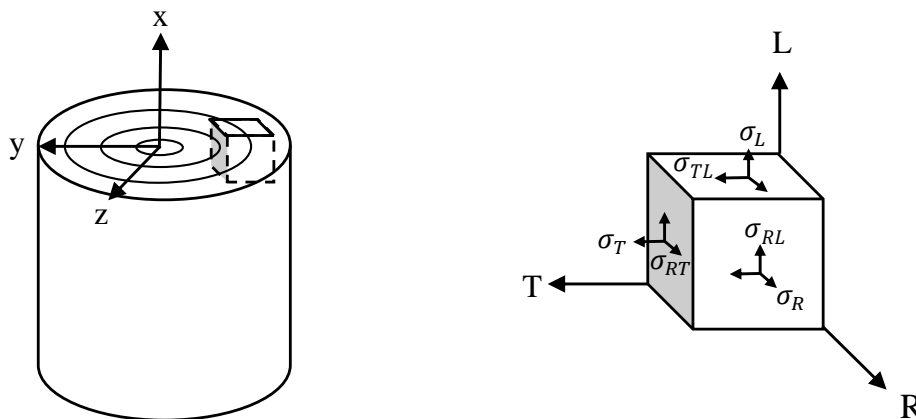


Figure 2.3: Definition of stress directions and nomenclature used in timber engineering.

As can be seen in Figure 2.3, the characteristic directions are defined by three mutually perpendicular planes of material symmetry; longitudinal (L), radial (R) and tangential (T). Due to the characteristics of the fibres, wood can be classified as an orthotropic material referring to the orthogonal directions. To describe the stiffness of wood within the elastic range twelve constants are necessary [Bodig and Jayne, 1982]:

Table 2.1: The stiffness of wood using increasing degree of simplification.

	Complete stiffness	Engineering stiffness
Modulus of elasticity (MOE)	$E_L, E_R, E_T$	$E_L, E_R = E_T$
Shear modulus	$G_{LR}, G_{LT}, G_{RT}$	$G_{LR} = G_{LT}, G_{RT}$
Poisson ratios	$\nu_{LR}, \nu_{RL}, \nu_{LT}, \nu_{TL}, \nu_{RT}, \nu_{TR}$	$\nu_{LR} = \nu_{LT},$ $\nu_{RT} = \nu_{TR},$ $\nu_{RL} = \nu_{TL}$

In engineering, the difference between radial and tangential direction are however often disregarded. Furthermore, the Poisson ratios are normally regarded as par wise equal thus reducing the number of material variables to six, often denoted  $E_{\parallel}$ ,  $E_{\perp}$ ,  $G_{\parallel}$ ,  $G_{\perp}$ ,  $\nu_{\parallel}$  and  $\nu_{\perp}$ .  $\parallel$  denotes parallel to the fibre direction and  $\perp$  perpendicular. Wood strength and stiffness when loaded perpendicularly are considerably less than when loaded parallel to the fibre direction [SS-EN 1194].

When considering timber, local defects is taken into account and it is therefore not possible to predict the mechanical behaviour of sawn timber using only the properties of clear wood. For example the fibre deviations around a knot cause large local stresses to arise due to loading. Strength and stiffness of timber are therefore determined using standardised methodology. The result is material parameters which better reflects strength on element level rather than on material level [Johansson, 2011].

## 2.4.2 Strength Grading

To optimize usage of a material of such varying properties as timber, strength grading is necessary. For example, bending strength for Norway spruce can vary between 10 and 90 MPa [Berbom Dahl, 2009]. Since wood is produced by nature there is small possibility to control the variation by changing manufacturing process. Instead estimates of the properties are determined and the timber is graded into different strength classes.

The characteristic strength value is defined as the 5%-fractile in the distribution of strength, see Figure 2.4.

However, it is not possible to determine all material properties in a non-destructive manner. Using a measured modulus of elasticity and density the timber strength can be roughly determined through measured relationships, which is specified in the European standards EN384 and EN408. Measurement methods include visual and machine grading and the methodology utilizes the elastic section modulus to predict timber properties non-destructively. As a consequence the strength values can only be used in design models based on elastic theory.

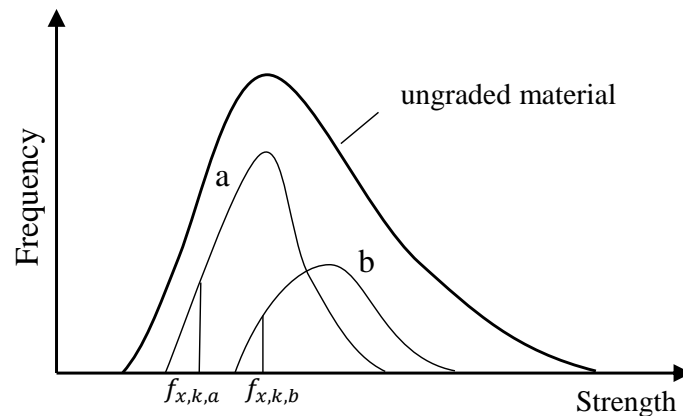


Figure 2.4: Principle variation of strength for graded and ungraded material. Characteristic values marked as  $f_{x,k,i}$ .

### 2.4.3 Influence of Moisture

As previously discussed, the physical properties of wood are affected by moisture content and hence the mechanical properties are affected as well. The lower moisture contents the higher strength and stiffness. The relation can be considered linear below the FSP while the variation is negligible above [Bodig and Jayne, 1982].

Testing shows the influence of moisture content varies for different loading directions in both strength and stiffness. The influence on stiffness is similar though not quite as sensitive as strength, which can be seen in Table 2.2 and 2.3.

Table 2.2: Stiffness change for an increase of moisture content of 1%. The linear approximation is valid for a moisture content ranging from 5% to the FSP. Values are for Sitka Spruce [Dinwoodie, 2000].

$E_L$	$E_R$	$E_T$	$\nu_{RL}$	$\nu_{TL}$	$\nu_{RT}$	$\nu_{TR}$	$G_{LR}$	$G_{LT}$	$G_{RT}$
-0.9%	-2.6%	-2.8%	-1.3%	1.7%	2.6%	1.5%	-1.0%	-1.5%	-2.0%

Table 2.3: Strength change for an increase of moisture content of 1%. The linear approximation is valid for a moisture content ranging from 8% to 20% [Johansson, 2011].

$f_c$	$f_{c,90}$	$f_T$	$f_{t,90}$	$f_v$
-5.0%	-5.0%	-2.5%	-2.0%	-3.0%

Again it should be noted that the influence on especially the strength of structural timber differs from that of clear wood, for which the values are determined. Tests indicate that the influence on structural timber is not as pronounced, particularly for some loading directions [Johansson, 2011]. The tension strength is almost independent while the compression strength is highly affected by the moisture content of full size timber.

#### 2.4.4 Influence of Temperature

Strength and stiffness of wood decreases with increasing temperature but the effect is relatively small for normal temperatures ( $-30^\circ\text{C}$  to  $+90^\circ\text{C}$ ). Hence the effect of temperature variation is not considered in design codes [Johansson, 2011].

#### 2.4.5 Influence of Size

Testing indicates that larger specimens break at lower average tension stress levels than smaller specimens, a phenomenon usually explained by the weakest link theory. The theory says “a chain subjected to tension is never stronger than its weakest link”. For wood the probability of a large imperfection occurring in the most loaded section is greater for larger specimen than for small. Brittle wood can be described using the Weibull theory assuming random imperfection sizes and positions. If  $V_1$ ,  $V_2$  are the two volumes and  $f_1$ ,  $f_2$  their respective strengths, the relation can be described using [Johansson, 2011]

$$\left(\frac{f_2}{f_1}\right) = \left(\frac{V_1}{V_2}\right)^{1/k} \quad (2.2)$$

$k$  is the shape function of the Weibull distribution. The modification factor  $\kappa_h$  is included in Eurocode 5 regarding this phenomenon.

Volume effect is also large for tension perpendicular to the grain which is especially relevant in curved elements such as arches.

### 2.4.6 Influence of Time

Wood experience a significant decrease of strength and stiffness over time. A 10 year duration of load (DOL) may reduce the strength to approximately 40% for solid wood [Hoffmeyer, 2003]. Especially important is reduction of bending strength and among the early research in the topic the work at Forest Product Laboratory, US, stands out. The findings reported in Wood [1951] is commonly referred to as “The Madison Curve” which describes strength versus time dependence for small specimens of clear wood as can be found in Figure 2.5.

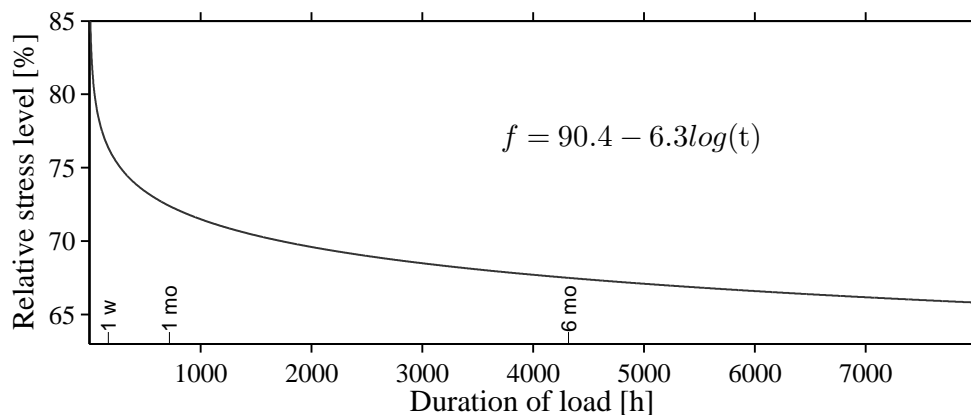


Figure 2.5: The Madison curve which describes the characteristic decrease of strength and stiffness over time.

where  $f$  is the relative stress level (%) and  $t$  is the effective DOL in hours. Note that DOL effects are particularly significant at short- and medium-term loading.

DOL studies of timber began in the 1970’s and continues until present day due to the complexity of the problem. The results do not correspond as some research indicate that the DOL effect is less while other claims it being of the same magnitude as of clear wood [Johansson, 2011]. There is also an effect of increased temperature and moisture both resulting in larger DOL effects.

## 2.5 Short- and Long-term Deformations of Timber Structures

Deformations occur in all timber structures, but the significance varies due to the utilization. Deformations can cause insufficient roof slopes and problems opening doors and windows. Special consideration must be paid to deflections so that non-structural components are not introduced in the load path.

Deformations are commonly divided into elastic deformations, viscoelastic deformations and mechano-sorptive deformations. Please note that plastic deformations may occur for higher stress levels but this effect will not be further discussed in this thesis.

### 2.5.1 Elastic Deformations

Instantaneous deformations due to tension, compression or bending are proportional to the load applied. In a load-deflection curve the proportionality is represented by a linear relation which upholds until a well-defined point known as the limit of proportionality, see Figure 2.6. Note that there is a difference between tension and compression.

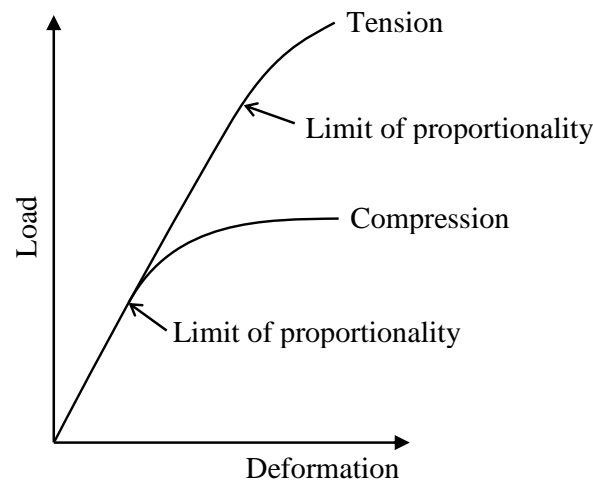


Figure 2.6: Load-deformation curve for wood in compression and tension. Limit of proportionality after which non-linear material behaviour occur is illustrated.

Below the limit of proportionality, the material is said to be linear elastic described by the modulus of elasticity.

### 2.5.2 Viscoelastic Deformations

An increasing deformation with time can be seen for timber elements subjected to constant load. The effect is due to viscoelastic behaviour and is commonly referred to as creep, which is illustrated as the change in deformation while no change in load in Figure 2.7. Most of the deformation will be recovered after load removal although a small permanent deformation remains.

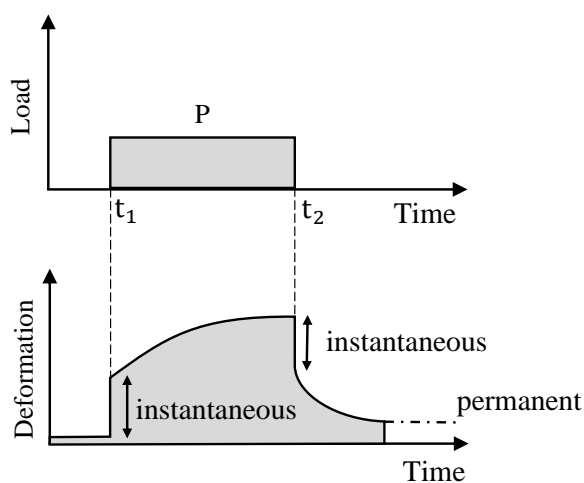


Figure 2.7: Time-deformation curve illustrating creep.

Temperature, stiffness, load direction, knots and moisture content all influence the magnitude of the creep. Due to its importance, moisture variations are however not included in a viscoelastic description but given a definition of its own, c.f. Section 2.5.3. For beams, creep may lead to failure at high load levels but deflections will be moderate for normal loading conditions [Mårtensson, 2003]. Furthermore, engineered wood products, such as glulam, may have different creep behaviour than sawn timber governed by the properties of the adhesive [Johansson, 2011].

The relative creep, i.e. total deflection divided by initial deflection, is in Figure 2.8 plotted for different types of beams. Note that spruce and glulam beams exhibit less creep than LVL- and I-beams for similar stress levels and that a significant part of the creep occurs during the first six months. For glulam it will take at least ten years to double the six months creep deflection [Ranta-Maunus and Kortessmaa, 2000].

### 2.5.3 Mechano-sorptive Deformations

Structural wood subjected to moisture content changes exhibits considerably larger deformations than if subjected to constant humidity conditions. The phenomenon has been studied since the 1960s by e.g. Armstrong and Christensen [1961] and is commonly referred to as the mechano-sorptive effect.

In Figure 2.9, the mechano-sorptive effect is illustrated in a deflection-time curve. The initial deflection  $\delta_i$  is due to the elastic response of the structure. If load and humidity is kept constant, pure creep  $\delta_c$  follows over time. However, if humidity varies the deflection curve will oscillate due to mechano-sorptive deflections  $\delta_{ms}$ .

The effect of moisture content variation on deformation is generally significantly larger than the effect of time, but it can be minimized using chemical treatment such as paint [Mårtensson, 2003].

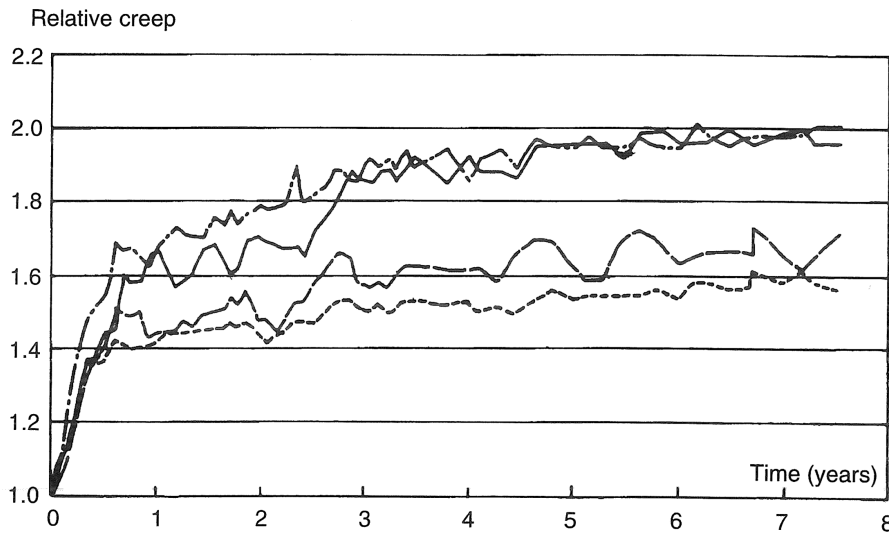


Figure 2.8: Average relative creep in sheltered environment. --- I-beam; — LVL; — Glulam; - - - Spruce. Source: Ranta-Maunus and Kortetmaa [2000]

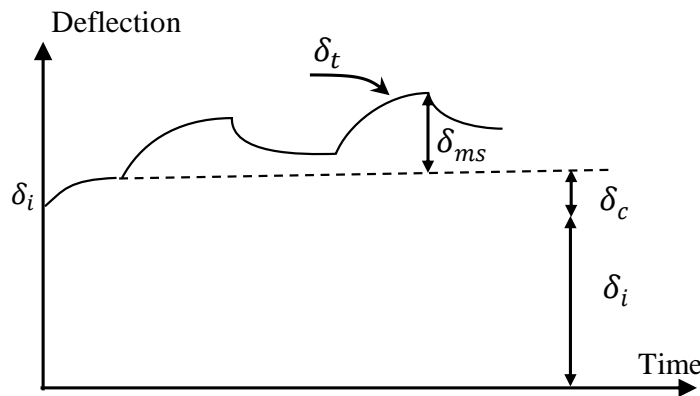


Figure 2.9: Mechano-sorptive deflections induced by varying moisture content.

## 2.6 Linear Elastic Behaviour

Depending on the cut orientation in the trunk and/or engineering simplifications, Cartesian or polar material axes can be used to model the elastic behaviour of wood. If tangential and radial material properties are assumed equal, which is common in timber engineering, the material classifies as transverse isotropic.

### 2.6.1 Orthotropy

Stresses at a point in a general continuum is represented by nine stress components  $\sigma_{ij}$  where  $\{i, j\} = \{1, 2, 3\}$ . The components act on the surface planes of a three dimensional element, see Figure 2.10.



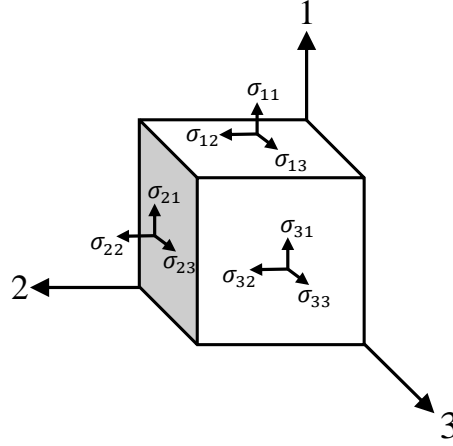


Figure 2.10: General definition of stress components on a three dimensional element.

Similarly the strain is represented by  $\epsilon_{ij}$ . Hooke's law defined the stress strain relation which in index notation is stated as

$$\sigma_{ij} = D_{ijkl}\epsilon_{kl}; \epsilon_{ij} = C_{ijkl}\sigma_{kl} \quad (2.3)$$

where  $D_{ijkl}$  designate the elastic stiffness tensor and  $C_{ijkl}$  the elastic flexibility tensor [Ottosen and Ristinmaa, 2005]. Please note that  $\mathbf{D}$  and  $\mathbf{C}$  are fourth order tensors containing  $3^4$  components each. In matrix notation Hooke's law is stated as

$$\boldsymbol{\sigma} = \mathbf{D}\boldsymbol{\epsilon}; \boldsymbol{\epsilon} = \mathbf{C}\boldsymbol{\sigma} \quad (2.4)$$

To characterize a material completely would thus require 81 elastic constants. Fortunately, basic mechanics and the general strain energy function implies minor and major symmetry, thus

$$D_{ijkl} = D_{jikl} = D_{ijlk} = D_{klij} \quad (2.5)$$

which reduces the number of independent elastic constants of an anisotropic material significantly to 21 [Ottosen and Ristinmaa, 2005]. Similarly holds for  $C_{ijkl}$ .

As stated in Section 2.4.1 wood is orthotropic since the elastic components remain unchanged (invariant) if the axis is reflected through one of its three mutually perpendicular symmetry planes. The corresponding orthogonal transformations implies further simplifications of the constitutive matrix to

$$\begin{bmatrix} D_{1111} & D_{1122} & D_{1133} & 0 & 0 & 0 \\ D_{2211} & D_{2222} & D_{2233} & 0 & 0 & 0 \\ D_{3311} & D_{3322} & D_{3333} & 0 & 0 & 0 \\ 0 & 0 & 0 & D_{1212} & 0 & 0 \\ 0 & 0 & 0 & 0 & D_{1313} & 0 \\ 0 & 0 & 0 & 0 & 0 & D_{2323} \end{bmatrix} \quad (2.6)$$

using Voigt matrix form. Invert the elastic stiffness tensor to obtain Hooke's law in the format [Ottosen and Ristinmaa, 2005]

$$\begin{bmatrix} \epsilon_{11} \\ \epsilon_{22} \\ \epsilon_{33} \\ \gamma_{12} \\ \gamma_{13} \\ \gamma_{23} \end{bmatrix} = \begin{bmatrix} \epsilon_{11} \\ \epsilon_{22} \\ \epsilon_{33} \\ \epsilon_{12} + \epsilon_{21} \\ \epsilon_{13} + \epsilon_{31} \\ \epsilon_{23} + \epsilon_{32} \end{bmatrix} = \begin{bmatrix} \frac{1}{E_{11}} & -\frac{\nu_{21}}{E_{22}} & -\frac{\nu_{31}}{E_{33}} & 0 & 0 & 0 \\ -\frac{\nu_{12}}{E_{11}} & \frac{1}{E_{22}} & -\frac{\nu_{32}}{E_{33}} & 0 & 0 & 0 \\ -\frac{\nu_{13}}{E_{11}} & -\frac{\nu_{23}}{E_{22}} & \frac{1}{E_{33}} & 0 & 0 & 0 \\ 0 & 0 & 0 & \frac{1}{G_{12}} & 0 & 0 \\ 0 & 0 & 0 & 0 & \frac{1}{G_{13}} & 0 \\ 0 & 0 & 0 & 0 & 0 & \frac{1}{G_{23}} \end{bmatrix} \begin{bmatrix} \sigma_{11} \\ \sigma_{22} \\ \sigma_{33} \\ \sigma_{12} \\ \sigma_{13} \\ \sigma_{23} \end{bmatrix} \quad (2.7)$$

Please note that the shear strain  $\gamma_{ij}$  equals the sum of  $\epsilon_{ij}$  and  $\epsilon_{ji}$  which by definition are equal. Major symmetry enforces the equality

$$C_{iijj} = \frac{\nu_{ij}}{E_{ii}} = \frac{\nu_{ji}}{E_{jj}} = C_{jjii} \quad (2.8)$$

Thus only three of six Poisson's ratios are independent. An orthotropic material is consequently governed by nine independent elastic constants.

The relations are for wood normally set up using the widely accepted LRT nomenclature according to Figure 2.11.

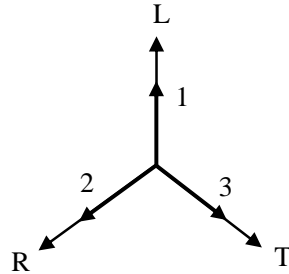


Figure 2.11: Reference coordinate system 123 relative to principal material system LRT

Consequently, the elastic flexibility tensor is given by [Bodig and Jayne, 1982]

$$\mathbf{C} = \begin{bmatrix} \frac{1}{E_L} & -\frac{\nu_{LR}}{E_R} & -\frac{\nu_{TL}}{E_T} & 0 & 0 & 0 \\ & \frac{1}{E_R} & -\frac{\nu_{TR}}{E_T} & 0 & 0 & 0 \\ & & \frac{1}{E_T} & 0 & 0 & 0 \\ & & & \frac{1}{G_{RT}} & 0 & 0 \\ \text{sym.} & & & & \frac{1}{G_{LT}} & 0 \\ & & & & & \frac{1}{G_{LR}} \end{bmatrix} \quad (2.9)$$

### 2.6.2 Transverse Isotropy

If a material is an invariant with respect to an arbitrary rotation about a given axis it is said to be transversely isotropic. This holds true for wood if radial and tangential material properties are assumed equal. The elastic stiffness tensor is then again reduced resulting in six independent elastic constants dependent of the longitudinal ( $L$ ) and perpendicular ( $P$ ) direction [Daniel and Ishai, 2005] [Reddy, 1997].

$$\mathbf{C} = \begin{bmatrix} \frac{1}{E_L} & -\frac{\nu_{LP}}{E_L} & -\frac{\nu_{LP}}{E_L} & 0 & 0 & 0 \\ & \frac{1}{E_P} & -\frac{\nu_{PP}}{E_P} & 0 & 0 & 0 \\ & & \frac{1}{E_P} & 0 & 0 & 0 \\ & & & \frac{1+\nu_{PP}}{G_{RT}} & 0 & 0 \\ & sym. & & & \frac{1}{G_{LP}} & 0 \\ & & & & & \frac{1}{G_{LP}} \end{bmatrix} \quad (2.10)$$

As mentioned in Section 2.4.1, the assumption of transversely isotropic materials is used in timber engineering. A common argument is that the variation between R and T is often lower than the variation along the stem from pith to bark. However, when testing clear wood specimens, the directions are commonly distinguished [Gustafsson, 2003].

Please note that transversely isotropic materials also are orthotropic.

### 2.6.3 Timber as an Orthotropic Elastic Material

A number of assumptions are required when applying orthotropic elastic theory to timber, some of which are illustrated in Figure 2.12. A bolt of wood (a) containing natural characteristics, c.f. Section 2.2, is idealised by ignoring these features (b). The bolt can be positioned by a polar coordinate system for which the long axis is  $L$ , the radial orientation is  $R$  and the curvature of the cylindrical growth rings is  $T$ .

However, wood is for the most part modelled in a Cartesian coordinate system as shown in Figure 2.12(d) [Bodig and Jayne, 1982]. Thus the curved growth rings must be modelled as planar growth layers. The error introduced by the assumption of rectilinear orthotropy for wood in the  $RT$ -plane is a function of specimen size and location in a stem. Notice the varying curvature in highlighted timber section in Figure 2.13.

Obviously the original location of the wood member in the log has great influence. Linearized ring curvature introduces larger errors for pieces taken near the pith than if taken in the periphery. Specimen 1 will thus be subjected to the least amount of error while for specimen 3  $T$  and  $R$  directions could be interchanged. By varying the size of specimens 4, 5 and 6, the error remains nearly constant. The error is thus minimized by a sample kept small in relation to the distance from the pith.

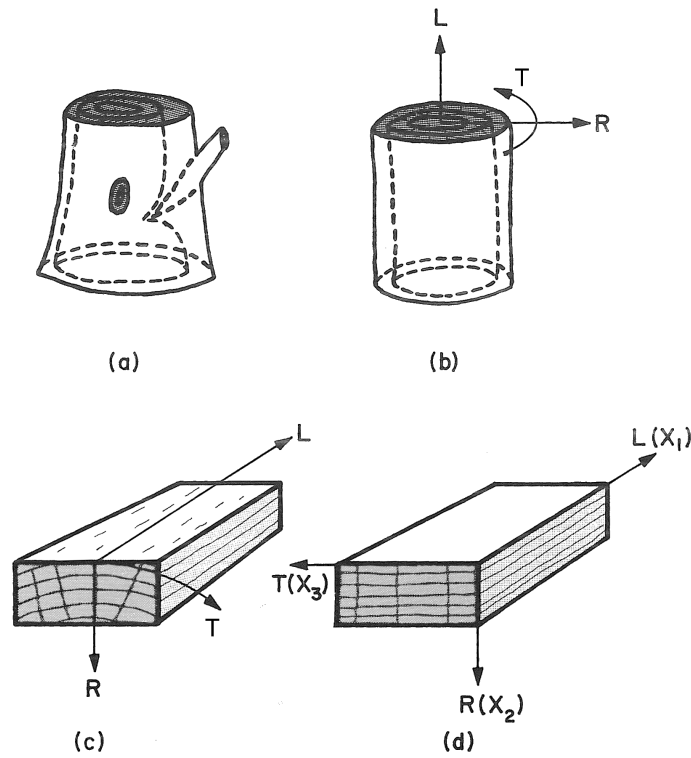


Figure 2.12: Reduction of a tree stem to an orthotropic model [Bodig and Jayne, 1982].

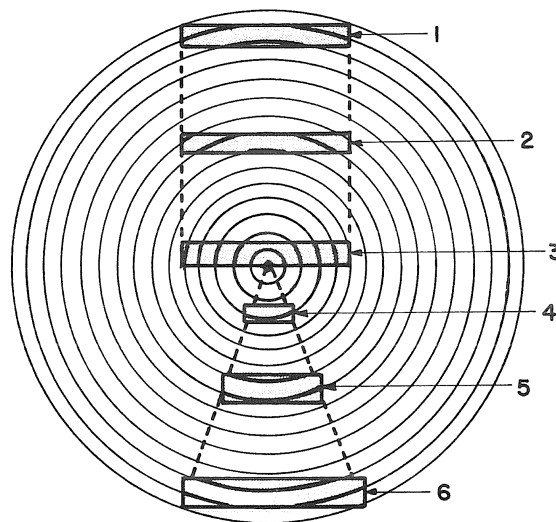


Figure 2.13: Varying influence of curvature in timber elements depending on originating location in the log [Bodig and Jayne, 1982].

# Chapter 3

## Glulam and Glulam Arches

### 3.1 Glulam

In order to exceed the naturally restricted dimensions of timber it is required to use engineered wood products. The oldest engineered wood product is glued laminated timber (glulam), first patented in 1906 by Otto Hetzer [Johansson, 2011]. Glulam consists of several finger jointed sawn boards, also known as laminations, bonded together with adhesives. The main fibre direction of the boards is aligned with the axial direction of the finished glulam beam.

In Sweden, standard straight glulam consists of 45 mm thick laminations with a width up to 215 mm. If needed, two or more glulam beams can be glued together to increase the total width. To optimize the element for bending, high strength laminations can be positioned in the outer higher stressed regions of the beam. Such element is called combined glulam in comparison to homogeneous glulam, see Figure 3.1.

Glulam beams can be produced with curvature, either to minimize deflections by a small pre-camber or as a curved beam. Curved beams are normally made using thinner laminations which are forced into the desired shape before hardening of the adhesive. The production method induces stress in the material and the curvature causes tensile stresses perpendicular to the grain in the apex which must be considered during design. Distortion of individual lamellas is not an issue in glulam production, however distortion of the glulam element itself can occur.

Since glulam is built up with several layers of laminations, local defects are limited in size and more evenly distributed over the volume in comparison with timber. The distribution reduces the probability of having a defect with serious influence on the element and consequently the total effect is less prominent. This dispersion effect results in a more homogeneous material than solid timber [Serrano, 2003], see Figure 3.2. Please note that glulam is not significantly stronger than equivalent timber.

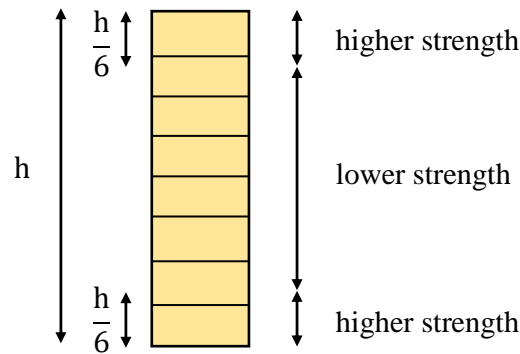


Figure 3.1: Combined glulam. Source: Johansson [2011].

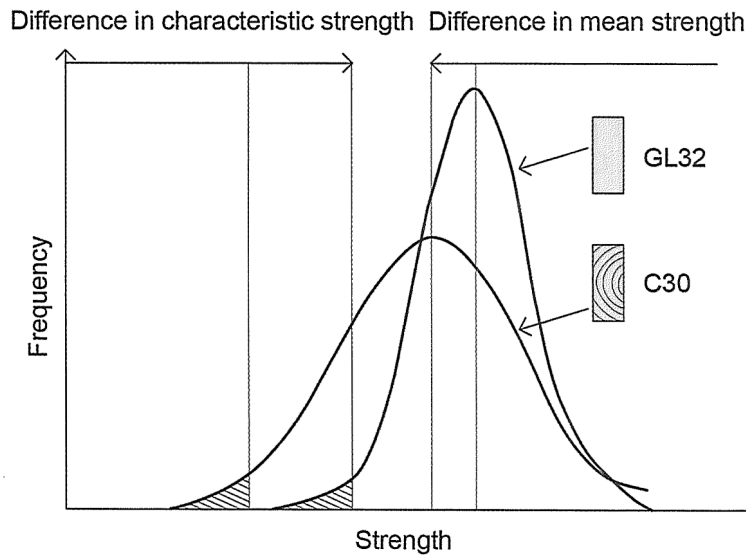


Figure 3.2: Strength distribution of timber and glulam. Source: Johansson [2011].

Though the material strength is not significantly greater than that of solid wood, the load carrying capacity of a glulam structure is. This is since very large dimensions of glulam can be made.

A typical feature of glulam is that the tensile strength of the laminations is higher than the bending strength of a beam. This does however raise the question about the stiffness of the finger joints, which has been found often comparable to that of clear wood [Serrano, 2003].

## 3.2 Arches

Arches were first used on a wide range of structures by the Ancient Romans. Stone was used as building material which has a low tensile strength. Since arches work mainly in compression it was a suitable geometry for span structures in stone. Due to simple scaffolding the arch often used was semi-circular, see Figure 3.3 [Crocetti, 2013].

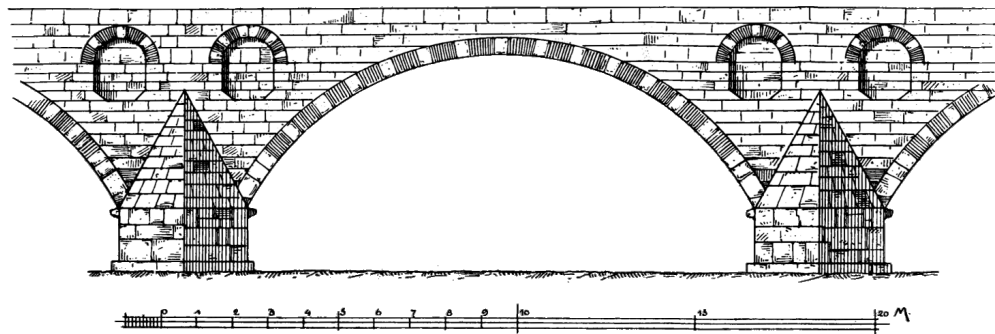


Figure 3.3: Macestus Bridge built by the Romans in the northwestern part of modern-day Turkey.

Today the arch geometry is chosen to minimize bending moment which is achieved by synchronizing the geometry with the thrust line of the dominating load combination, commonly referred to as the funicular shape. However, bending cannot be eliminated since several load combinations must be considered, each with their individual thrust line. Using equations of equilibrium on a three-hinged arch subjected to horizontally uniformly distributed load (UDL) it can be shown that bending moment is zero for any given position of the arch if it is shaped according to Equation 3.1.

$$y = \frac{4f}{L^2} (Lx - x^2) \quad (3.1)$$

where  $f$  is the arch rise and  $L$  is the total span of the arch. An arch shaped of this quadratic equation is called a parabolic arch. To limit the horizontal reaction forces rise-span ratio should be chosen greater than 0.14 [Carling, 2008]. For functional reasons other arch forms, such as elliptic or catenary, can be preferable. Common arch terminology is presented in Figure 3.4.

Arches can be zero, two or three hinged. To minimize internal stresses due to movements during service life, e.g. moisture content variation or uneven foundation settlement, the statically determinate three hinged arch is usually preferable for spans up to 60-70 m [Crocetti and Mårtensson, 2011]. Using a three hinged arch the two structure parts can be transported separately with an individual length of approximately up to 30m.

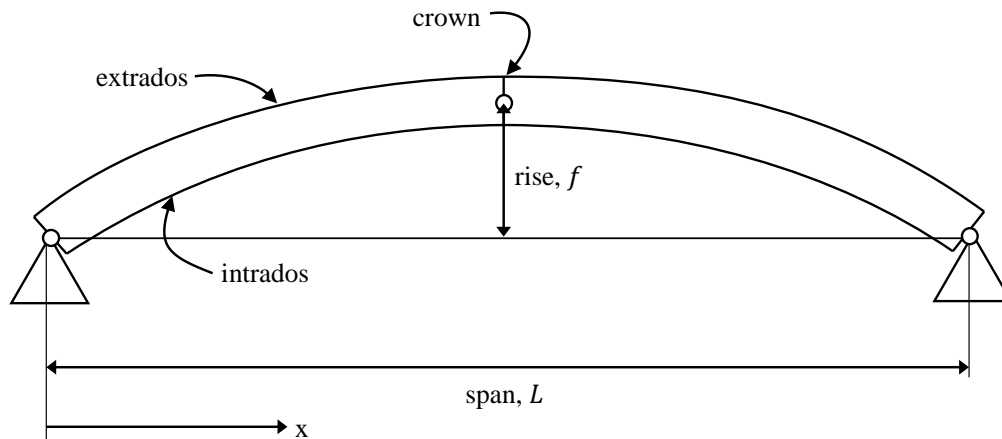


Figure 3.4: Parabolic arch with terminology.

### 3.3 Glulam Arches

Due to the large forces in wide span structures, such as arches, timber is generally used in larger glulam elements. Glulam can be produced in curved shapes with varying depth without a great increase in production cost which makes it ideal for light weight arch structures.

#### 3.3.1 Crown and Abutment

The stability of glulam arches are influenced by the types of joints of which the elements are attached to each other and to the foundation. It is of great importance for joints in large span structures to be designed in such manner that the static function of the element becomes the intended. Common types of connections for glulam arches are presented below.

##### 3.3.1.1 Abutment Hinge

A frequently used hinge is found in Figure 3.5. In this design, the transferred bending moment is small and thus not needed to be considered during the arch design [Carling, 2008]. While in-plane rotation of the arch is allowed, rotation out-of-plane and around the longitudinal axis is restricted. However, the glulam arch is not designed to take bending moment perpendicularly thus lateral bracing is needed.



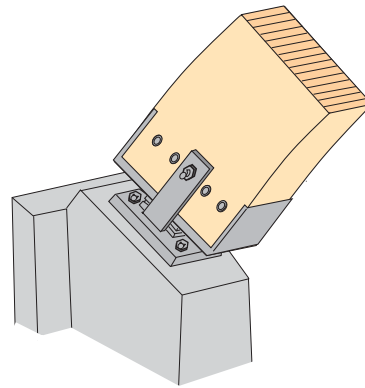


Figure 3.5: Common abutment hinge design. Source: Carling [2008].

### 3.3.1.2 Crown Hinge

Crown hinges for smaller spans are designed using nail plates. However, for large shear forces nail plates generates significant moments due to eccentricity which is not desirable. Instead a welded shim is introduced which can be designed as shown in Figure 3.6.

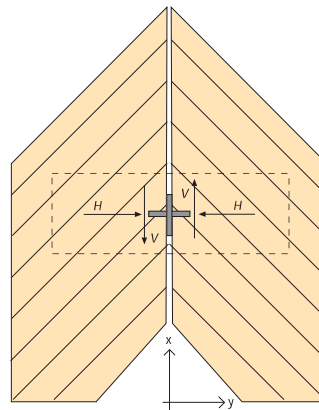


Figure 3.6: Common crown hinge design using welded shims. Source: Carling [2008].

The shim transfers shear force causing negligible eccentric moment while nail plates are used for the occasional horizontal tension.

## 3.3.2 Lateral Support

The glulam arch is commonly not designed with respect to perpendicular bending moment, thus lateral support is needed. The traditional design is a secondary structure of purlins, however load bearing profiled sheets are growing increasingly popular.

### 3.3.2.1 Purlin Joint

The joint which attaches the purlins to the arch is preferably designed using one of several types of fabricated connectors of which two frequently used can be seen in Figure 3.7.

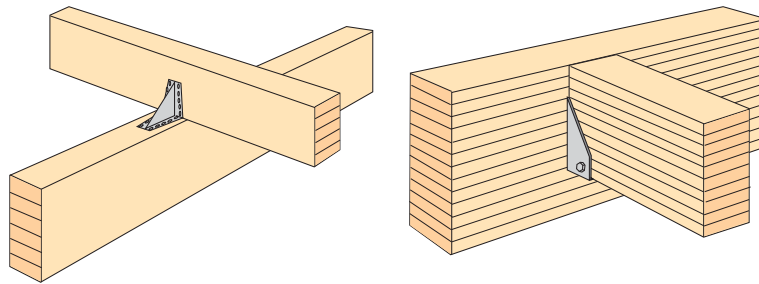


Figure 3.7: Purlin joint using reinforced angle (left) and hanger (right). Source: Carling [2008].

Using angles, purlins transfer vertical loads mainly by contact pressure while horizontal forces are transferred by nails. Please note that the angles can be placed under the purlin to obtain greater bending moment capacity which can be favourable regarding out-of-plane buckling of the arch.

Especially when the extrados and secondary structure is to be aligned, hangers are preferred. Horizontal forces are transferred from purlin to hanger by contact pressure while vertical forces are transferred from the hanger to the arch by nails.

Please note that when lateral support joints are designed to act in compression, the secondary structure needs to be designed with respect to buckling.

### 3.3.2.2 Load Bearing Profiled Sheets

Self-supporting roof structures is growing increasingly popular in large buildings due to cost efficiency in comparison to the use of purlins, see Figure 3.8. The high profiled steel sheathing supports insulation, installations and variable vertical loads through bending while horizontal loads from wind are transferred through diaphragm action.

The profiled sheets are typically fastened using two screws in every profile valley for mid-structure elements while six to eight in the gables [Andersson, 2014]. Due to the numerous fasteners, profiled sheathing can be considered as a more effective lateral bracing for the primary structure than purlins in terms of bracing capacity.

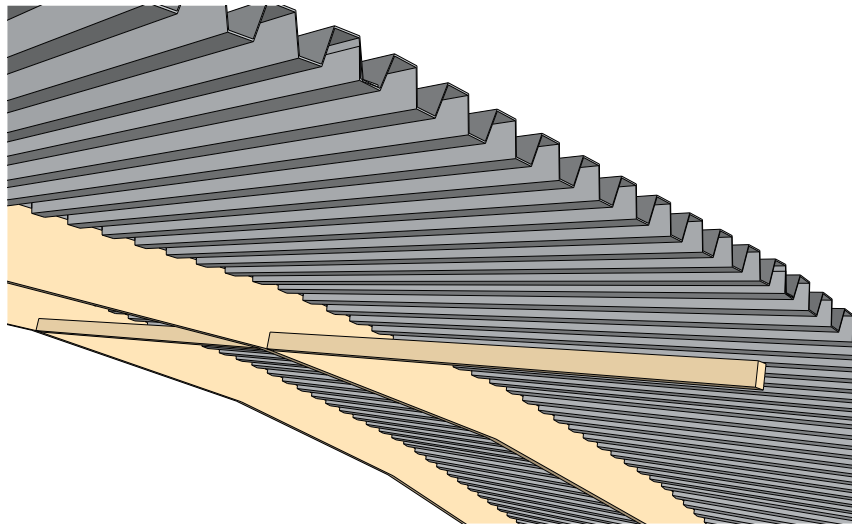


Figure 3.8: Bracing of arch structure by load bearing profiled sheets.

### 3.3.3 Global Lateral Stability

It is essential to achieve lateral stability not only of a structural element, i.e. using lateral bracing, but also of the entire structural system. The three fundamental methods of achieving lateral stability are diagonal bracing, shear wall and rigid joints. When additional capacity or redundancies are required more than one method can be used simultaneously.

Diagonal bracing using steel cables are usually preferred for glulam arches, which is illustrated in Figure 3.9. A secondary structure, such as purlins or load bearing profiled sheets, is used to transfer horizontal loads to the bracing structure.

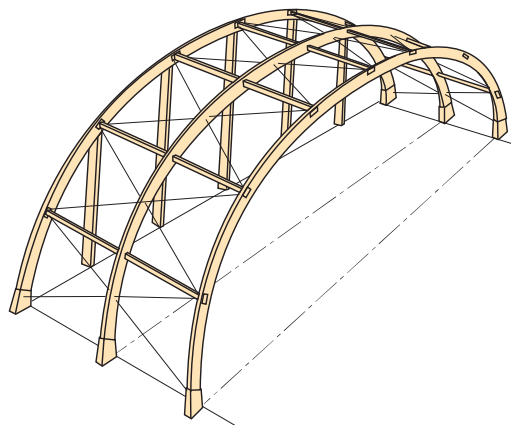


Figure 3.9: Lateral stability of glulam arches using diagonal bracing. Source: Carling [2008].

### 3.3.4 Additional Stresses in Arches

In comparison with traditional beam design, two additional stress phenomena are needed to be considered when designing glulam arches.

#### 3.3.4.1 Bending stress in the apex zone

During the production of curved glulam beams, individual lamellas are forced into a curvature which induces considerable bending stresses. However, these bending stresses are reduced due to material relaxation thus resulting in relative small strength reductions [Hudson, 1960]. Depending on the curvature and thickness of the lamella, these stresses should be considered.

Under the action of a pure moment on a uniform section of a curved beam the bending stress will not be linearly distributed over the cross-section unlike that of a straight beam, see Figure 3.10.

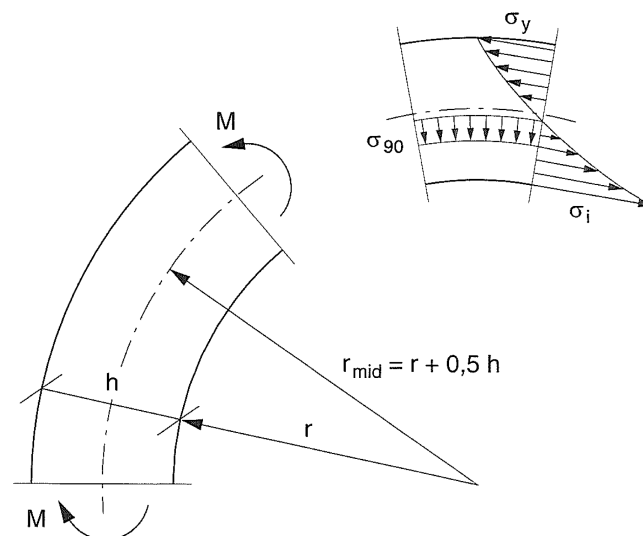


Figure 3.10: Curved beam of rectangular cross-section subjected to constant bending moment  $M$  resulting in a non-linear stress distribution. Source: Larsen and Riberholt [1999].

This is due to the fact that the face of the cross-section nearly stays perpendicular to the neutral axis, but since the original fibre lengths are increasing from intrados to extrados the strains (thus the stresses) will not vary linearly. Solutions for a rectangular cross-section can be found in [Lekhnitskii, 1968].

3.3.4.2 Radial stress in the apex zone

As can be seen in Figure 3.10 radial stresses will also arise due to the curvature. Consider the direction of compression forces in Figure 3.11. The curvature will cause a force component perpendicular to the grain which the material must withstand.

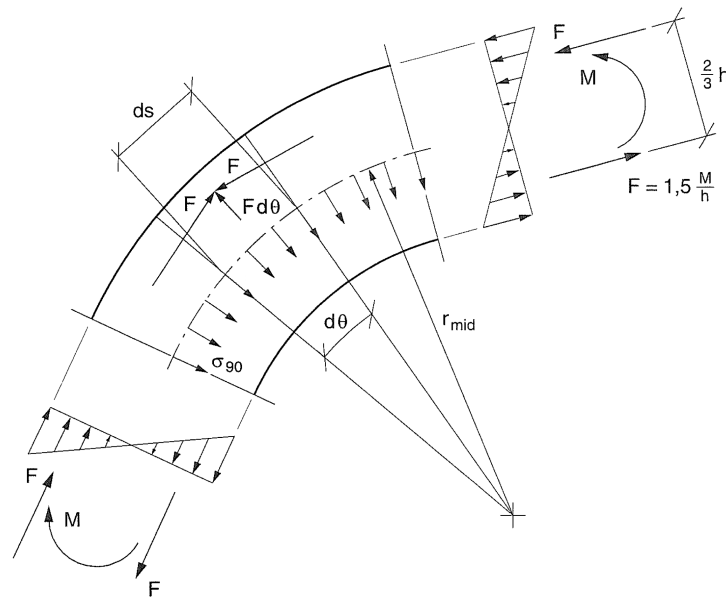


Figure 3.11: Internal forces  $F$  and tensile stresses perpendicular to grain at the centreline of a curved beam,  $\sigma_{90}$ . Source: Larsen and Riberholt [1999].

The radial stresses are especially significant for glulam arches since the tensile strength perpendicular to grain is very low.



# Chapter 4

## Instability Phenomenon

A structure is considered stable if a small increase of loading results in a small increase of deflections. However, if the structure is in an unstable state of equilibrium a small disturbance or increase of the load can result in a finite, but often very large, deformation. A comparison can be made to a ball on a hill versus in a valley, see Figure 4.1. These structural instabilities often results in collapse since the magnitude of the deformations can induce large stresses and ultimately material failure [Runesson et al., 1992].

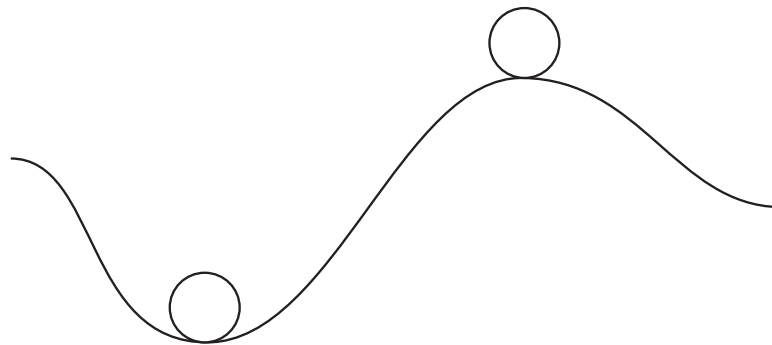


Figure 4.1: A ball in a stable and unstable state of equilibrium.

While material failure often is the limiting failure mode for short and bulky elements, instability is typically addressed to slender structural elements subjected to compressive axial or transversal loading. The most common instability phenomena are buckling and lateral torsional buckling, which can be analysed using different orders of theory. In the following chapter buckling and lateral torsional buckling will be presented for straight and curved beams.

## 4.1 Order of Theory

The mathematical definition of instability is expressed in terms of potential energy. The potential energy is dependent only of the actual configuration and not of how it is achieved. Equilibrium is reached for constant potential energy while the type of equilibrium is determined by the change of potential energy for a change of configuration around the equilibrium position. A stable equilibrium is characterised by a local minimum of the potential energy while a local maximum characterises an instable equilibrium [Runesson et al., 1992]. Please relate to Figure 4.1.

Three distinct orders of theory exist for various degrees of simplifications. In 1<sup>st</sup> order theory deformations and internal forces are directly proportional to the applied loading, i.e. forms linear systems. It is assumed that the deformations are small and thus they are neglected when considering the equations of equilibrium. The structure is analysed in the initial configuration and the principle of superposition is applicable.

If the deformations are small but being considered in the equilibrium equations the 2<sup>nd</sup> order theory is used. Stresses and deflections are no longer proportional to the axial load. Their values will also be dependent on the magnitude of the deflections produced [Timoshenko and Gere, 1961]. Stability analysis according to 2<sup>nd</sup> order theory with pre-defined, known or assumed, compressive normal force is also known as linear buckling analysis.

A higher level of realism is obtained if the deformations are not treated as small and the real geometry is continuously being used to derive the equilibrium equations. Analysis according to the 3<sup>rd</sup> order is difficult to achieve without the use of finite element method since new equilibrium states are needed to be calculated for each small increase of loading. 3<sup>rd</sup> order analysis is also referred to as non-linear buckling analysis.

## 4.2 Buckling

As previously mentioned, slender structural members subjected to compressive axial loading may reach a critical load for which the member becomes unstable. Though unstable, the member (column) may theoretically withstand further increased loading. Since an unstable condition is reached the member may however suddenly buckle due to small disturbances causing large in-plane deformations. Such disturbances always exist in reality.



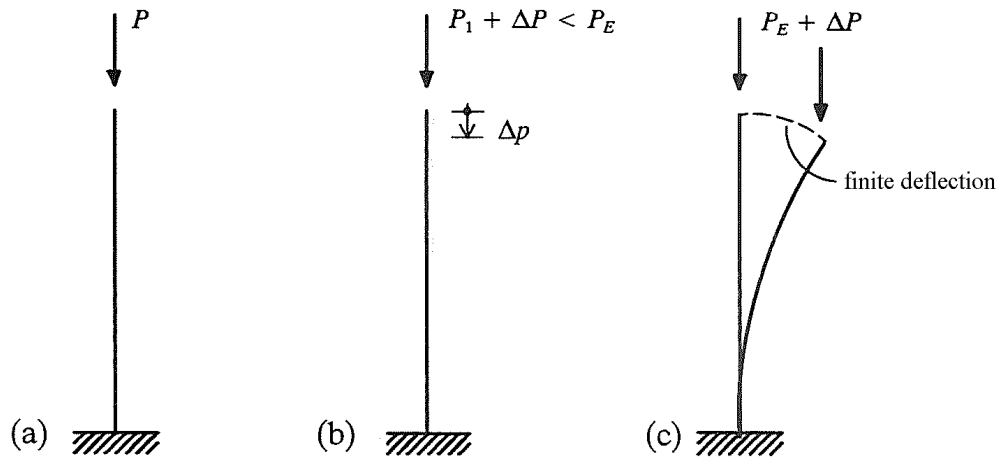


Figure 4.2: (a) Axial loaded column. Sensitive to instability. (b) Stable state of equilibrium. (c) Unstable state of equilibrium. Source: Runesson et al. [1992]

### 4.2.1 Buckling of Columns

Figure 4.2 illustrates buckling of a column. A small increase of axial loading  $\Delta P$ , in total smaller than the buckling load  $P_E$ , causes only a small increase in axial deformation (Figure 4.2b). However, a small increase  $\Delta P$  of  $P_E$  may also cause a finite horizontal displacement (Figure 4.2c); an unstable equilibrium.

A general expression for the buckling load of an initially straight column subjected to axial loading through the centreline of gravity is presented in Equation 4.1.

$$P_{cr} = \frac{\pi^2 EI}{(\beta L)^2} \quad (4.1)$$

where

- $EI$  bending stiffness of the column [ $Nm^2$ ]
- $L$  unsupported length of the column [ $m$ ]
- $\beta$  Euler effective length factor depending on the support conditions according to Figure 4.3.

In the section above the column was treated as straight and with loading directly in the centre of gravity. Practically, there are always imperfections such as eccentric loading, initial bow shape or residual stresses within the member. Depending on the magnitude of imperfection the critical buckling load will never be achieved, see Figure 4.4. The buckling load will instead be seen as the theoretical limit of the analysed member [Runesson et al., 1992].

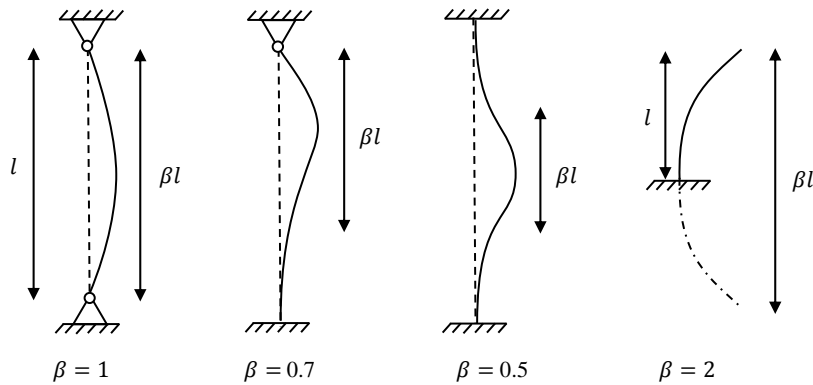


Figure 4.3: Euler effective length factor  $\beta$  for different support conditions.

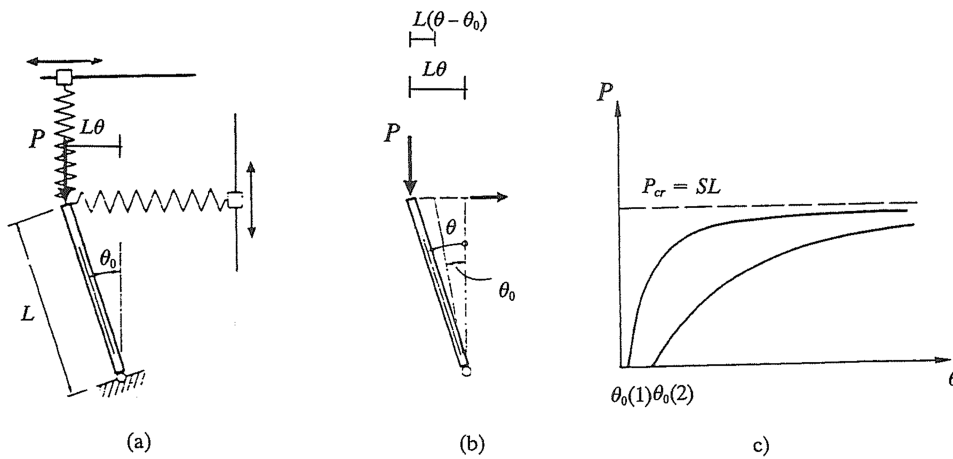


Figure 4.4: Stiff column with initial imperfection. The critical load is plotted for increasing initial angle in two systems (a and b), theoretical buckling load as dashed line. Source: Runesson et al. [1992].

### 4.2.2 Buckling of Beam-columns

Beams subjected to axial and lateral loads simultaneously are known as beam-columns [Timoshenko and Gere, 1961], see Figure 4.5.

Since the lateral loads will cause eccentricity for the axial loading, internal forces, stresses and deflections of the beam will not be proportional to the magnitude of the axial load. Hence 2<sup>nd</sup> or 3<sup>rd</sup> order analysis is necessary.

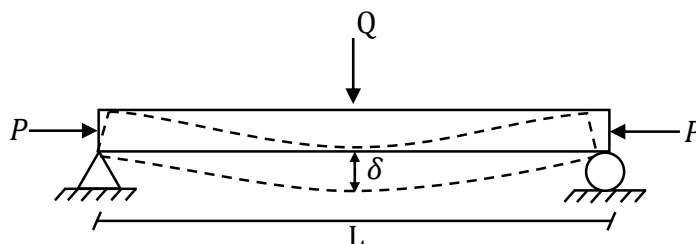


Figure 4.5: Simply supported beam subjected to axial ( $P$ ) and lateral ( $Q$ ) point loads.

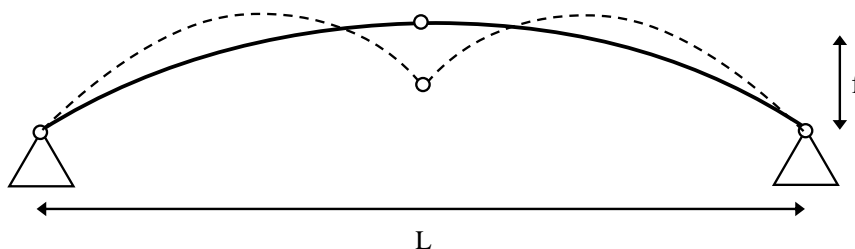


Figure 4.6: First in-plane buckling mode for a parabolic arch.

### 4.2.3 Buckling of Arches

Since a parabola is the funicular shape of a uniform load no bending of the arch will occur while subjected to such load. By gradually increasing the load on the parabolic arch a condition at which the equilibrium becomes unstable can be reached. The shapes of buckling modes are dependent of boundary conditions, and for a three-hinged parabolic arch the first in-plane buckling mode is illustrated in Figure 4.6.

For a parabolic arch with constant cross-section and uniform load the critical load can be expressed by the following formula [Timoshenko and Gere, 1961]:

$$q_{cr} = \gamma_4 \frac{EI}{L^3} \quad (4.2)$$

where

- $EI$  bending stiffness of the arch [ $Nm^2$ ]
- $L$  span [ $m$ ]
- $\gamma_4$  numerical factor depending on the ratio  $f/L$  and the number of hinges in the arch, see Figure 4.7

The dashed lines corresponds to symmetrical forms of buckling. In these cases asymmetrical buckling will still occur and to obtain values of  $\gamma_4$  curves for arches without central hinge must be used [Timoshenko and Gere, 1961].

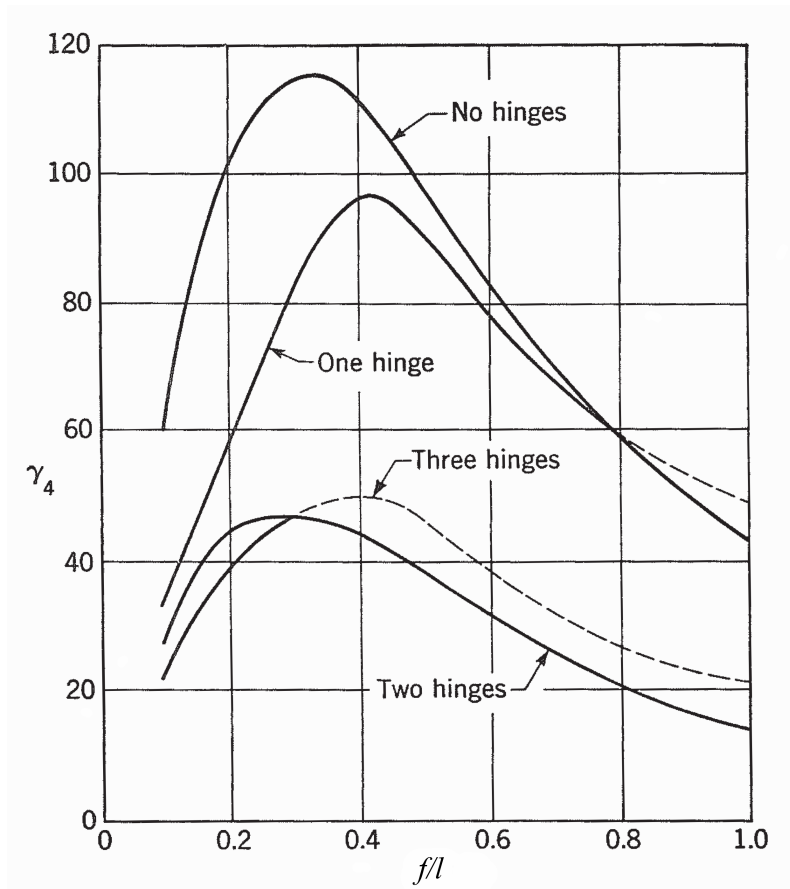


Figure 4.7: Numerical factor  $\gamma_4$  expressed graphically as a function of  $f/L$ . Source: Timoshenko and Gere [1961]

### 4.3 Lateral Torsional Buckling

Lateral torsional buckling represents a limit state where beam deformation includes in- and out-of-plane deformations as well as twisting. This can occur when a beam is loaded transversally, though risk of instability increases for simultaneous axial loading [Runesson et al., 1992]. As for buckling, in order for the phenomenon to occur the cross-section needs to be slender, i.e. the flexural rigidity of the beam in the plane of bending is large in comparison with the lateral bending rigidity.

#### 4.3.1 Lateral Torsional Buckling of Beams

Equations can be written for the beam in its deformed position: one for bending in the strong axis, one for bending in the weak axis and one equation associated with torsion. These can then be combined to determine the critical moment of the beam  $M_{crit}$ . A load on the beam greater than the critical moment may induce lateral torsional buckling, see Figure 4.8.

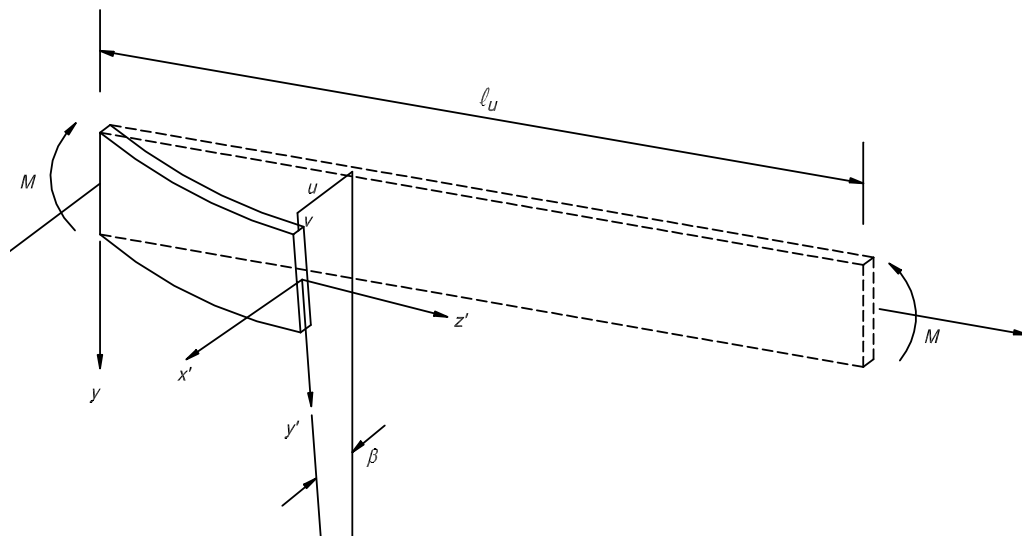


Figure 4.8: Simply supported beam with critical end moments causing lateral buckling. Source: American Forest and Paper Association [2003]

The lateral torsional buckling seen in Figure 4.8 corresponds to an unrestrained rectangular cross-section with a concentrated load in the centre of gravity. The critical moment can be calculated using Equation 4.3 [Runesson et al., 1992].

$$M_{cr} = \frac{\pi}{L_e} \sqrt{EI_y GJ} \quad (4.3)$$

where

- $E$  modulus of elasticity [ $Pa$ ]
- $I_y$  moment of inertia with respect to the weak direction [ $m^4$ ]
- $G$  shear modulus [ $Pa$ ]
- $J$  torsion constant [ $m^4$ ]
- $L_e$  effective length of beam [ $m$ ]

As can be seen in Equation 4.3, the critical moment can be significantly increased by reducing the effective length of a beam, for which it can deform, using lateral bracing. For increasing stiffness of the lateral bracing,  $M_{crit}$  is increased until the buckling mode is eliminated, see Figure 4.9. However, after the first buckling mode a stiffer mode will occur which needs to be verified.

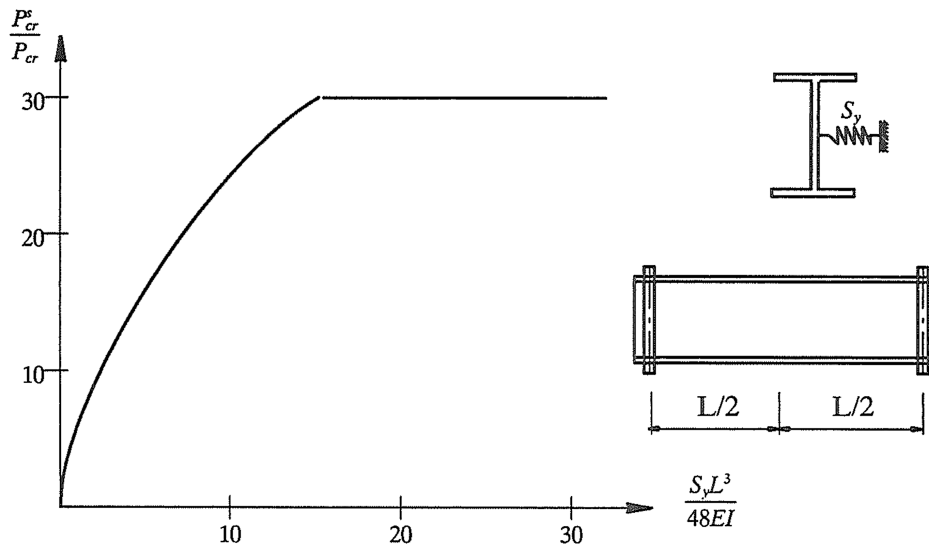


Figure 4.9: Simply supported beam with lateral spring at  $L/2$ . Critical load ratio plotted for increasing spring stiffness illustrating buckling mode elimination [Runesson et al., 1992]. Please note that the stiffer buckling mode will have an inflection point at the point of bracing, thus not effected by the spring stiffness. Source: Runesson et al. [1992]

### 4.3.2 Lateral Torsional Buckling of Arches

Since arches are mainly subjected to axial compression the risk of buckling is profound. For some load cases bending moments can be introduced and increase the risk of lateral torsional buckling. However, a useful theoretical model of the capacity with respect to lateral torsional buckling of curved beams is, to the authors' knowledge, not yet presented. Using beam analogy it is usually possible to identify the lower lateral torsional buckling modes, but in order to obtain numerical values a finite element model needs to be introduced, c.f. Chapter 7. The relevant arch buckling modes in this thesis are presented in Section 5.1.

# Chapter 5

## Arch Structure Studied

The reference arch model used in this thesis is presented in Figure 5.1 and 5.2. The model is a three-hinged parabolic arch situated inside a large span structure, such as a sports hall, in the south of Sweden. The roofing consists of continuous trapezoidal steel sheets which also is used as part of the bracing structure. The structural design is verified using Eurocode (EC) and later compared with finite element analysis.

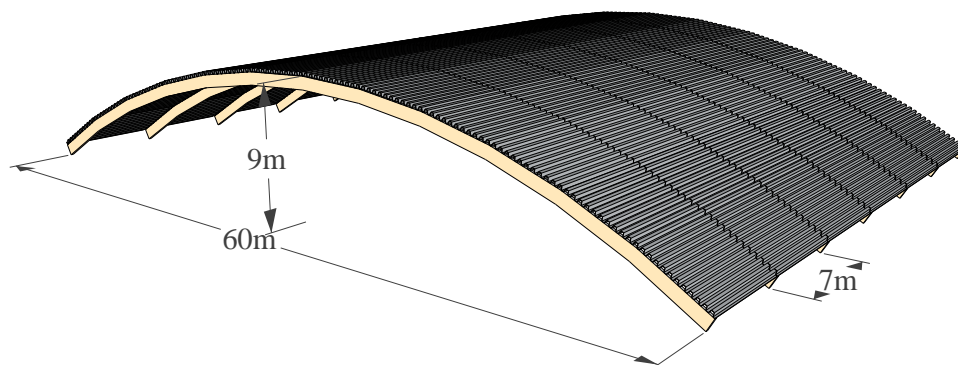


Figure 5.1: Large span arch building with trapezoidal roof sheathing.

### 5.1 Geometry

The arch is a three hinged arch of a parabolic shape with the rise-span ratio of 0.15, slightly larger than the common limit, c.f. Section 3.2. The spacing of the arch members is set to 7 m. The cross-section of the reference model is constant along the arch axis and its height by width is 1800x190 mm<sup>2</sup>. Due to the slenderness of the cross-section lateral supports are introduced along the intrados of the arch, see Figure 5.2 and Table 5.1.

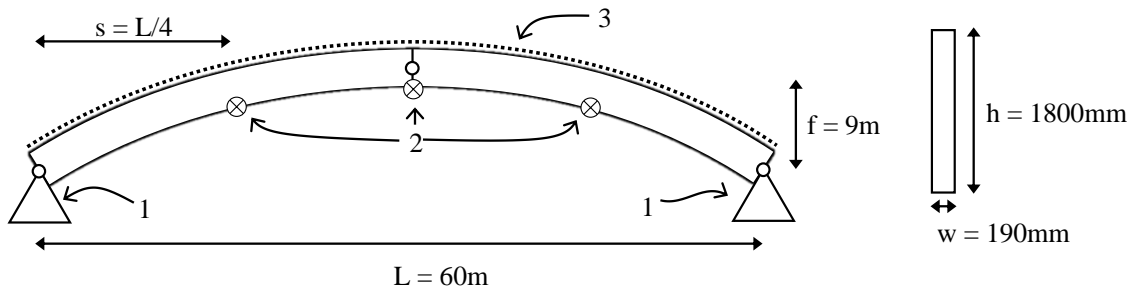


Figure 5.2: Boundary conditions of the arch model studied, see Table 5.1.

Table 5.1: Boundary conditions specifications.

Point	Boundary condition
1	Fixed support in both ends
2	3 point intrados lateral support
3	Continuous extrados lateral support by roof

The boundary conditions described will shape the buckling modes of the arch. The first out-of- and in-plane buckling modes for the presented model are shown in Figure 5.3.



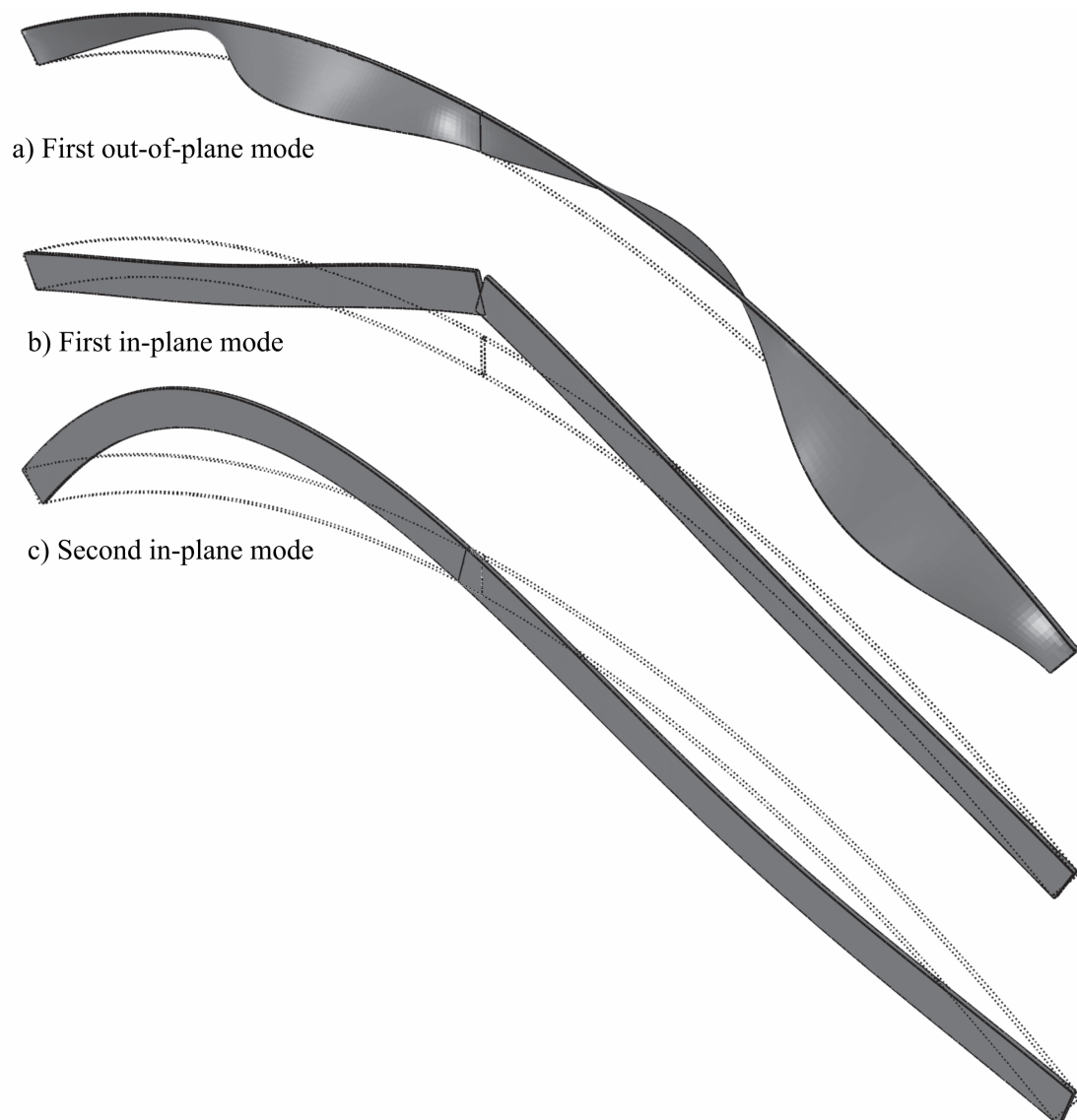


Figure 5.3: Buckling modes of a 3-hinged parabolic arch with intrados lateral support; out-of-plane (a) and in-plane (b,c).

Please note the similarity of Figure 5.3(a) to beams subjected to bending moments in Figure 4.8. The characteristic deformation of lateral torsional buckling is found between the intrados lateral bracing. Consider the effective buckling length with and without this lateral support. An asymmetrical load induces compression along a section of the arch intrados which further enhances instability failure.

The extent of the lateral support can be arranged in many different configurations preventing the structure to fail due to lateral torsional buckling. A comprehensive configuration of lateral support changes the first buckling mode from out-of-plane to in-plane after which no significant increase in load bearing capacity can be made. The configuration used in this thesis has been chosen in order to evaluate lateral torsional stability, hence out-of-plane modes occur prior to in-plane.

## 5.2 Material

The material used is a homogenous glulam of Eurocode class GL32h. The use of a combined glulam class such as GL32c were not found suitable since large normal forces are induced over the whole cross section (opposed to beams subjected to pure bending). The chosen glulam class GL32h has the following properties [SS-EN 1194]:

$f_{mk}$	=	32 MPa	Characteristic bending strength
$f_{ck}$	=	29 MPa	Characteristic compression strength parallel to grain
$f_{v,k}$	=	3.8 MPa	Characteristic shear strength
$f_{t,90,k}$	=	0.5 MPa	Characteristic tension strength perpendicular to grain
$E_{0.05}$	=	13 700 MPa	Characteristic modulus of elasticity parallel to grain
$G_k$	=	850 MPa	Characteristic shear modulus

## 5.3 Design Loads

The design loads are derived using load cases and distributions stated in the European rules for structural design, Eurocode, further presented in Chapter 6. The load cases considers permanent and variable loads in order to standardise building requirements. Variable loads typically varies over time and includes wind, snow and imposed loads depending of occupancy.

### 5.3.1 Permanent Load

The self-weight of a structure is represented by permanent loads. Since the cross-section and roofing is constant along the length of the arch the permanent load is simplified to a uniformly distributed load, see Figure 5.4.

Self-weights of the arch member, roofing and installations are approximated in Appendix A.1 with respect to the arch spacing of 7 meters. The total load is

$$q_{self-weight} = 13.1 \text{ kN/m horizontal}$$

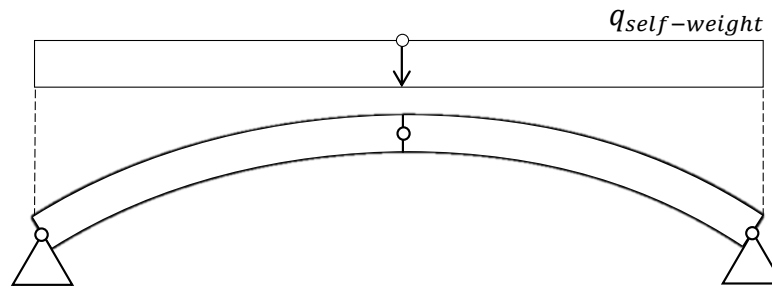


Figure 5.4: Arch with permanent loads considered as UDL.

### 5.3.2 Snow Load

The characteristic snow load is the weight of snow with the probability of 2% to be exceeded during a given year. However, the distribution of snow on a structure is influenced by many factors including the shape of the building, surrounding terrain and local climate for which the characteristic value is modified accordingly. Another variable regarding snow loads is the consideration of snowdrift due to wind.

Two load cases are considered during design; snow with and without snowdrift. Without snowdrift the snow is represented by a uniformly distributed load while snowdrift is represented by a asymmetrical triangular load case, see Figure 5.5. The triangular load represents an exceptional snow drift which can cause negative moments in the arch.

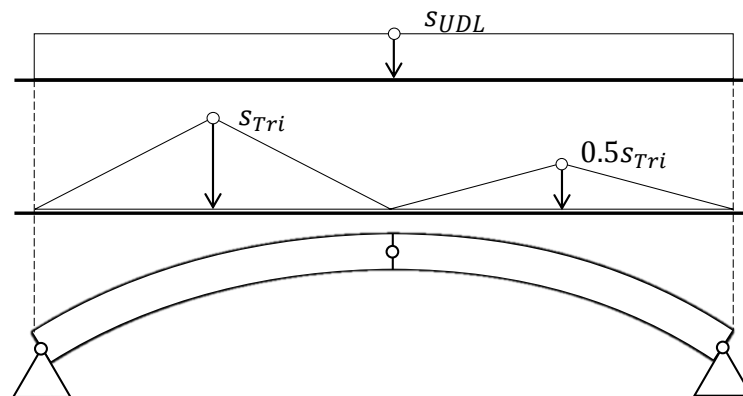


Figure 5.5: Snow loads on arches according to Eurocode; symmetric and asymmetric.

The loads are derived in Appendix A.2 to:

$$s_{UDL} = 1.6 \text{ kN/m}^2$$

$$s_{Triangular} = s_3 = 3.4 \text{ kN/m}^2$$

The value of the triangular load model will henceforth be referred to the maximum load, i.e.  $s_{Triangular}$ . Please note that in comparison to  $s_{UDL}$  the total force applied is only 37,5%.

### 5.3.3 Wind Load

With similar background as for snow loads, standardised wind load models are stipulated in Eurocode. The characteristic wind load is the average wind velocity during 10 minutes with the probability of 2% to be exceeded during a given year on the height of 10 meters above ground. As for snow, shape factors and topology is taken into account.

The wind load is primarily the result of dynamic effects. Most structures have a considerable natural dampening and are insensitive to short dynamic loads such as wind gusts. These characteristics allow an equivalent static load to be used in EC. The wind load model on an arch roof according to EC is found in EKS 9 (1.1.4, 13§), see Figure 5.6.

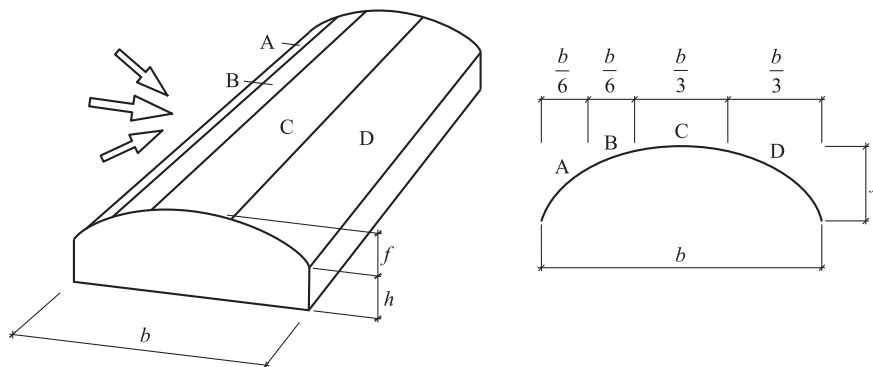


Figure 5.6: Wind load model of arch roof with rectangular base. Source: EKS9 figure C-6

While external surfaces are most exposed to winds, wind can cause high and low pressure within a structure which needs to be considered during the design. The main effect of wind on roof structures is that it is subjected to upwardly directing forces which may become larger than the self-weight of the structure.

### 5.3.4 Load Combination

Variable and permanent loads should be considered acting simultaneously on a structure. However, the probability of a worst case scenario, e.g. high winds and snow simultaneously, is low. To determine a more reasonable load combination, one of the variable loads is considered dominant while remaining are reduced.

Considering the relevant loads presented above, eight possible load combinations are needed in order to determine the designing load case. Calculations are found in Appendix A.4 and the combinations are presented in Figure 5.7.

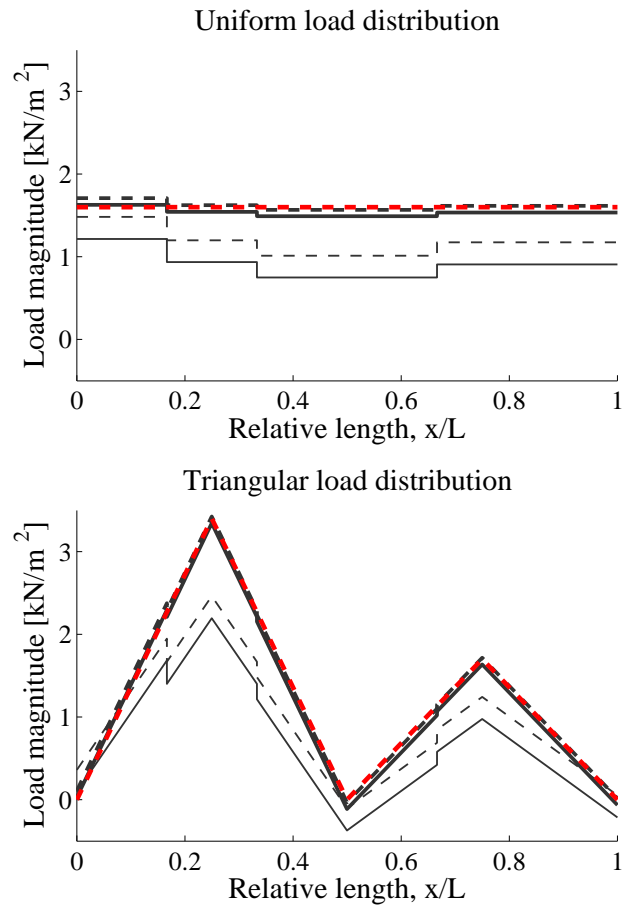


Figure 5.7: Identification of worst load case by possible combinations according to Eurocode. Main load: Snow (bold), wind (regular). Internal relative wind pressure: Positive (solid line), negative (dashed line). Used load combination in red.

Due to small influence the wind load is neglected in the further studies, resulting in two possible load cases to be considered according to Figure 5.8.

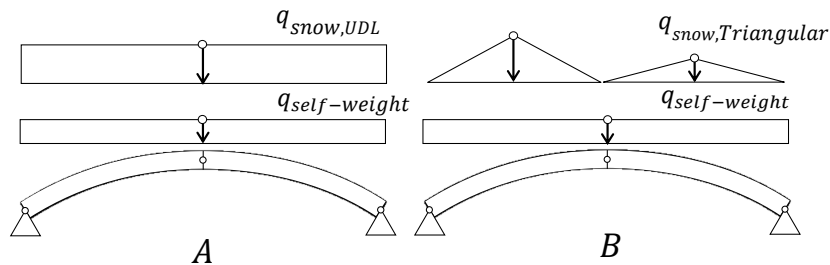


Figure 5.8: Two load cases illustrated. A) Self-weight and uniformly distributed snow B) self-weight and snow subjected to snowdrift.

## 5.4 Internal and Reaction Forces

In addition to self-weight, the parabolic arch is subjected to variable loads according to Section 5.3, see Figure 5.9. The three hinge design forms a statically determinate structure of which the internal forces can be determined analytically according to 1<sup>st</sup> order theory.

The triangular distributed snow load model will induce significant bending moment in the arch whereas the uniform will induce maximum normal forces. Thus it is of importance to separately find maximum internal forces and to identify possible critical positions of combination effects.

Calculations can be found in Appendix B while the result of the triangular and UDL load case is presented below.

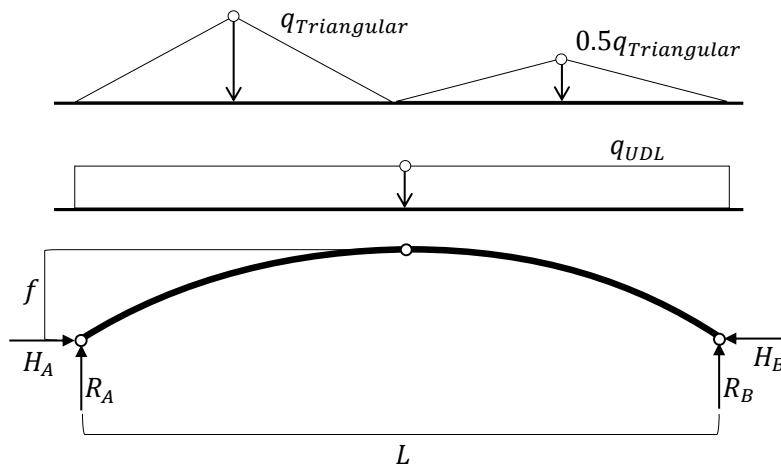


Figure 5.9: Free body diagram of parabolic arch with load models according to Eurocode.

### 5.4.1 Uniformly Distributed Load

Using static equilibrium and analytical calculations the internal forces for the arch subjected to a UDL was found. As previously discussed in Section 3.2, the parabolic shape does not obtain any bending moments for UDL, hence no shear forces neither. The normal force distribution is illustrated in Figure 5.10.

The maximum normal force is found at the abutments while the minimum is found at the crown, see Table 5.2.

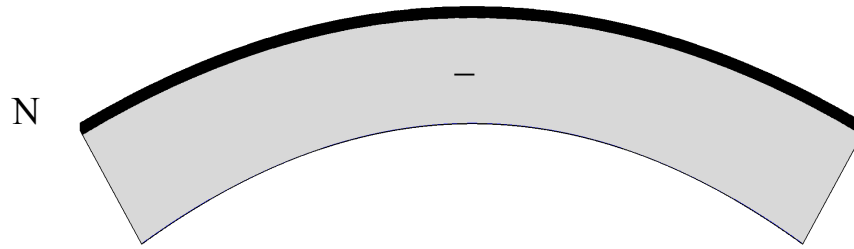


Figure 5.10: Normal force distribution over a parabolic arch subjected to UDL.

Table 5.2: Maximum internal forces in parabolic arch subjected to UDL.

	Self-weight	Snow
Normal force, $N_{max}$	762 kN	682 kN
Shear force, $V_{max}$	$\approx 0$ kN	$\approx 0$ kN
Bending moment, $M$	$\approx 0$ kNm	$\approx 0$ kNm

Since the normal force variation for shallow arches is small, it is for UDL assumed constant henceforth.

### 5.4.2 Triangular Distributed Load

While a parabola is the funicular shape to an UDL, bending moments and shear forces are expected for the triangular load case while a lower normal force. The internal forces are analytically calculated in Appendix B.2 and the results are found in Figure 5.11 and Table 5.3.

Table 5.3: Maximum internal force with corresponding internal forces at same location.

Internal force	Max value	Position	Simultaneously	
$N_{max}$	550 kN	0	41 kN	0 kNm
$V_{max}$	72 kN	$\approx L/2$	445 kN	348 kNm
$M_{max}$	811 kNm	$L/4$	470 kN	0 kN
$M_{min}$	-157 kNm	$\approx 3L/5$	456 kN	0 kN

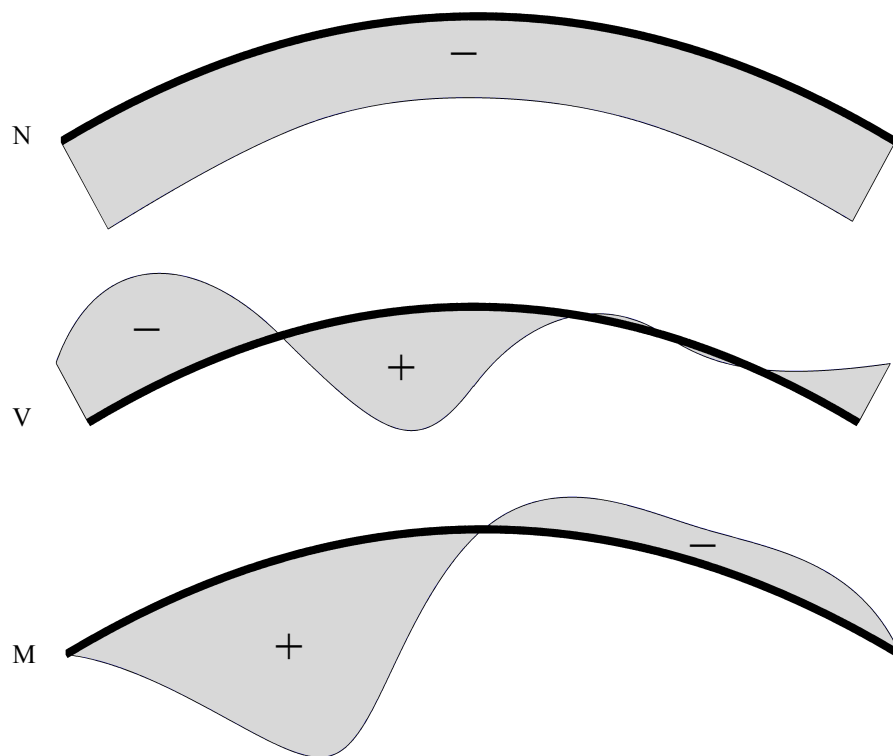


Figure 5.11: Internal forces for triangular load case. Normal force, radial shear force and bending moment distribution respectively.



# Chapter 6

## Design According to Eurocode

The Eurocode (EC) is a set of documents comprising rules for structural design using different materials in the European Union (EU). While the codes are equal for every member nation there may be, when considered appropriate, national choices of certain design rules or values [Porteous and Kermani, 2013].

In this chapter the studied arch presented in Chapter 5 will be verified according to EC using the following standards:

- The Eurocode framework for structural design is EN1990, Eurocode 0: Basis of structural design.
- The Eurocodes with regulations regarding snow and wind loads are EN1991, Eurocode 1: General actions on structures, Part 1-3 snow loads and part 1-4 wind load respectively.
- The Eurocode for design of timber structures is EN1995, Eurocode 5: Design of timber structures.

Within Eurocode it is possible to address instability using both first and higher order of analysis. Since it is an aim of this thesis to compare Eurocode hand calculations with FEM results, an analytical first order analysis approach has been chosen.

All calculations and variable definitions are presented in Appendix C.

## 6.1 Design Forces

The characteristic internal forces were determined analytically in Chapter 5. The uncertainties in the load models are considered in Eurocode with the use of partial safety factors. Since this thesis focuses on structural failure, the design forces are calculated using the ultimate limit state [EKS 9 eqn 6.10b] with safety class 3 according to Equation 6.1. The design loads are presented in Table 6.1.

$$X_d = \gamma_d \{1.2X_G + 1.5X_Q\} \quad (6.1)$$

Table 6.1: Design internal forces.

	Position	N [kN]	V [kN]	M [kNm]
$N_{max}^{1)}$	0	1938	0	0
$V_{max}^{2)}$	$\approx L/2$	1582	108	522
$M_{max}^{2)}$	$L/4$	1620	0	1217
$M_{min}^{2)}$	$\approx 3L/5$	1600	0	-236

1) Uniformly distributed load

2) Triangularly distributed load

## 6.2 Modification Factors

In order to take model uncertainties and property variations into account certain reduction coefficients are used. In the following a short description of the modification factors used in Eurocode 5 are presented.

### 6.2.1 Modification Factor $k_{mod}$

Timber behaves differently when exposed to different load durations and moisture levels, c.f. Chapter 2. The design standards quantifies this with the use of a modification factor,  $k_{mod}$ , which is multiplied with the characteristic strength according to Equation 6.2.

$$f_d = k_{mod} \frac{f_k}{\gamma_M} \quad (6.2)$$

The structural design standard defines five different load duration classes and three service classes accounting for load duration and humidity conditions respectively. For each combination of load duration and service class a value for  $k_{mod}$  is proposed, ranging from 0.5 to 1.1 (c.f. SS-EN 1995-1-1, 3.1.3).

In order to take account for uncertainties in the effects of geometric and material property deviations a partial factor  $\gamma_M$  is introduced. Typical value for glued-laminated timber is  $\gamma_M = 1.25$ .

### 6.2.2 Deformation Factor $k_{def}$

Deformation of a member or a structure can be calculated for both instantaneous deflections and long-time deflections including creep behaviour. As explained in Chapter 2 the creep behaviour is a function of several factors including moisture level and material. In Eurocode 5 the design process is simplified using a deformation factor,  $k_{def}$ , which is applied to the elastic modulus according to Equation 6.3. The deformation factor is dependent on the type of material as well as its moisture content (expressed with a service class) and it ranges from 0.6 to 2.0 for glulam [Porteous and Kermani, 2013].

$$E_{mean,fin} = \frac{E_{mean}}{(1 + k_{def})} \quad (6.3)$$

The deformation factor is applied to long term loads such as self-weight. Variable loads are instead converted to an equivalent long term load using quasi-permanent load modification factors (c.f. SS-EN 1990, 6.5.3). When validating the strength of a structure at ULS the elasticity and shear modulus should be reduced with respect to load duration and moisture condition. This is done in order to achieve the final mean values adjusted according to Equation 6.4 [SS-EN 1995-1-1, 2.3.2.2]:

$$E_{mean,fin} = \frac{E_{mean}}{(1 + \psi_2 k_{def})} \quad (6.4)$$

## 6.3 Influence of Curvature

In addition to the regular design verifications the apex zone must be validated with respect to stress condition, c.f. Section 3.3 and Figure 6.1.

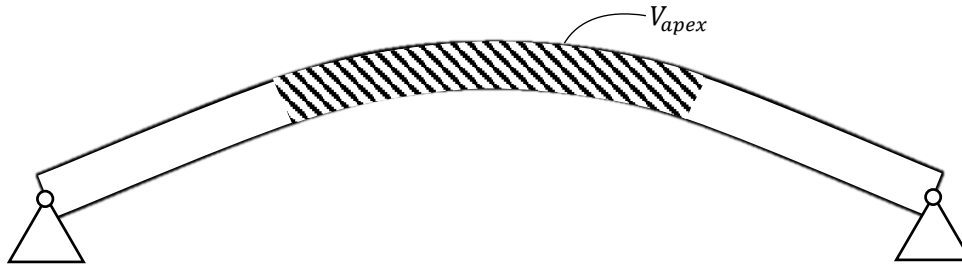


Figure 6.1: Curved beam with apex volume highlighted.

Due to the non-linear stress distribution over the cross-section (see Section 3.3.4) a modification factor,  $k_l$ , is introduced. The maximum bending stress,  $\sigma_{m,0,d}$ , is defined in SS-EN 1995-1-1 eqn 6.42 as:

$$\sigma_{m,d} = k_l \frac{6M_{ap,d}}{bh_{ap}^2} = 12 \text{ MPa} \quad (6.5)$$

The maximum stress must then be checked by the capacity of the cross-section according to Equation 6.6.

$$\sigma_{m,d} \leq k_r f_{m,d} \Rightarrow 12 \leq 20.5 \text{ MPa} \quad OK! \quad (6.6)$$

The maximum tensile stress perpendicular to grain in a curved beam is defined in SS-EN 1995-1-1 eqn 6.54 as Equation 6.7 and checked in Equation 6.8.

$$\sigma_{t,90,d} = k_p \frac{6M_{ap,d}}{bh_{ap}^2} = 0.1 \text{ MPa} \quad (6.7)$$

$$\sigma_{t,90,d} \leq k_{dis} k_{vol} f_{t,90,d} \Rightarrow 0.1 \leq 0.69 \text{ MPa} \quad OK! \quad (6.8)$$

Where  $k_p$  is a modification factor addressing the magnitude of the radial tension stress, see Section 3.3.4.

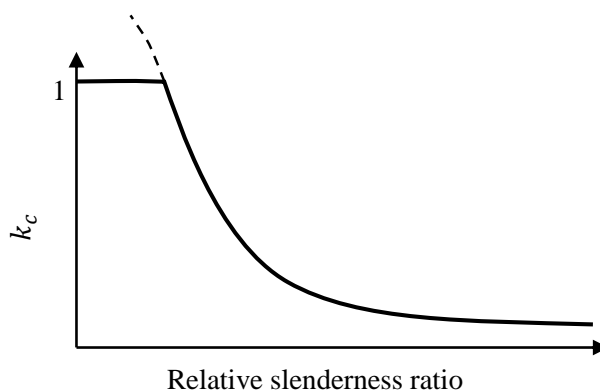


Figure 6.2: Buckling reduction factor  $k_c$  as a function of relative slenderness ratio. For bulky elements no reduction is required since material failure will occur prior to buckling.

## 6.4 Normal Force Capacity with regard of Instability

A member subjected to axial load has a tendency to buckle laterally due to geometrical imperfections, high slenderness ratio,  $\lambda$ , or a combination of both. Eurocode implements the use of slenderness ratio from which a strength reduction factor  $k_c$  is obtained, see Figure 6.2.

The compressive stress of the member must be less than the strength of the member at the design condition in Equation 6.9.

$$\sigma_{c,0,d} \leq k_c f_{c,0,d} \quad (6.9)$$

As seen in Figure 6.2 the strength reduction factor is highly influenced of the slenderness ratio,  $\lambda$ . The slenderness ratio is defined as the effective length of the member divided by its radius of gyration. Since a constant cross-section is used the radius of gyration is constant throughout the length of the member. When the member is short and bulky, failure will be due to timber failing under compression stress rather than buckling, represented by the initial constant part of the curve.

To estimate the in-plane buckling length of an equivalent column an effective length factor  $\beta = 1.25$  is used [Crocetti and Mårtensson, 2011].

$$L_{e,IP} = \beta s = 1.25 \cdot 31.7 = 40 \text{ m} \quad (6.10)$$

where  $s$  is half the arch length.

Since the arch is considered to be laterally supported along the whole length of the extrados the classic buckling behaviour is restricted. Instead torsional buckling will occur as the intrados buckles laterally, see Figure 6.3 left.

The buckling reduction within Eurocode is only defined for straight elements. For curved elements a second order FE analysis is commonly used to provide the critical load. However, it is the aim of this thesis to keep FE analysis separated from the Eurocode calculations, hence an analytical approach has been chosen.

In order to analytically evaluate the critical compressive load for such out-of-plane buckling an analogy is made to torsional buckling of a cruciform strut, see Figure 6.3 right. The internal edge of each quadrant of the cruciform cross-section can be considered restrained from lateral movements, similar to the lateral support of the arch. The critical load for the cruciform cross-section is hence divided by four in order to obtain a critical load estimation of the arch. Note that no regard has been taken to initial imperfection, which is considered in Eurocode.

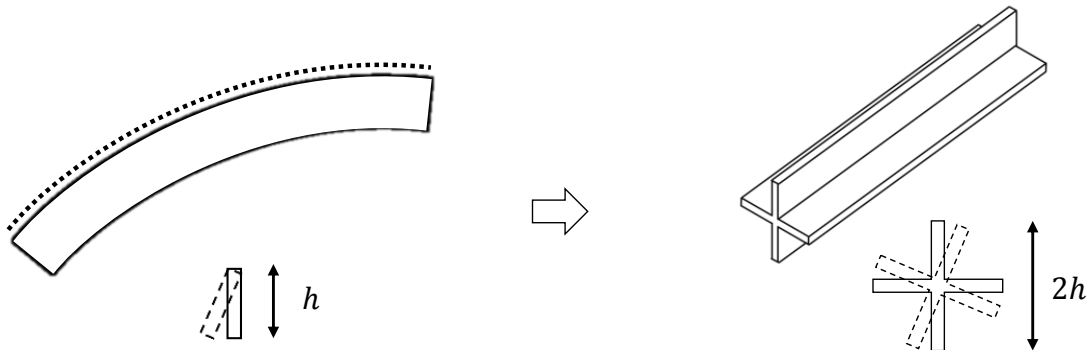


Figure 6.3: Analogy between lateral buckling of arch and torsional buckling of a cruciform strut.

## 6.5 Bending Moment Capacity with regard of Instability

Members subjected to flexure may fail due to lateral torsional instability, see Section 4.3. Eurocode 5 treats this matter by using a relative slenderness for the structural member.

For a member with the effective length of  $l_{ef}$ , restrained against torsional movements at its ends and subjected to pure moment applied at its ends the elastic critical bending stress according to Eurocode is [SS-EN 1995-1-1 eqn 6.31]:

$$\sigma_{m,crit} = \frac{M_{y,crit}}{W_y} = \frac{\pi\sqrt{E_{0.05}I_z G_{0.05}J}}{l_{ef}W_y} = 10.7 \text{ MPa} \quad (6.11)$$

In order to account for lateral buckling of a member the bending stress in the member must be less than or equal to the reduced bending strength [SS-EN 1995-1-1 eqn 6.33]:

$$\sigma_{m,d} \leq k_{crit}f_{m,d} \quad \Rightarrow \quad 2.3 \leq 0.33 \cdot 20.5 = 6.77 \text{ MPa} \quad OK! \quad (6.12)$$

where  $k_{crit}$  is the lateral buckling reduction factor determined from the relative slenderness.

## 6.6 Shear Strength

When a member is subjected to bending, shear stress will also arise perpendicular to the longitudinal axis. According to elastic theory the shear stress at any level in the member is calculated according to Equation 6.13.

$$\tau = \frac{VS}{Iw} \quad (6.13)$$

where

- $\tau$  shear stress [ $Pa$ ]
- $V$  shear force [ $N$ ]
- $S$  static moment of area [ $m^3$ ]
- $I$  moment of inertia [ $m^4$ ]
- $w$  width of member [ $m$ ]

For a rectangular section of width  $w$  and height  $h$  the maximum shear stress will occur at mid-depth with a magnitude according to Equation 6.14.

$$\tau = \frac{3V}{2wh} \quad (6.14)$$

The shear capacity of the arch will then be (see Appendix C.9):

$$V_{Rd} = \frac{3}{2}w_{eff}hf_{V,d} = 438 \text{ kN} \quad (6.15)$$

$$V_{Ed} \leq V_{Rd} \quad \Rightarrow \quad 108 \leq 438 \text{ kN} \quad OK! \quad (6.16)$$

## 6.7 Total Load Bearing Capacity

In order to evaluate the total load bearing capacity of the arch specific sections are controlled with respect to the sectional forces acting, see Figure 6.4.

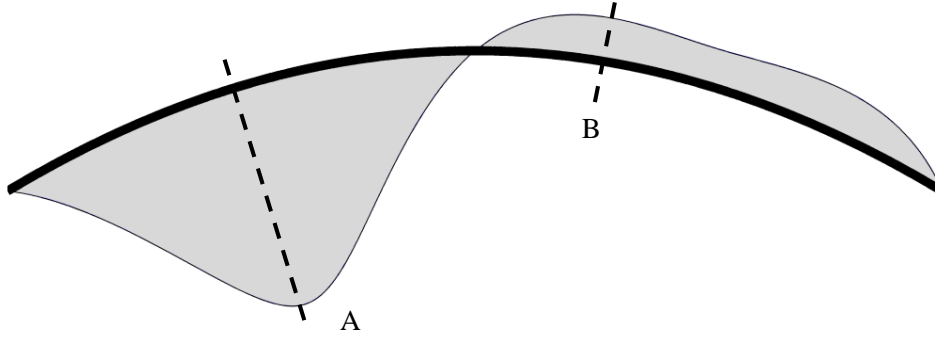


Figure 6.4: Section controls: A) Positive bending moment, compressed edge restrained from lateral buckling, B) Negative bending moment and compressed edge free to buckle laterally.

### 6.7.1 Compressed Edge Restrained from Lateral Buckling

With a relative slenderness greater than 0.3 buckling behaviour needs to be considered. Hence no plastic stresses are allowed to be utilized and the member fails when the material reaches its failure strength in the extreme fibre. For a member subjected to combined axial compression and bending moment Eurocode 5 stipulates a verification according to the constraints below [SS-EN 1995-1-1 eqn 6.23-24]:

$$\frac{\sigma_{c,0,d}}{\sigma_{Rd,cruciform}} + k_m \frac{\sigma_{m,y,d}}{f_{m,y,d}} + \frac{\sigma_{m,z,d}}{f_{m,z,d}} = 0.99 < 1.0 \quad OK! \quad (6.17)$$

$$\frac{\sigma_{c,0,d}}{k_{c,y} f_{c,0,d}} + \frac{\sigma_{m,y,d}}{f_{m,y,d}} + k_m \frac{\sigma_{m,z,d}}{f_{m,z,d}} = 0.96 < 1.0 \quad OK! \quad (6.18)$$

### 6.7.2 Compressed Edge Unrestrained from Lateral Buckling

For members which has a relative slenderness greater than 0.75 the effects of lateral torsional stability needs to be considered. When combined action from moment about the major axis and compressive force the stresses should fulfil the following condition [SS-EN 1995-1-1 eqn 6.35]:

$$\left( \frac{\sigma_{m,d}}{k_{crit} f_{m,d}} \right)^2 + \frac{\sigma_{c,0,d}}{k_{c,z} f_{c,0,d}} = 0.49 < 1.0 \quad OK! \quad (6.19)$$



## 6.8 Eurocode Verification Summary

The presented verifications are summarized in Table 6.2.

Table 6.2: Verification summary.

Verification of	Status	Reference
Stresses in apex zone	OK	Appendix C.6.1 and C.6.2
Bending stress	OK	Appendix C.8
Compression stress	OK	Appendix C.7
Shear stress	OK	Appendix C.9
Combined stresses	OK	Appendix C.10



# Chapter 7

## Finite Element Method and Abaqus

### 7.1 Finite Element Method

Problems occurring in structural mechanics can usually be described by differential equations. Some problems can be solved analytically but due to complex geometry or boundary conditions the analytical solutions may not be available. Using finite element method the problems are instead solved approximately with a numerical approach [Ottosen and Petersson, 1992], see Figure 7.1.

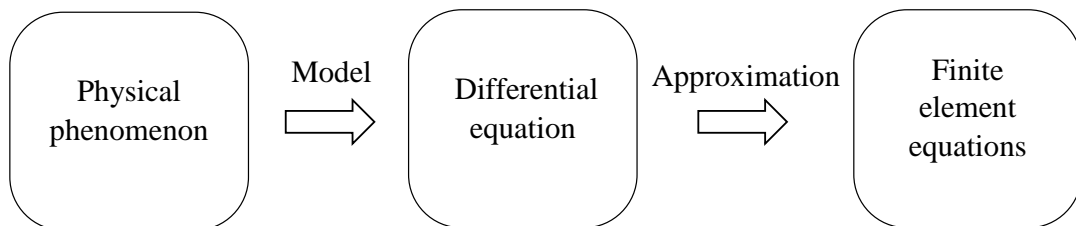


Figure 7.1: Analysis scheme from physical phenomenon to FEM.

The differential equations used to describe a physical phenomenon are assumed valid over a certain small region of a model. Instead of finding a solution for the entire model it is characteristic for the finite element method to divide the region into smaller parts, i.e. finite elements. An approximation is then carried out over each element assuming linear or quadratic variation. By using a great amount of elements even a model with highly non-linear variation can be modelled using finite element method [Ottosen and Petersson, 1992]. The collection of all such elements building up a model is called a finite element mesh, see Figure 7.2.

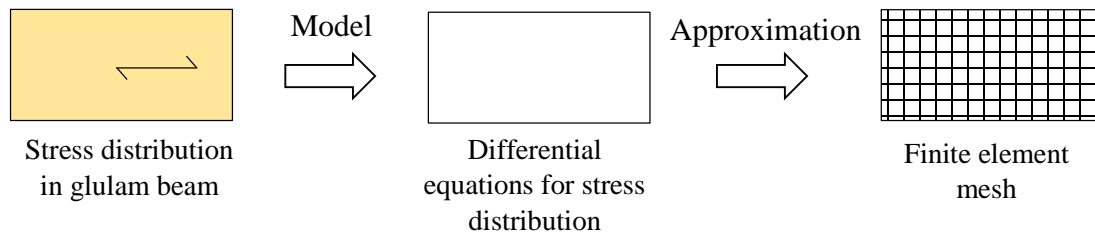


Figure 7.2: Illustration of modelling steps in order to represent a physical phenomenon.

As FE method is a numerical solution to a general differential equation the method can be applied to a wide variety of problems, e.g. heat conduction and the flexural behaviour of three-dimensional bodies such as plates.

To further illuminate the solution technique a heat conduction problem is illustrated in an example below. The example consists of only a few unknowns, i.e. degrees of freedom or DOF, which are needed to analyse how the temperature varies over the length of the bar. The property of a material to conduct heat is called thermal conductivity, which can be seen as the resistance of the system to a physical change.

In structural analysis the unknown DOF consists not of temperature but displacements and rotations. The resistance of a system to such changes depends on material properties, boundary conditions and geometry which all are included in the stiffness matrix  $\mathbf{K}$  representing the system.

In general the problems analysed often involves thousands of unknown and such equation systems cannot be solved by hand. Instead the FE method is entirely depending on the use of computers making it possible to analyse complex geometry.

**Example.** The temperature variation along a one-dimensional bar is to be modelled using FE method. The bar is divided into several elements with linear approximation between the elements nodes. The temperature at these nodes is assumed to be equal to the real temperature  $T(x)$ . These points are called nodal points and are usually located on the boundary of each element.

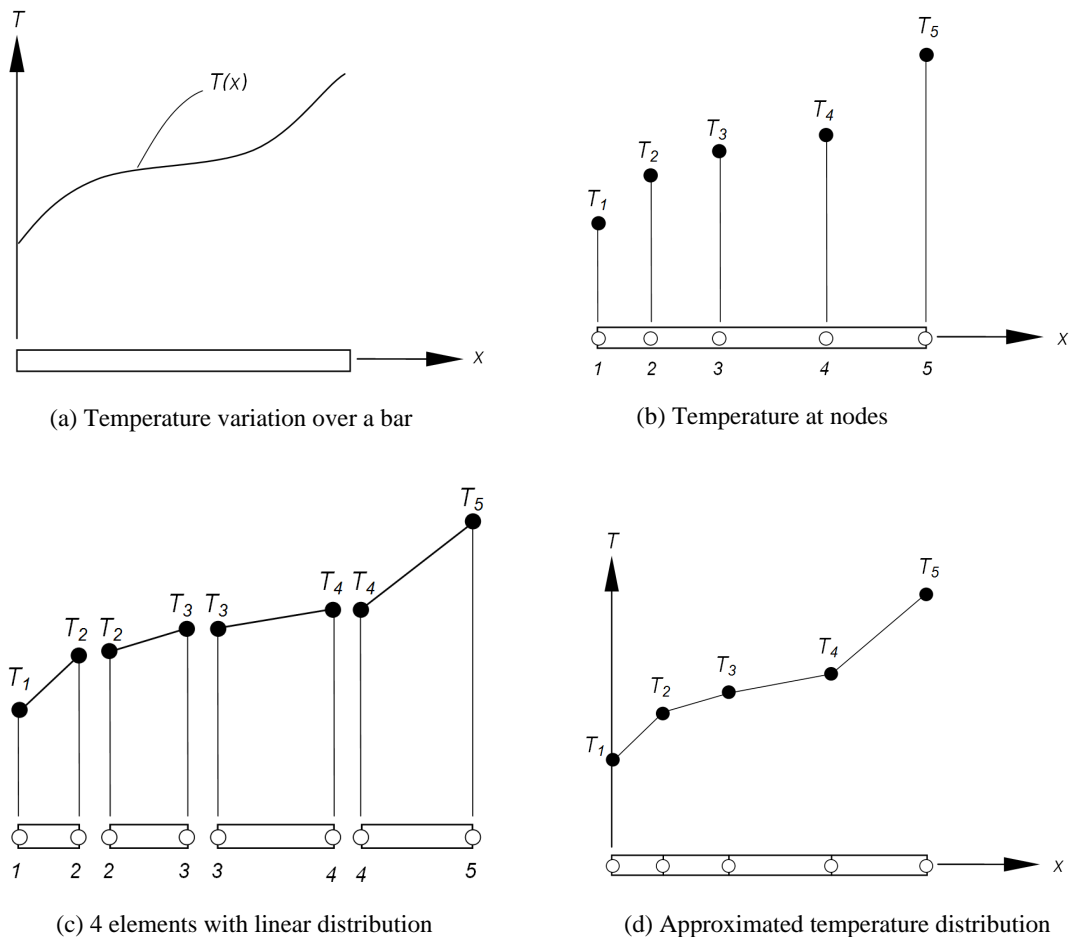


Figure 7.3: Example of approximations using FEM. Source: Persson [2010].

By introducing elements the original problem with infinitely many unknowns has been replaced with a problem of finite number of unknowns. In general, more unknowns used to approximate a problem will result in higher accuracy and the numerical solution from a well-defined FE analysis will converge to the true value.

## 7.2 Linear Elastic Buckling Analysis

Analysing buckling load using eigenvalues provides the critical load for which the structure reaches its buckling strength. By numerical solutions the load at which the stiffness matrix becomes singular is identified and expressed as a load multiplier,  $\lambda$ . This eigenvalue is multiplied with the assigned load to achieve the critical load. The eigenvalue problem is formulated in Equation 7.1.

$$(\mathbf{K}_0 + \lambda_i \mathbf{K}_\Delta) \mathbf{v}_i = 0 \quad (7.1)$$

where

- $\mathbf{K}_0$   $n \cdot n$  stiffness matrix originating from the base state where  $n$  is number of DOF. Any preloads defined on the structure are included.
- $\mathbf{K}_\Delta$   $n \cdot n$  stiffness matrix due to the type of loading.
- $\lambda_i$  scalar eigenvalue for the corresponding eigenmode,  $i = 1, 2, 3, \dots, n$
- $\mathbf{v}_i$  eigenvector containing the normalized mode shape,  $i = 1, 2, 3, \dots, n$

When conducting a buckling analysis usually the lowest mode is of greatest interest since it is most likely to occur. It should be noted that the eigenvector contains normalized magnitudes of deformation at the critical load, i.e. the maximum displacement component is 1.0. Hence the real deflection is not presented using linear buckling analysis.

## 7.3 Non-linear Buckling Analysis

Utilizing non-linear analysis the structural model can include plastic deformations and, as of interest in this report, initial imperfections and large deflection responses. Non-linear buckling analysis allows a more accurate prediction of critical load for a structure in comparison to a linear eigenvalue analysis. The latter is still commonly used since the computational cost is low and gives a good estimate of the upper bound of the critical load.

Non-linear analysis takes large deformations into account when solving equilibrium states and the loading can be applied using either a load- or displacement-controlled algorithm or a combination of both. When using a load controlled analysis the load is gradually increased until the structure becomes unstable and the limit point is reached, i.e. a small increase in load causes very large deflections. The analysis will then stop since a further increase of load will not yield a corresponding equilibrium.

In order to use non-linear analysis a disturbance of the structural system must be introduced. There are several methods to introduce disturbances in a finite element model. A generic method has been used in this thesis by applying scaled imperfections of buckling modes. This method is to be considered as a severe yet reasonable type of imperfection since the entire geometry is given an imperfection in which the geometry is most prone to take when buckling. As can be seen in Figure 7.4, the critical load decreases for increasing initial imperfections.

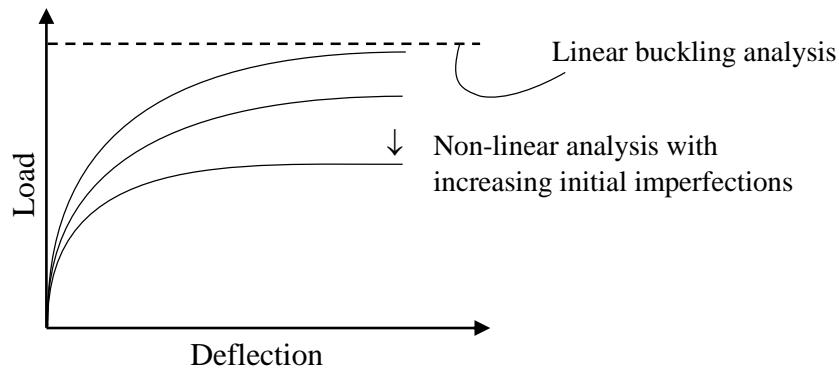


Figure 7.4: Load-displacement curve for increasing imperfections.

A simple load or displacement controlled algorithm experiences a so called snap-back and snap-through phenomenon due to highly non-linear response, see Figure 7.5. To study the response of the structure beyond the limit point a path following algorithm is required, which is a combination of load- and displacement controlled algorithm. This allows to identify potential post-buckling capacity, c.f. Krenk [2009]. It is not commonly utilized in the design of building structures but can be beneficial as it produce some sort of redundancies.

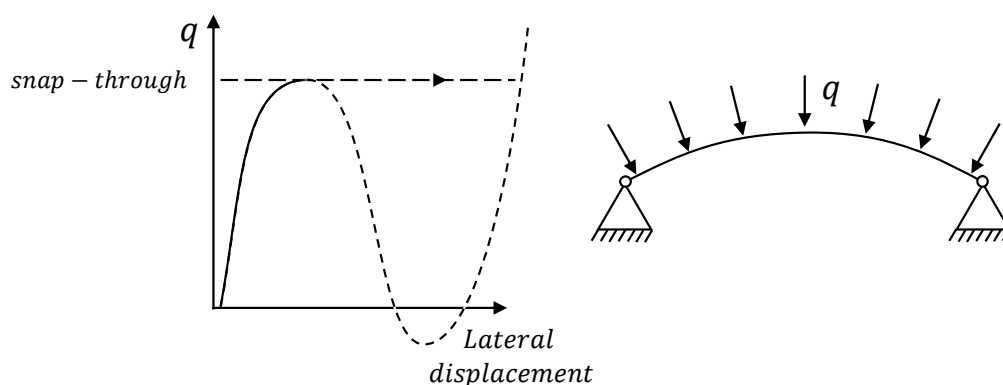


Figure 7.5: Post-buckling analysis using a path following analysis (dashed line) as opposed to conventional load-controlled algorithm causing snap-through phenomenon.

## 7.4 Element Types

A geometry is divided into a finite number of elements of which there are generally three families. These families are presented in the following section and will further be compared in Section 8.6.

### 7.4.1 Characterising Elements

There are several types of elements suitable for different types of problems. Five aspects characterises the behaviour [Dassault Systèmes Simulia Corp., 2010]:

- Family
- Degrees of freedom
- Number of nodes
- Formulation
- Integration

To model an arch, three families are applicable namely solid-, shell- and beam elements, see Figure 7.6.

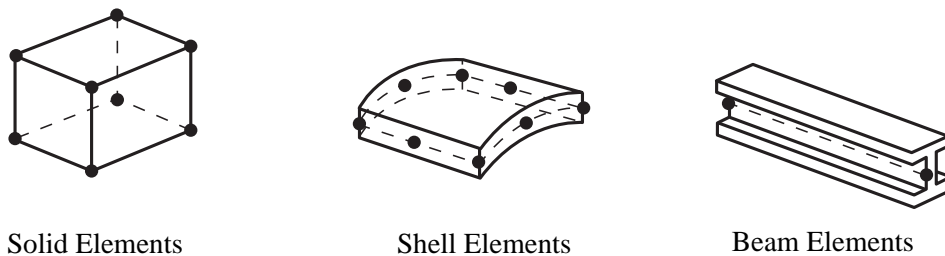


Figure 7.6: Element families commonly used in structural engineering.

Directly related to the element family is the number of degrees of freedom, DOF, which are the fundamental variables calculated during the analysis. For a stress and displacement simulation DOF includes translations and for some elements also rotations. DOF are defined in a number of points within an element, called nodes. For each element family, the number of nodes can be varied in order to obtain linear or quadratic variation over the element, see Figure 7.7. An optimized analysis generates accurate results using a minimum number of nodes.

Formulation refers to the mathematical theory used to define the behaviour of the element. For solid material analysis Lagrangian formulation is used while numerical techniques are used to integrate various quantities over the volume of each element.



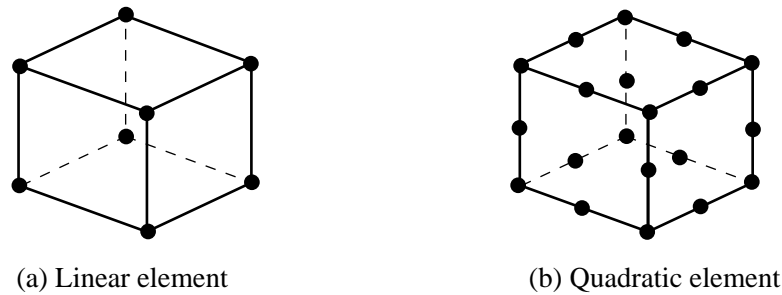


Figure 7.7: Linear 8-node solid element and quadratic 20-node element.

### 7.4.2 3D Solid Element

Solid elements enable meshing in three dimensions since the element contains nodes in three dimensions, see Figure 7.8. A brick is numerically preferable over a tetrahedral even though tetrahedral elements are sometimes advantageous for advanced geometries.

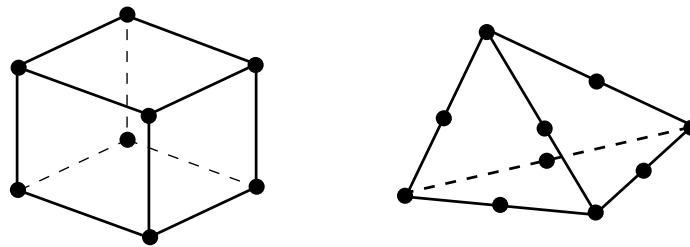


Figure 7.8: Solid elements in brick and tetrahedral shape.

Solid elements have only translation DOF and rotation is enabled by the three dimensional distribution of nodes.

### 7.4.3 3D Shell Element

A three dimensional shell element found in Figure 7.9 is actually a two dimensional element given a theoretical stiffness for the third dimension, thus reducing the DOF. Shell elements are normally rectangular in shape though triangular exists subjected to similar limitations as tetrahedral solids.

Using a 3D shell element enables to combine the simplicity of a 2D element and the versatility of a 3D element, thus reducing the number of computations in comparison with a 3D solid element. Loads are applied in 2D and by using 3D DOF a three dimensional result is obtained.

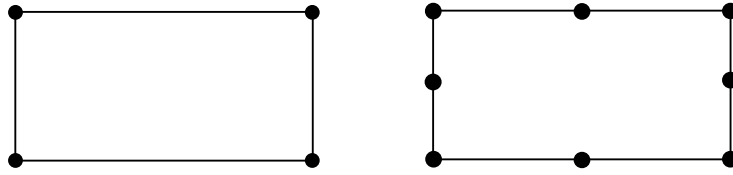


Figure 7.9: Shell elements, linear and quadratic.

#### 7.4.4 3D Beam Element

Beam elements further simplify the geometry using a single line of two or three nodes for linear or quadratic distribution respectively, see Figure 7.10. In order to analyse a two or three dimensional problem beam elements use both translation and rotations DOFs in each node. The rotational DOF enables the beam element to represent a 3-dimensional behaviour.

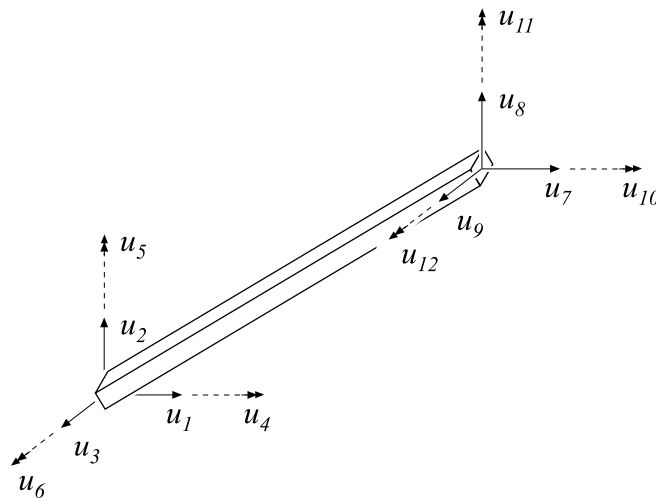


Figure 7.10: Beam element with illustrated DOFs.

## 7.5 Abaqus

There are numerous commercial FEM software on the market which are either applicable to general or specific types of problems. Software designed for specific problems are often used to obtain a more effective workflow. However, such software usually includes different assumptions which may affect the result.

In order to gain full control over the analysis, a general FEM software has been used in this thesis; Abaqus FEA. Abaqus was initially designed to address non-linear behaviour and as a result it has an extensive range of material models which has made it popular with academic and research institutes.

Abaqus is a software suite for FE analysis and computer-aided engineering. The specific software used in this thesis is Abaqus CAE and Abaqus Standard. Abaqus CAE is used in pre and post processing defining the model and visualizing the result while Abaqus Standard is used to run the actual analysis. Abaqus Standard employs a traditional FEM implicit integration scheme which is suitable for static and low-speed dynamic events.

In order to obtain an effective workflow customized scripts using Python language has been used as direct input to Abaqus Standard.



# Chapter 8

## Arch FE Model Studied

The arch model presented in Chapter 5 is modelled using the commercial FE software Abaqus. In the following chapter specific characteristics of the FE model will be presented, including verification study and method of analysis.

### 8.1 Introduction

After decades of study, buckling of curved beams continues to be a subject of great interest. There are generally three methods which have been used in the derived theories [Yang and Kuo, 1994]:

1. The equilibrium approach was used by e.g. Timoshenko and Gere [1961] in solving for critical loads of a solid curved beam under the two special cases of uniform bending or uniform compression. Experience indicates that the theory can yield very good solutions for solid curved beams. It is however difficult to consider coupling effects [Yang and Kuo, 1994].
2. Vlasov [1961] used the analogy approach based on straight beam theory. Please note that the idea of starting with the straight-beam theory is not meritless, although the analogy relations used in their derivations should be questioned.
3. More recent studies use energy methods such as virtual displacements and potential energy. The methods are all derived from the so-called first principles for curved beams, with no reference made to the straight-beam equations.

Discrepancies do however exist among the various theories. The lack of consistency in terms of method formulation and definition of control variables makes them difficult to compare. To justify superiority of one theory over the others experimental testing seems to be the only recourse. However, there are very few tests conducted [Yang and Kuo, 1994].

It has been argued that straight-beam elements cannot be used to model buckling of curved beams, particularly for the cases with large curvatures or small warping rigidity. Hence solutions using straight-beam elements should not be considered a valid base for judging the rationality of various curved-beam theories. However, more recent studies indicate that a curved beam can indeed be represented as an infinite number of infinitesimal straight elements by introducing an additional stiffness matrix; the joint moment matrix [Yang et al., 1991].

However, straight elements have been used in the FE analysis due to the simplicity of implementation in Abaqus and small difference from theoretical values calculated according to Timoshenko and Gere [1961].

## 8.2 Straight Member Approximation

In simpler commercial FEM software it is common that only straight members can be analysed and the common praxis is then to represent an arch by several straight members.

Depending on the type of analysis, such beam approximation can affect the accurateness of the analysis. In order to evaluate the accuracy of the instability load a linear buckling analysis has been conducted for geometries consisting of an increasing number of straight members, see Figure 8.1.

The results are found in Table 8.1, in which *Error* describes the deviation from theoretical values, c.f. Section 4.2.3, while *Diff* describes the deviation from previous results. In order to compare the results with theoretical data the analysis was made using an arch with isotropic material.

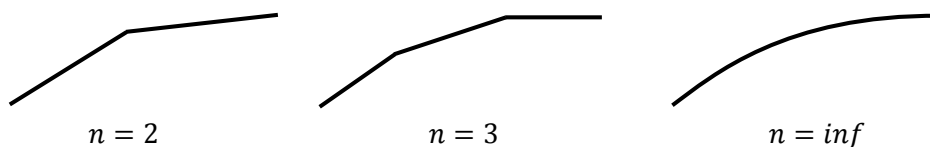


Figure 8.1: Straight member approximation of arch geometry.

Table 8.1: Influence of straight member approximation of in-plane linear buckling analysis of parabolic arch.  $L = 60\text{m}$ ,  $f = 9\text{m}$ ,  $width = 0.1\text{m}$ ,  $height = 1\text{m}$ , steel, element S8R. Symmetry was used.

No. straight members	Critical load [kN/m]	Diff [%]	Error [%]
3	263		2.06
5	251	4.58	-2.41
10	246	2.16	-4.48
20	247	-0.19	-4.29
40	241	2.18	-6.34
infinite	250	-2.43	-2.77
<i>Theoretical</i>	<i>258 kN/m</i>		

The increasing number of straight members does surprisingly not converge for the specific analysis which should be regarded as an uncertainty for such approximations. However, in order to exclude possible secondary errors due to such approximation the geometry used henceforth is the one referred to as “infinite”. The geometry is an equation driven parabolic arch imported from Solidworks, thus the straight members of the arch is assumed to be only the individual finite elements which are straight.

## 8.3 Material Model

A model that accounts for all characteristics of wood, timber and glulam is not computationally effective [Serrano, 2003]. Failure modes of glulam can be due to bending, tension failure parallel to grain, shear failure or instability. The scope of this report is instability thus failure due to plastic deformations is not analysed in detail. An elastic model is then reasonable to be assumed, in both tension and compression.

### 8.3.1 Linear Elastic Material Model

The material properties of wood are discussed in Section 2.6, for which a rectilinear transverse isotropic material model is implemented in this thesis. Thus the tangential and radial direction are assumed equal and modelled using a Cartesian coordinate system.

As a result of the dispersion effect of local imperfections in glulam discussed in Section 3.1, a simplification in the material model is therefore introduced by neglecting the influence of local defects such as knots resulting in a homogenous material. However, the global stiffness used is the characteristic value according to the european standard SS-EN 1194 which has taken local defects into account. The influence of finger joints are also neglected in a similar manner. The characteristic values from Eurocode are complemented by material parameters from Berbom Dahl [2009] resulting in the material properties in Table 8.2.

Table 8.2: Material properties of glulam quality GL32h complemented by Norway spruce characteristics. Stiffnesses in MPa.

$E_L$	$E_R, E_T$	$\nu_{LR}, \nu_{LT}$	$\nu_{RT}, \nu_{TR}$	$\nu_{RL}, \nu_{TL}$	$G_{RL}, G_{LT}$	$G_{RT}$
$E_1$	$E_2, E_3$	$\nu_{12}$	$\nu_{13}$	$\nu_{23}$	$G_{12}, G_{13}$	$G_{23}$
13 700	460	0.495 <sup>1)</sup>	0.43 <sup>1)</sup>	0.02 <sup>1)</sup>	850	34 <sup>1)</sup>

1) From Berbom Dahl [2009]  
Remaining from SS-EN 1194

### 8.3.2 Failure Criterion

An elastic material model does not necessarily contain a failure limit restricting strains nor stresses. A stability analysis can, especially for small initial imperfections and/or rigorous bracing, result in large stresses before instability occurs thus a failure criterion is required. Failure criteria can be defined using stresses, strains or displacements. In accordance with ultimate limit state in Eurocode, stresses are used in this thesis.

There are multiple failure criteria defined using both linear and quadratic forms used in solid mechanics, e.g. Tsai-Hill, Tresca and Von-Mises. However, the failure criterion adopted in Eurocode is based on first order analysis hence it includes coefficients accounting for the risk of buckling.

If the member is considered to be restrained from buckling Eurocode adopts a failure criterion where the cross-section to some extent can achieve plasticity. If, on the other hand, buckling effect have to be taken into account no benefit is taken of any plastic behaviour in the member and the member fails when the most stressed fibre reaches the capacity. Eurocode combines normal and bending stresses in a linear manner according to Equation 8.1-8.2.

$$\frac{\sigma_{c,0,d}}{k_{c,y}f_{c,0,d}} + \frac{\sigma_{m,y,d}}{f_{m,y,d}} + k_m \frac{\sigma_{m,z,d}}{f_{m,z,d}} \leq 1.0 \quad (8.1)$$



$$\frac{\sigma_{c,0,d}}{k_{c,z}f_{c,0,d}} + k_m \frac{\sigma_{m,y,d}}{f_{m,y,d}} + \frac{\sigma_{m,z,d}}{f_{m,z,d}} \leq 1.0 \quad (8.2)$$

In order to obtain a similar failure criterion in the FE analysis a maximum stress theory described in Equation 8.3 is used, thus no stress interaction is considered.

$$\left[ \frac{\sigma_c}{f_{ck}}, \frac{\sigma_{c90}}{f_{c90k}}, \frac{\sigma_t}{f_{tk}}, \frac{\sigma_{t90}}{f_{t90k}}, \left| \frac{\sigma_v}{f_{vk}} \right| \right] \leq 1.0 \quad (8.3)$$

$f_i$  are the failure strength values stated in Table 8.3. Similar to the elastic material parameters, the characteristic failure strength is from Eurocode in order to obtain comparable results.

Table 8.3: Characteristic failure strength for glulam GL32h according to SS-EN 1194.

Direction	Fail strength
$f_{ck}$	29 MPa
$f_{tk}$	22.5 MPa
$f_{c90k}$	3.3 MPa
$f_{t90k}$	0.5 MPa
$f_{vk}$	3.8 MPa

The failure envelope of maximum stress theory is plotted in Figure 8.2, where it is compared to the Tsai-Hill theory which do consider stress interaction. Please note that maximum stress theory is not always a conservative approach.

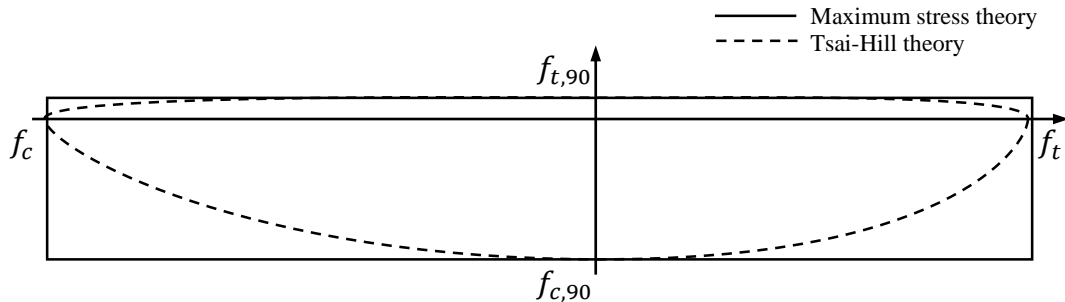


Figure 8.2: Failure envelope for Tsai-Hill and Maximum stress theory.

In the finite element calculations the maximum stress theory (MSTRS) is used in order to obtain the material failure limit. The MSTRS represents the maximum utilization rate of all nodes in the model. However, unwanted stress concentrations occur due to the linear material model. Since no plasticity is defined, strains can become so large that small portions of the structure can be exposed to stresses beyond the yield stress or even failure stress due to the lack of stress redistribution. If failure stress is reached the node would be represented by a MSTRS value of  $> 1.0$ . How stress concentrations are treated is described in Section 8.8.2.

## 8.4 Boundary Conditions

Boundary conditions are used to restrict element movements in known contact points. The boundary conditions in the reference model are described in Figure 8.3 and the following section.

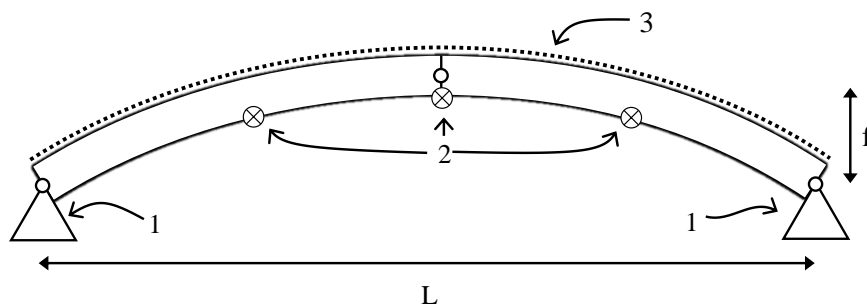


Figure 8.3: Arch geometry with indexed boundary conditions.

Please note that no eccentricities are included in the reference model.

### 8.4.1 Hinges

In each end the arch support, index 1 in Figure 8.3, is pinned in one point, i.e. translations are constrained in all directions. In order to obtain a realistic stress distribution over the cross-section yet allowing rotation a multi-point constraint, MPC, was used. Rotation is only allowed about the out-of-plane axis.

Similarly, the top hinge was defined using MPCs combined with another constraint connecting the master nodes of each arch element. The constraint only allows rotation between the elements about the out-of-plane axis.

### 8.4.2 Lateral Support

The extrados lateral support, index 3 in Figure 8.3, is a self-supporting roof system which either can be modelled by a total elimination of out-of-plane displacements or by assigning a more realistic stiffness to the connection. Please note that in either case such a system has a negligible bending moment capacity hence it cannot resist torsion of the arch.

In order to determine a realistic stiffness a force-displacement curve for the specific type of fasteners used is needed, which is found in Figure 8.4 for various types of connections in timber. One finds that almost full capacity for screws is reached after a displacement of 8mm.

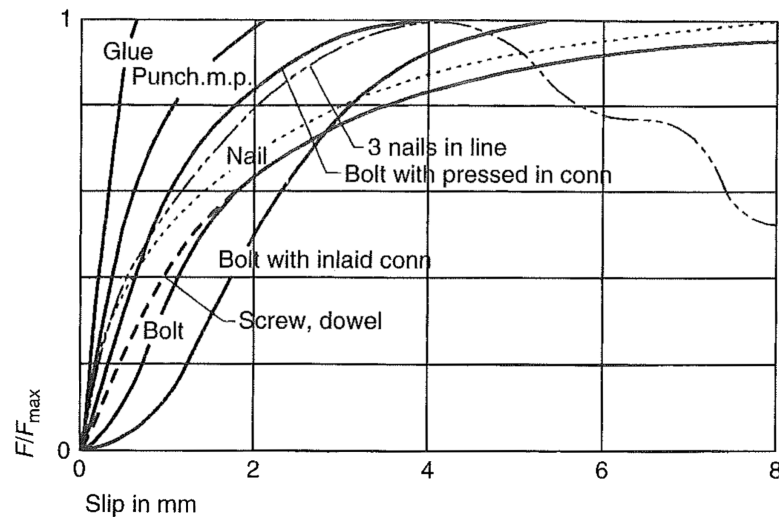


Figure 8.4: Load-slip curves for various fasteners. Screws are used in the lateral support. Source: Larsen [2003].

According to the roof system manufacturer Lindab the dimensions of the screws are 6.5x51 mm which makes it possible to determine the characteristic  $F_{max}$  according to Eurocode 5 [SS-EN 1995-1-1, 8.5] (calculations in Appendix D).

$$F_{max} = 3950 \text{ N}$$

Furthermore, two screws are used in every profile bottom spacing 315 mm apart. By combining these findings with Figure 8.4 it is possible to estimate the lateral displacement stiffness of the system. By sectionally linearizing the force-displacement curve one obtains a non-linear spring behaviour according to Figure 8.5 which has been implemented.

Please note that any deformations of the steel roof structure during the instability failure are neglected, which results in a slightly stiffer spring response than what is realistic. Possible interaction between screws in groups is neglected.

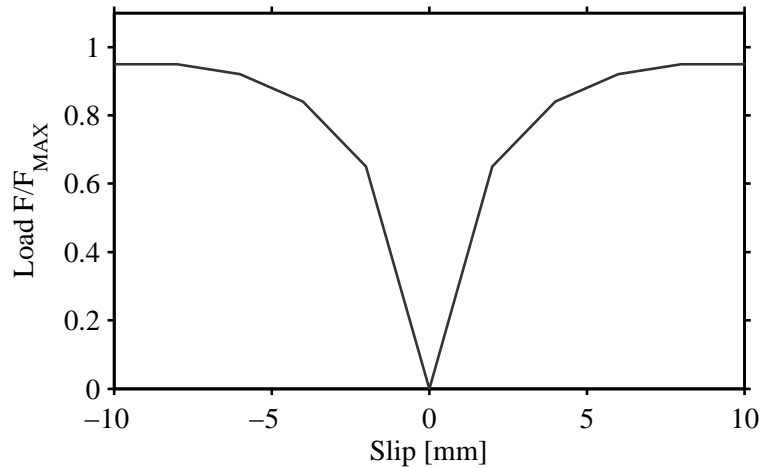


Figure 8.5: Slip-force curve implemented in FE model.

To further prevent lateral torsional buckling in the arch, the extrados lateral support is accompanied by three bracing beams fixed at the intrados, c.f. Section 5.1. The bracing is designed to act in pure tension so that the stiffness is only dependent of the elongation. The spring stiffness  $k$  is then determined in Equation 8.4 for a timber beam 150x70mm (see Appendix D.2):

$$k = \frac{EA}{L} = 18.3 \text{ MN/m} \quad (8.4)$$

Please note that there is normally a slip for members acting in tension, thus such bracing system used in our model normally acts in compression. Due to bracing buckling and interaction throughout an entire system such behaviour is non-linear and it is not within the scope of this thesis to analyse global effects.

## 8.5 Loads

The load cases applied to the arch model are uniformly distributed load and triangular distributed load respectively, see Section 5.3. In order to analyse the differences for each load type the uniformly and triangular distributed loads are applied separately during the analyses. A combined load model is later used in order to compare FE results to Eurocode.

All loads are applied on the extrados with direction parallel to the vertical axis. The loads are modelled as conservative forces, i.e. the force applied does not follow the rotation of the arch member.

### 8.5.1 Uniform Load Distribution

Distributed load is in Abaqus defined with respect to the curved edge of the member,  $ds$  in Figure 8.6. In order to obtain a uniformly distributed load with respect to the horizontal axis the load is modified according to:

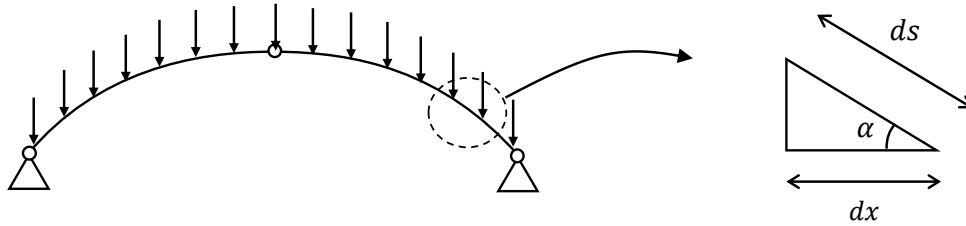


Figure 8.6: Distributed load is by default assigned to the curved length,  $ds$ . A function is determined to obtain a distributed load over horizontal length,  $dx$ .

The default applied load is

$$F = q \cdot ds \quad (8.5)$$

However, in order to obtain a horizontally UDL, a correction factor must be introduced according to

$$F_{hor,UDL} = F \frac{dx}{ds} = q \cdot ds \frac{dx}{ds} = q \cdot \cos(\alpha) dx \quad (8.6)$$

Where  $\alpha$  is derived from the derivative of the parabolic shape function to

$$\alpha = \tan^{-1} \left( \frac{4f}{L^2} (L - 2x) \right) \quad (8.7)$$

thus

$$q(x) = q \cdot \cos \left( \tan^{-1} \left( \frac{4f}{L^2} (L - 2x) \right) \right) \quad (8.8)$$

### 8.5.2 Asymmetric Triangular Load Distribution

The asymmetric triangular load case, Figure 8.7, is representing snow drift. No redistribution of the distributed load, as for the UDL, has been applied to this model.

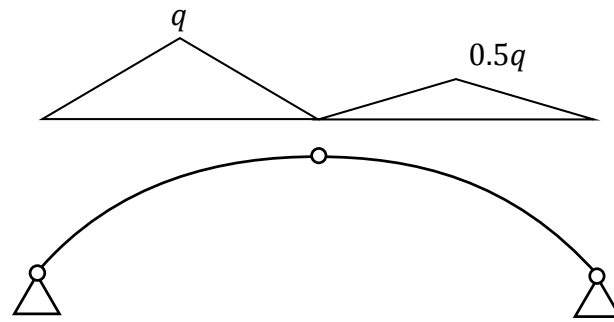


Figure 8.7: Asymmetric triangular distributed load model according to Eurocode [SS-EN 1991-1-3, 5.3.5].

## 8.6 Elements and Mesh

Choosing element type is not a trivial task, neither is the number of elements needed to obtain results of reasonable accuracy. Convergence studies of standard element types in presented element families (c.f. Section 7.4) have been conducted for buckle analysis by Persson [2010]. Using quadratic elements and a simple geometry, he concludes that all families converges to the theoretical buckling value of a column for a reasonable amount of elements with a relative error of  $\pm 0.02\%$ . Lateral torsional buckling of a simply supported beam resulted in a relative error of for all families less than  $\pm 0.4\%$  where solid elements resulted in the minimum relative error.

For a parabolic arch geometry with isotropic material, the linear buckling load has been calculated using quadratic elements of shell and solid elements. The results are found in Table 8.4. In order to compare with the theoretical findings, c.f. Section 4.2.3, an isotropic material model has been chosen. *Err* describes the deviation from the theoretical values while *Diff* describes the deviation from previous result. Please note that beam elements have been excluded from the analysis since relevant geometric features of this thesis is not applicable, e.g. edge loading and bracing.

Table 8.4: Mesh convergence study of in-plane linear buckling analysis of parabolic arch using different element types.  $L = 60\text{m}$ ,  $f = 9\text{m}$ ,  $width = 0.1\text{m}$ ,  $height = 1\text{m}$ , steel. Symmetry was used.

No. elements	Solid [kN/m]	Diff [%]	Err [%]	Shell [kN/m]	Diff [%]	Err [%]
15	2925		2.46	2770		-2.97
20	2917	0.27	2.18	2742	1.02	-3.95
25	2915	0.07	2.11	2732	0.35	-4.29
35	2914	0.02	2.09	2728	0.17	-4.45
70	2913	0.06	2.03	2726	0.07	-4.52
275	2909	0.12	1.90	2725	0.03	-4.54
1 000	2902	0.23	1.67	2725	0.01	-4.55
7 000	2884	0.63	1.03	2725	0.01	-4.56
<i>Theoretical</i>	2885 kN/m					

As expected, the study indicates a convergence for an increasing number of elements and regardless of element family. Additional testing clearly confirms that quadratic elements converges significantly faster than linear. More surprisingly was the differentiation between the converged values for each element type. For a fairly more complex geometry such as a parabolic arch, not only is the theory inconsistent, c.f. Section 8.1, but the different element formulations seem to significantly influence the converged results.

Quadratic shell elements with reduced integration, S8R, and a element size resulting in 275 elements are chosen for this thesis. The result of the convergence study indicates a fast converged error of -4.5% in comparison to the theoretical value. However, consideration has also been taken to the considerably shorter running time than for solid elements which needs an unreasonable amount of elements in order to obtain accurate results.

Reduced integration is used to form the element stiffness, which significantly reduces running time and usually provides more accurate results [Dassault Systèmes Simulia Corp., 2010]. However, when using reduced integration a specific type of element deformation can occur which produces no strains, hence no force to resist. The phenomenon is known as hourglassing which in the model is minimized using standard Abaqus hourglass control.

## 8.7 Verification of Model

In order to verify the accuracy of the model, several simulations have been conducted in order to determine whether different particulars performs in the intended manner.

### 8.7.1 Multi-point Constraints

In order to acquire a model without stress concentrations due to boundary conditions at a single point, multi-point constraints (MPCs) are introduced. These constraints allow the structure to redistribute stresses in a manner more similar to real life supports where the contact is distributed over the cross-section.

Stress distributions of abutment with and without MPCs are illustrated in Figure 8.8.

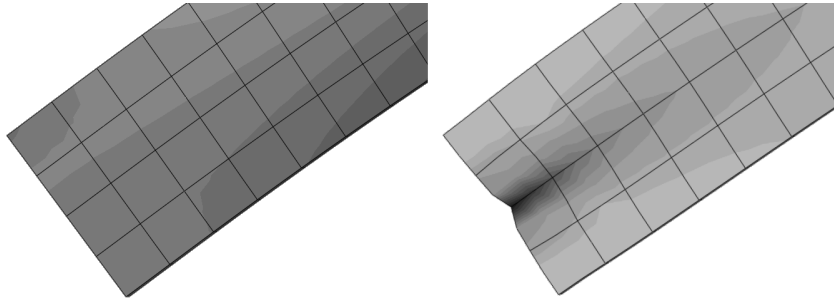


Figure 8.8: Stress distribution with and without MPCs. Significant stress concentrations when no MPCs are used.

### 8.7.2 Failure Stress Criterion

In order to validate the stress failure criterion a simply supported beam model was used. For a given UDL  $q$ , the beam will fail due to stresses exceeding the strength values.

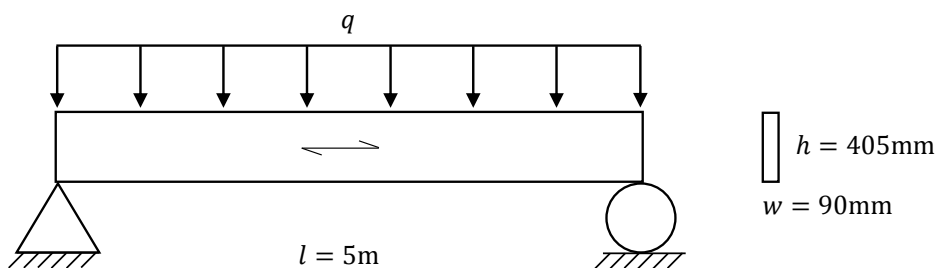


Figure 8.9: Simply supported beam subjected to UDL to visualize fail criterion according to maximum stress theory.



Maximum stress will occur at mid span due to the maximum bending moment. Using the same wood material model as in the arch analysis the tension parallel to grain is decisive, see Equation 8.9.

$$\sigma_{11} = \frac{M}{W} = \frac{ql^2/8}{wh^2/6} < f_t \Rightarrow q_{fail} = f_t \frac{wh^2/6}{l^2/8} = 17.71 \text{ kN/m} \quad (8.9)$$

An identical analysis was conducted in ABAQUS using the maximum stress failure criterion defined in Section 8.3.2. Material failure occurs when the MSTRS value reaches one, which is illustrated in Figure 8.10 where an increasing value is represented by a darker shade. Since the strength is lower in tension maximum MSTRS values are expected at the lower part of the beam. Failure load for both analytical calculations and simulations are found in Table 8.5.



Figure 8.10: Illustration of MSTRS failure criterion on a simply supported beam subjected to UDL. Failure nodes marked in black.

Table 8.5: Comparison between analytical and simulated material failure using MSTRS criterion.

Analytical failure	Simulated failure	Error
17.71 kN/m	17.73 kN/m	0.2%

With small deviations from the analytically calculated failure load the maximum stress failure criterion is found suitable.

### 8.7.3 Springs

The arch is laterally stabilized continuously at the extrados of the arch by a load bearing profiled steel sheet. These connections can be represented by uniformly distributed non-linear springs. In addition to the non-linearity, it is of importance that the springs does not affect the behaviour in any other direction than the intended.

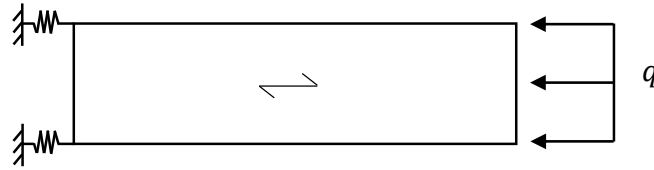


Figure 8.11: Non-linear spring test setup using a symmetric stiff column.

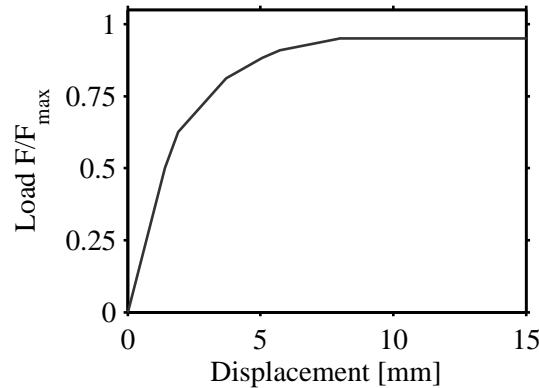


Figure 8.12: Load-displacement of test column using non-linear elastic spring elements.

In order to verify the non-linearity of the spring, a simple column test was used, only supported by spring elements. The test setup is illustrated in Figure 8.11 while the results are found in Figure 8.12.

The non-linear behaviour is hereby confirmed for lateral movements in both directions. Similar tests indicates that the springs do not affect force distribution nor deflections in any other direction than the intended.

## 8.8 Method of Analysis using Abaqus

### 8.8.1 Linear Buckling Analysis

In the linear buckling analysis performed with ABAQUS no non-linearities such as springs are simulated. The intrados and extrados spring support is considered rigid i.e. no deflection out-of-plane is permitted. Moreover are the calculations performed in the so called base state, i.e. no second order effects are considered.

From a linear buckling analysis only the eigenvalue or the critical load is achieved accompanied with the eigenvector representing the mode shape with normalized deflections.

Eigenvalue buckling analysis can use preloading to create a stress state in the structural member. Using linear perturbation without preload corresponds to classic Euler buckling analysis. However, all structures have self-weight which induces internal stresses in the members. These internal stresses and initial deflection can produce eigenvalues deviating from the classic Euler case. Density was however not included in the linear buckling analysis.

### 8.8.2 Non-linear Buckling Analysis

The non-linear buckling analysis in ABAQUS permits the use of third order effects, i.e. equilibrium is calculated in the deformed state and for large deformations. Furthermore, the non-linear analysis is able to capture the behaviour of the spring boundary conditions at the intrados and extrados and calculate the stress levels for each load increment.

If not else specified the initial imperfections are scaled versions of the first out-of-plane and second in-plane buckling modes, see Figure 5.3. Eurocode uses the same method and stipulates a geometric imperfection to be used when conducting non-linear analysis. The magnitude for in-plane imperfections correspond to  $L/400$ , seen in Figure 8.13 .

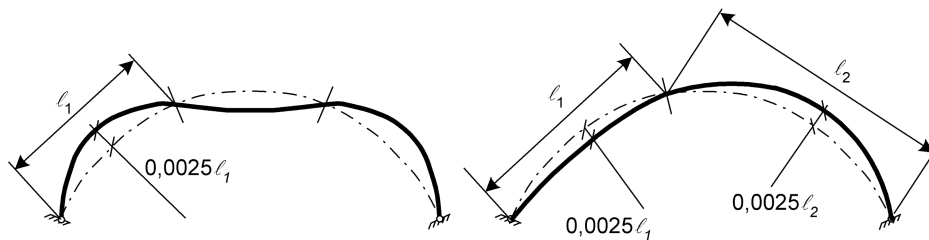


Figure 8.13: Example of specified in-plane imperfections according to Eurocode 5. The eccentricity should be no less than  $e = 0.0025l_i$  corresponding to an imperfection of approximately  $L/400$ . Source: [SS-EN 1995-1-1 figure 5.3]

However, out-of-plane imperfections are restricted to  $L/500$  [SS-EN 1995-1-1, 10.2 (1)] using the definitions found in Figure 8.14.

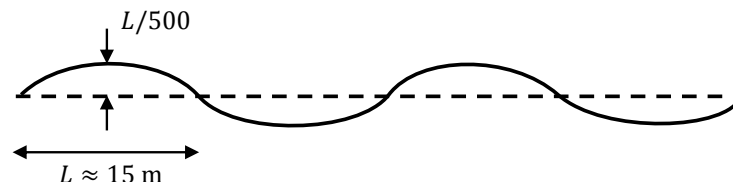


Figure 8.14: Schematic figure of out-of-plane imperfection. Solid line represents the intrados and dashed line represent the extrados which is fastened to the roofing along its whole length. Please compare with Figure 5.3a.

For each non-linear analysis during the parametric study two values are presented: Non-linear buckling and Non-linear material failure. In order to illustrate the difference of these two values an example is presented below.

**Example.** An arch member is subjected to small initial imperfections and a uniformly distributed load with increasing magnitude until the point of buckling, see Figure 8.15.

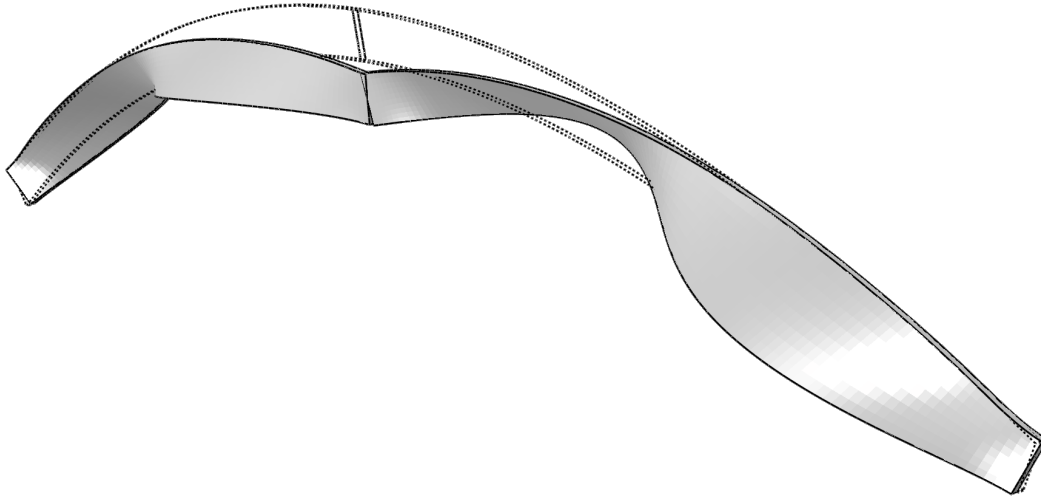
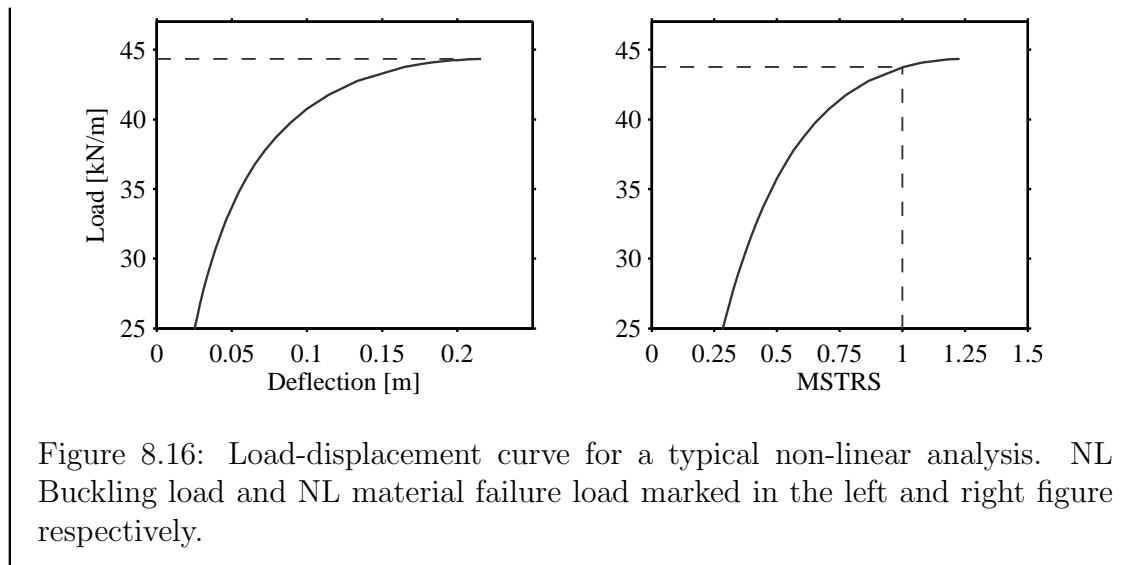


Figure 8.15: Non-linear analysis of arch subjected to uniformly distributed load up to point of lateral buckling.

The critical load corresponding to the non-linear buckling load is shown in the left part of Figure 8.16. This is the limit value for which a load controlled analysis can achieve, c.f. Section 7.3. The material can on the other hand fail due to stress prior to the geometrical buckling. If the failure criteria is greater than or equal to one the member is considered to fail due to stresses, see right part of Figure 8.16. Note that instability failure commonly refers to geometrical failure, i.e. the left plot in the figure.



As previously discussed, stress concentrations not representative to the true behaviour of the structure will arise. If not dealt with, these concentrations will significantly underestimate material failure.

Stress concentrations commonly occur at sharp edges, in nodes at which boundary conditions or where connecting elements are set. In the reference model stress concentrations is present in the four corners of each arch member and where the springs are located. Since MPCs are used at all hinges, no stress concentrations occur at the supports nor in the crown. The MSTRS value of these specific nodes are excluded in the material failure analysis.

Material failure occur at the FEM analysis increment where a MSTRS value first is 1.0 (after concentration exclusion). If the exact value of 1.0 is not present in an increment, linear interpolation is used between the two closest load increments. To minimize the error, small increments is used when necessary.

### 8.8.3 Abaqus Nomenclature

The algorithms used in this thesis are included in Abaqus using the steps in Table 8.6 below. Different calculation increments are used in the different steps to obtain required results.

Table 8.6: Abaqus nomenclature of FEM algorithms.

Type of analysis	Abaqus step
Linear analysis	Linear perturbation, Buckle
General non-linear analysis	Static general



# Chapter 9

## Arch FE Analysis and Discussion

To obtain a deeper understanding of the instability phenomenon of arches the presented model will in this chapter be subjected to several parametric studies of the system sensitivity. The analyses can be divided into two groups: sensitivity analyses of system constants and system variables. The system constants are parameters which normally do not vary during the service life of the structure while system variables do, e.g. cross-section slenderness and moisture content respectively. The parametric studies comprises geometrical features, support conditions and material properties.

The arch geometry and boundary conditions can be found in Section 8.4. The critical load,  $q_{UDL}$  and  $q_{TRI}$ , refers to the load at which failure occur due to the load models defined in Section 5.3. According to Section 5.3.2,  $q_{TRI}$  is defined by the maximum value of the asymmetrical triangular load. To allow easy comparison between the uniform and triangular load model results, a total critical load  $F_{UDL}$  or  $F_{TRI}$  is defined as the sum of all vertical load applied to the structure. Dashed lines in plots refers to material failure.

### 9.1 Lateral Support

Lateral support is often modelled as infinitely stiff points at which no lateral displacements can occur. However, this is not a conservative approach regarding the design of the structure. To obtain more realistic boundary conditions the lateral support is modelled using linear and non-linear spring elements according to Section 8.4.2. In order to determine the structure sensitivity to extrados spring stiffness, a parametric study is conducted by varying the maximum force,  $F_{max}$ , of the spring according to Figure 9.1. Note that springs with greater maximum force also are a stiffer connection.

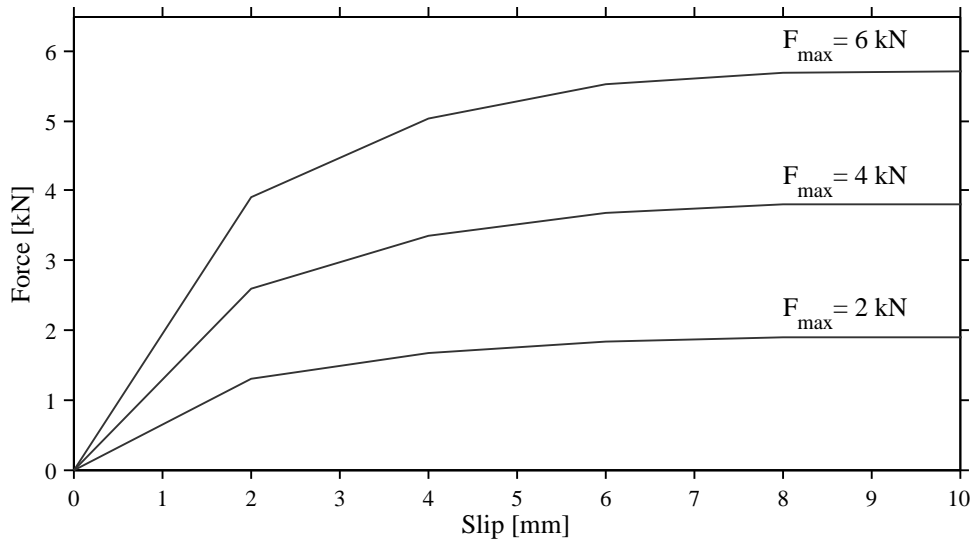


Figure 9.1: Load-slip curve for screws with increasing  $F_{max}$ .

The intrados lateral support was varied using different linear spring constants,  $k$ . The resulting sensitivity analysis is presented in Figure 9.2 and 9.3 below.

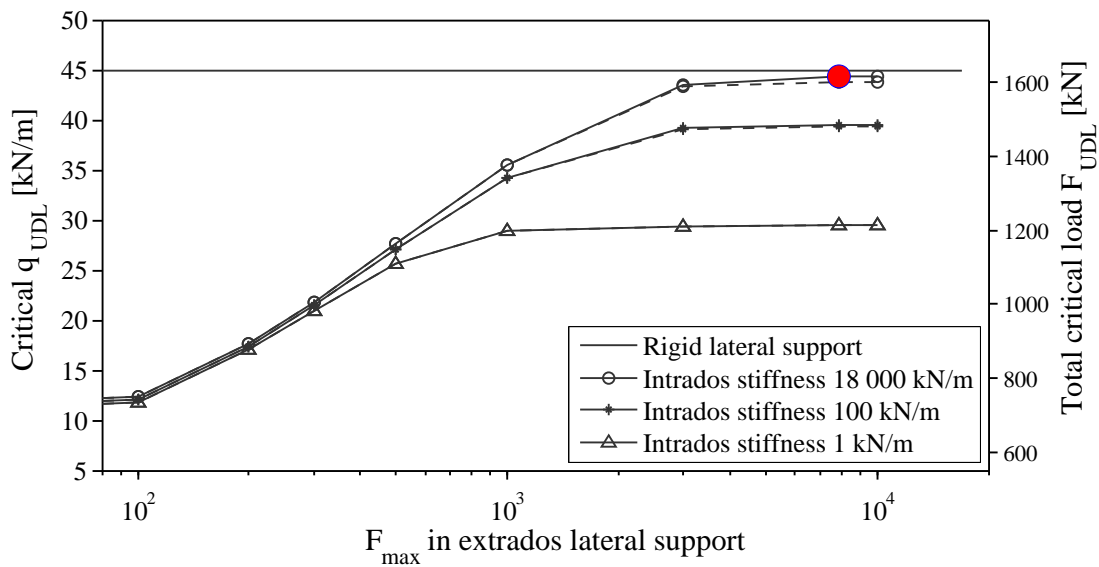


Figure 9.2: Non-linear critical load for increasing maximal force in extrados springs. Solid lines represents geometrical instability while dashed lines represents load at which material failure occurs. Horizontal line is non-linear analysis of rigid lateral support while highlighted dot is the reference spring stiffness calculated.



While subjected to UDL, geometrical instability is the main cause of failure. Increasing extrados rigidity results in higher critical loads. In terms of optimisation with respect to instability a less amount of or smaller screws can be used. However, the screws also transfers lateral load due to wind thus an extra capacity is required.

The calculated intrados lateral support is very stiff. The analysis indicates that the critical load converges for  $k$ -values over 10 000 kN/m (only three different stiffnesses are plotted in Figure 9.2 to obtain a clear plot), hence this type of tension support can be designed significantly more slender, c.f. Section 8.4.2. The linear assumption made for the intrados support also appears reasonable due to the convergence.

A similar analysis has been conducted for triangular load, see Figure 9.3.

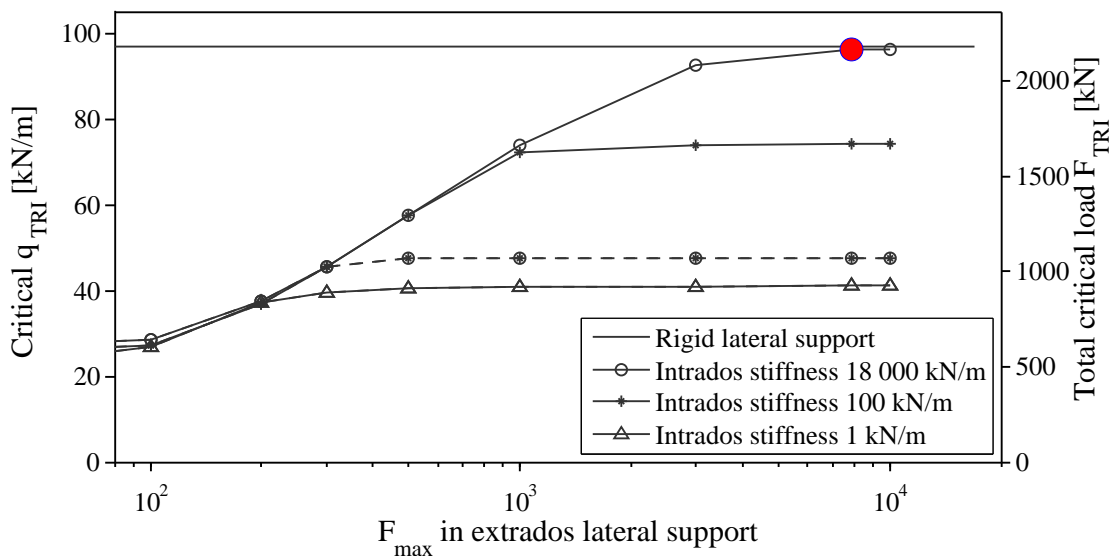


Figure 9.3: Similar to Figure 9.2 but for triangular load.

Please note the difference between geometrical instability and material failure. For intrados support stiffnesses exceeding only 1 kN/m material failure will occur prior to instability due to the bending moment caused by the asymmetrical load model.

As can be seen in both Figure 9.2 and 9.3, the effect of springs for the reference arch with continuous extrados support is not considerable. For a similar analysis with purlin design, c.f. [Persson, 2010].

It is convenient to conclude that a stiff secondary structure is consistently beneficial. It holds true on element level, but when regarding structural systems a stiff secondary structure can cause progressive collapse, c.f. Dietsch and Winter [2010]. Hence a global analysis considering interaction between arch members should be made during the structural design.

## 9.2 Geometry

### 9.2.1 Slenderness

The risk of instability phenomenon is closely related to the slenderness of an element, c.f. Chapter 4. A slender element is more prone to buckling than a bulky element. However, bending moment capacity of an element is increased cubically with height while only linear with the width hence these properties must be balanced against each other to obtain an optimal cross-section.

For a given cross-sectional area, the influence of width and height ratio on the critical buckling load of the arch has been analysed in Figure 9.5 and 9.6. Examples of analysed cross-sections are presented in Figure 9.4. The non-linear analysis was conducted using small imperfections based on the first linear buckling mode for each specific geometry.

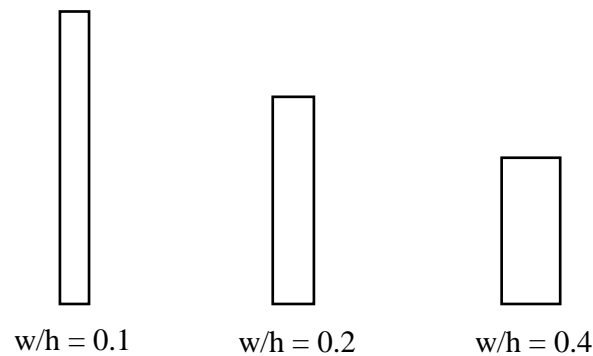


Figure 9.4: Examples of cross-sections with increasing width to height ratios for a given cross-sectional area,  $wh = \text{const.}$

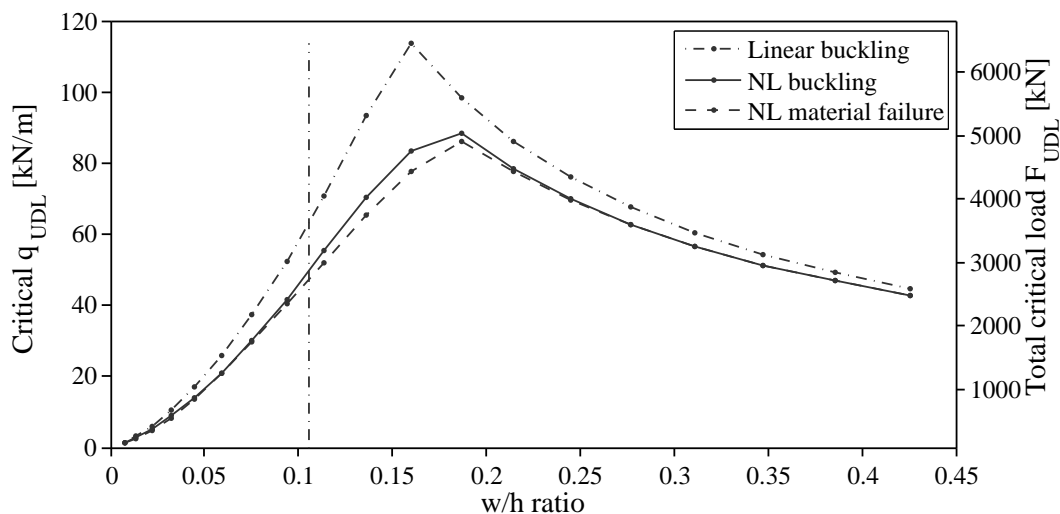


Figure 9.5: Critical UDL plotted for increasing width to height ratio. Reference model ratio represented by vertical dash dot line.

Keep in mind that the parabolic arch shape is the funicular shape to a uniformly distributed load hence no bending moment will occur. The optimum ratio in Figure 9.5 thus cannot be explained by beam analogy of buckling load versus bending moment capacity. Instead, the width to height ratio determines the first buckling mode at which the divergence point between the modes determines the optimum value. On the left hand side of the optimum the first out-of-plane buckling mode occurs while on the right hand side the first in-plane buckling mode occurs, see Figure 5.3a and 5.3b respectively.

As expected, the non-linear analysis is not as clear as the linear in terms of an optimum ratio. Nonetheless, the results indicate an effective cross-section ranging from 0.16-0.18 in width over height ratio while subjected to UDL.

Dissimilar to UDL, the asymmetrical triangular distributed load stipulated by Eurocode will however induce bending moment in the arch. A similar analysis has been conducted and the result can be seen in Figure 9.6.

The geometrical instability follows the same trend for triangular load as for UDL but for a ratio of 0.16-0.19. However, the material failure due to bending stresses occurs significantly prior to instability. The optimum ratio with respect to material failure is 0.08.

Regarding geometrical instability an optimum width-height ratio of 0.16-0.19 seems plausible for both load models. However, the optimum for failure stress criteria deviates considerably due to the triangular load model. Note that the triangular load model never acts unaccompanied by UDL, hence the practical relevance of the material failure optimum is low.

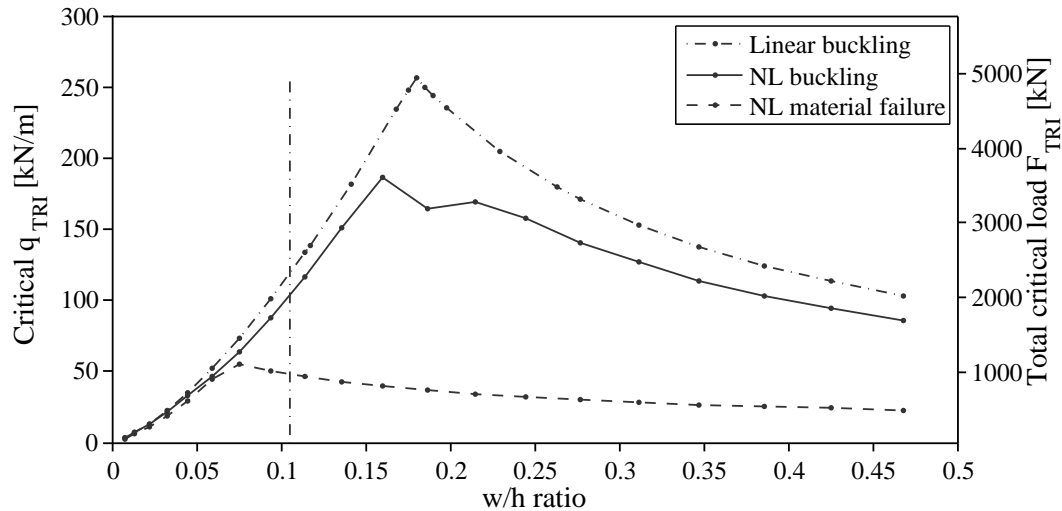


Figure 9.6: Critical triangular load plotted for increasing width to height ratio. Reference model ratio represented by vertical dash dot line.

This result is valid for the type and location of lateral support presented in Section 5.1. It is evident that the reference model width-to-height ratio is too small to obtain the optimum critical load. However, by adding additional lateral support the optimum ratio should decrease. Thus a similar analysis can be conducted for each setup of lateral support in order to find the corresponding optimum ratio.

### 9.2.2 Arch Rise

While often limited in span, an arch designer has usually more influence over the arch rise. Not only does the height influence apex stresses and curvature stresses in lamellas, but the rise also influence the geometrical instability of the arch.

Illustrated in Figure 9.8 is how the buckling load of the parabolic arch varies with the rise-span ratio  $f/L$ . For low ratios a significant horizontal force is needed to resist the UDL, causing high compression stresses in the arch which ultimately will buckle. However, as the ratio increases the effective buckling length increases which effectively lower the buckling capacity. These two buckle variables results in the existence of an optimum  $f/L$  ratio.

A linear parametric study has been conducted for an increasing value of  $f/L$  ratio, see Figure 9.8 and 9.9. Examples of the geometries are presented in Figure 9.7.

Optimum rise-span ratio for the analysed arch subjected to UDL is  $f/L = 0.4$ , which coincides with the findings of Timoshenko and Gere [1961] given a three-hinged arch, c.f. Section 4.2.3. However, when subjected to the triangular load model the optimum ratio is 0.3, see Figure 9.9.

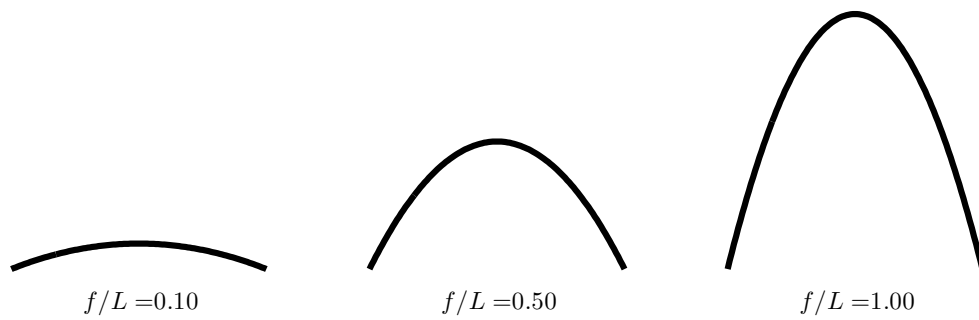


Figure 9.7: Parabolic arch geometry for increasing  $f/L$  ratio.

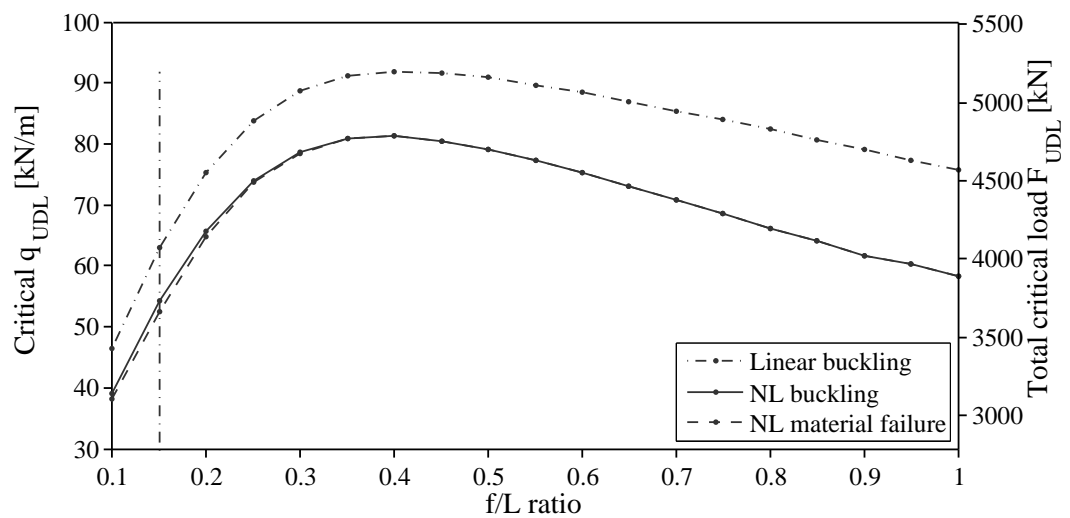


Figure 9.8: Instability analysis for parabolic arch subjected to UDL for increasing rise-span ratio. Reference model ratio marked with vertical line.

Please note that the triangular load model is not modified to the angle of the arch, c.f. Section 8.5.2, which affects this analysis considerably especially for large  $f/L$  ratios. Furthermore, only a linear analysis has been conducted for which it is reasonable to assume that material failure occur prior to geometrical instability, similar to the findings in Figure 9.3 and 9.6. The sudden change at  $f/L$  ratio of 0.9 is due to change of buckling mode from the first out-of-plane to the first in-plane mode.

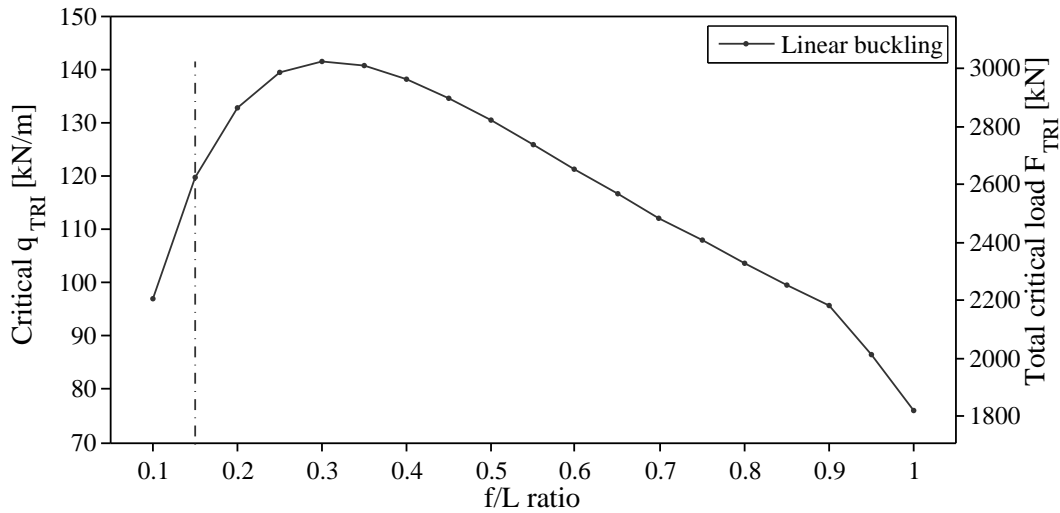


Figure 9.9: Linear buckling analysis for parabolic arch subjected to triangular load model for increasing rise-span ratio. Reference model ratio marked with vertical line.

### 9.3 Instability with respect to Imperfections

In theoretical analyses it is often convenient to use perfect geometries. Geometrical imperfections are random in nature which makes them difficult to quantify and model. However, imperfections can have a significant impact on element and system stability, c.f. Section 4.1 and 8.8.2, but is also crucial for a non-linear FE analysis. It is expected that the nonlinear analysis including geometrical imperfections result in lower critical loads than linear analysis and that the critical load should reduce for larger imperfections.

The most prominent buckling modes for the arch structure was determined using an imperfection sweep over the first 20 buckling modes. The structure was subjected to a small imperfection based on the respective buckling mode and the results are found in Figure 9.10.

The analysis concludes that the first in- and out-of-plane buckling modes are representative in order to determine the non-linear critical load.

In order to determine whether or not a parabolic arch is sensitive to imperfections the following analysis has been conducted for asymmetrical triangular distributed load as well as uniformly distributed load for scaled imperfections of the first in- and out-of-plane modes.

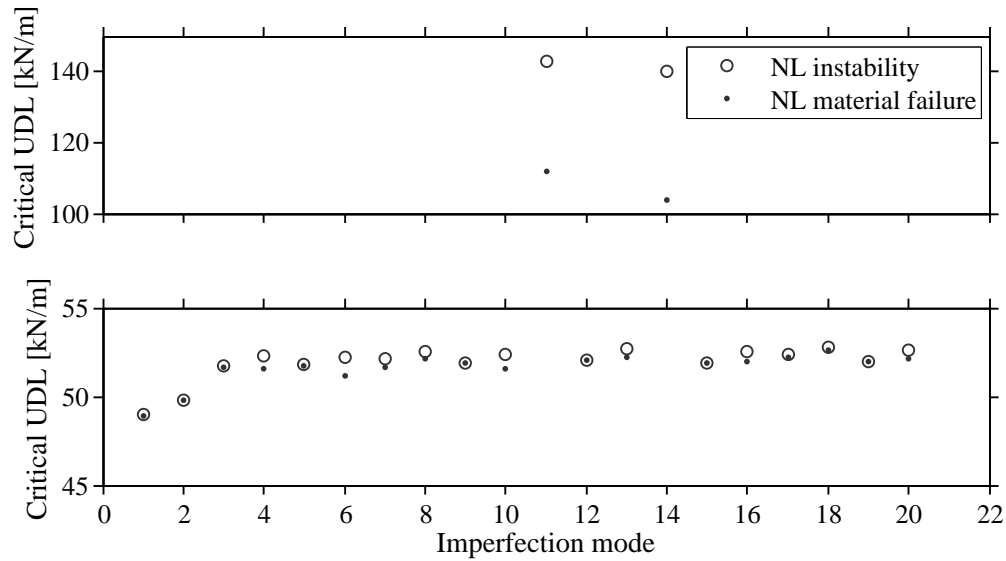


Figure 9.10: Arch member subjected to small imperfections based on various linear buckling modes. Mode 11 and 14 are in-plane buckling modes with considerable higher critical loads.

### 9.3.1 In-plane Imperfections

The sensitivity analysis of the arch member for in-plane imperfections with UDL and asymmetrical triangular load cases, c.f. Section 5.3, are presented below. The initial imperfections according to Eurocode, c.f. Section 8.8.2, corresponds to the first and second out-of-plane mode in our model.

The size of the initial imperfection is given relative to the element inflection points, which is illustrated in Figure 9.11 for the two analysed in-plane modes.

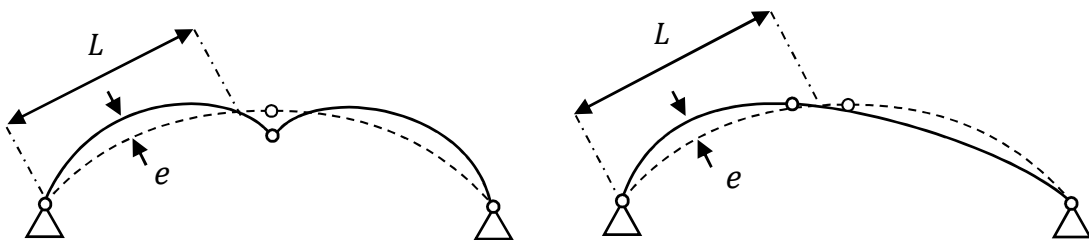


Figure 9.11: Scaled in-plane imperfections based on the 1<sup>st</sup> and 2<sup>nd</sup> in-plane buckling modes.

9.3.1.1 UDL model

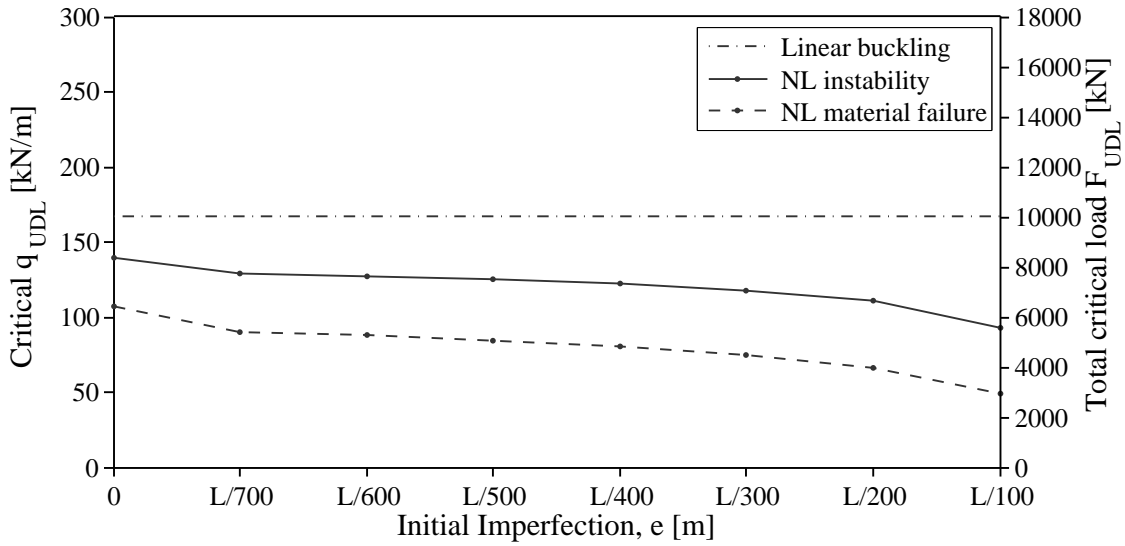


Figure 9.12: Critical UDL for different initial imperfections based on 1<sup>st</sup> in-plane buckling mode.

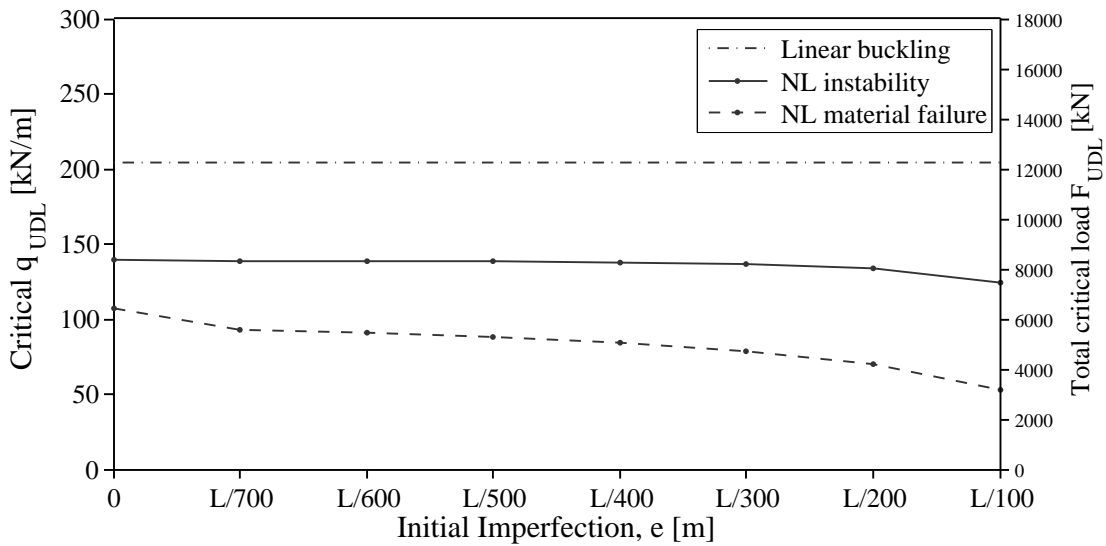


Figure 9.13: Critical UDL for different initial imperfections based on 2<sup>nd</sup> in-plane buckling mode.

As seen in Figure 9.13 the structure is fairly insensitive to imperfections of the second buckling mode.



### 9.3.1.2 Triangular load model

A clear decreasing buckling strength for increasing imperfections is hard to find for the triangular load model, as can be seen in Figure 9.14 and 9.15.

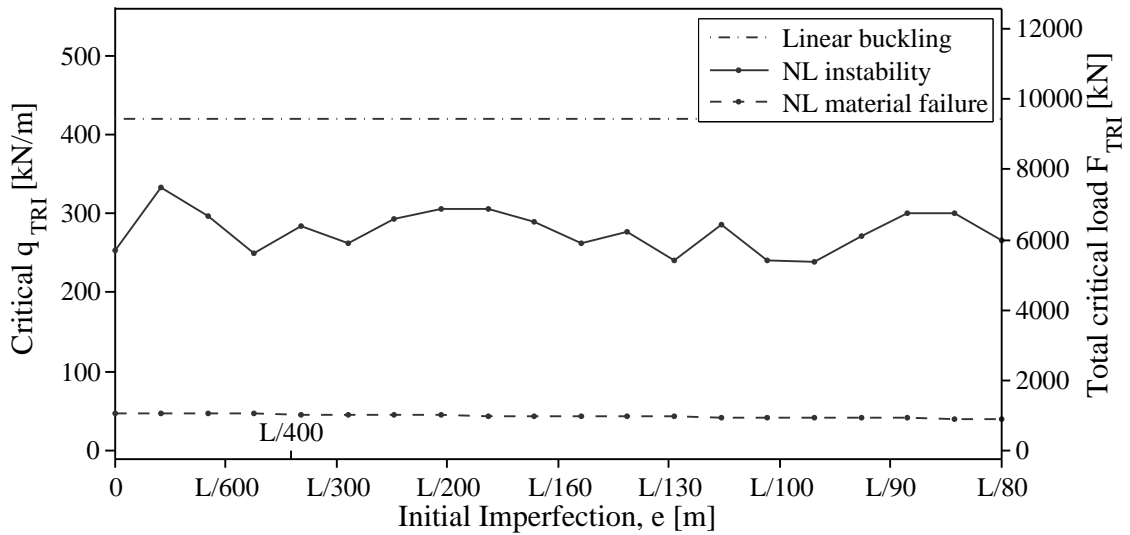


Figure 9.14: Critical triangular load for different initial imperfections based on 1<sup>st</sup> in-plane buckling mode.

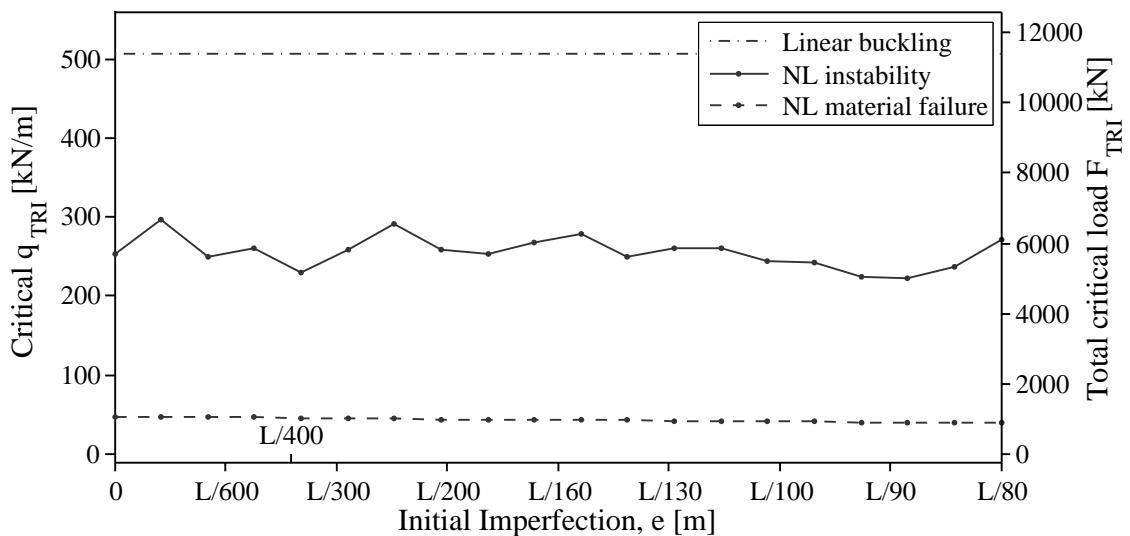


Figure 9.15: Critical triangular load for different initial imperfections based on 2<sup>nd</sup> in-plane buckling mode.

Since the loading is asymmetrical the in-plane deflections will increase in a shape similar to the second buckling mode, see Figure 9.11. Small in-plane disturbances will not affect the critical load and variations of this is considered to be due to numerical deviations during analysis.

Note that the material failure level is fairly constant throughout the range of imperfections. The asymmetrical load induces large bending moments and in combination with normal forces under which the member fails in compression due to large in-plane deformations.

### 9.3.2 Out-of-plane Imperfections

Imperfections based on the first out-of-plane buckling mode, see Figure 9.16, are applied to the structure with a variety of magnitudes. According to Eurocode 5 [SS-EN 1995-1-1 section 10] the initial imperfections should be assumed to have a magnitude of approximately  $L/500$ , c.f. Section 8.8.2.

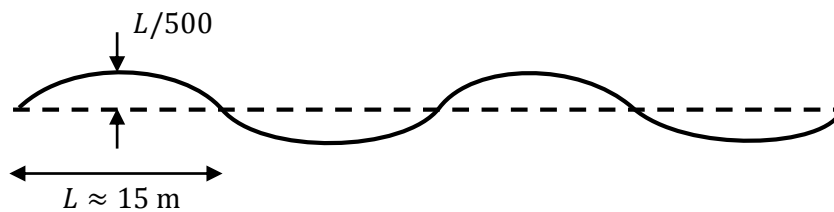


Figure 9.16: Top view of initial out-of-plane imperfections. Solid line represents the intrados edge and the dashed line the extrados edge fastened to the roofing. The magnitude of imperfection is shown for the value Eurocode specifies.

Please recall from Section 5.1 that the analysed reference arch is geometrically stronger in-plane than out-of-plane hence generally lower critical loads is expected in comparison with in-plane imperfections.

#### 9.3.2.1 UDL model

A small difference in load between non-linear instability and material failure reveals that an elastic buckling will occur for OP imperfections subjected to UDL, see Figure 9.17.

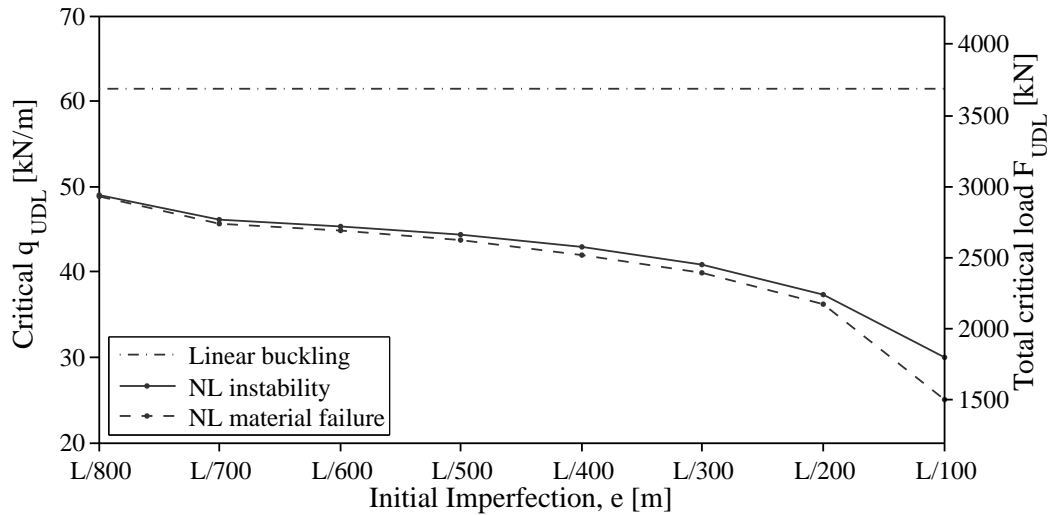


Figure 9.17: Critical UDL for different initial imperfections according to the 1<sup>st</sup> out-of-plane buckling mode.

### 9.3.2.2 Triangular load model

The influence of out-of-plane imperfections on the critical triangular load was also analysed, see Figure 9.18.

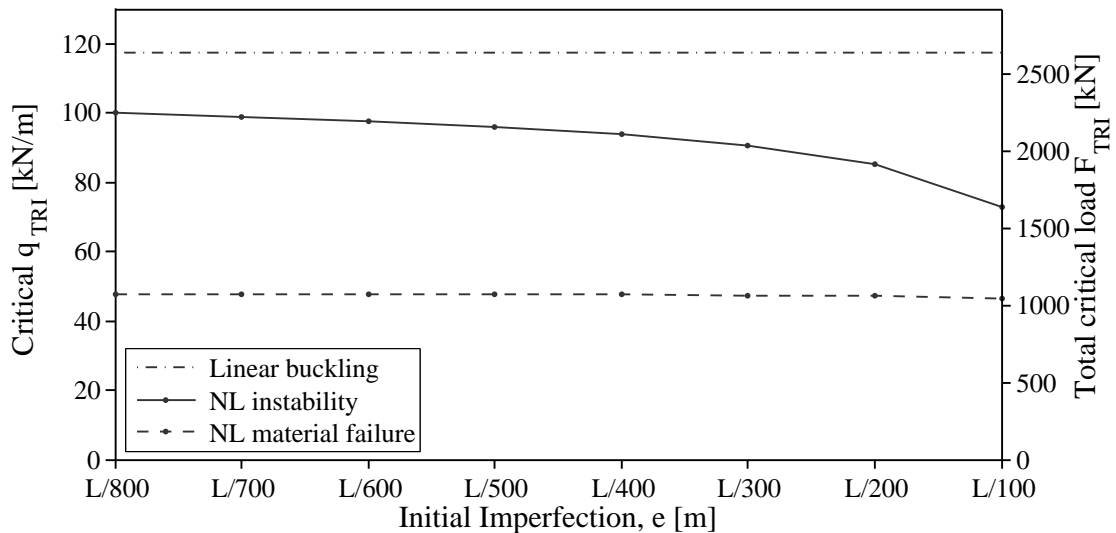


Figure 9.18: Critical triangle load for different initial imperfections according to the 1<sup>st</sup> out-of-plane buckling mode.

### 9.3.3 Linear Combination of Imperfection Modes

A geometry often contains multiple combinations of small imperfections, both in-plane and out-of-plane. The following study is conducted to determine if any combination effects exists.

An imperfection out-of-plane is clearly dominating the behaviour of the structure making it buckle laterally even for small out-of-plane imperfections and moderate in-plane imperfections. In Table 9.1 and Figures 9.19-9.20 a comparison is made for different imperfections and magnitudes.

The imperfections are based on the first buckling mode of in-plane and out-of-plane respectively. Since the out-of-plane imperfection is dominating the behaviour of the member values for zero out-of-plane imperfections are neglected in the plots.

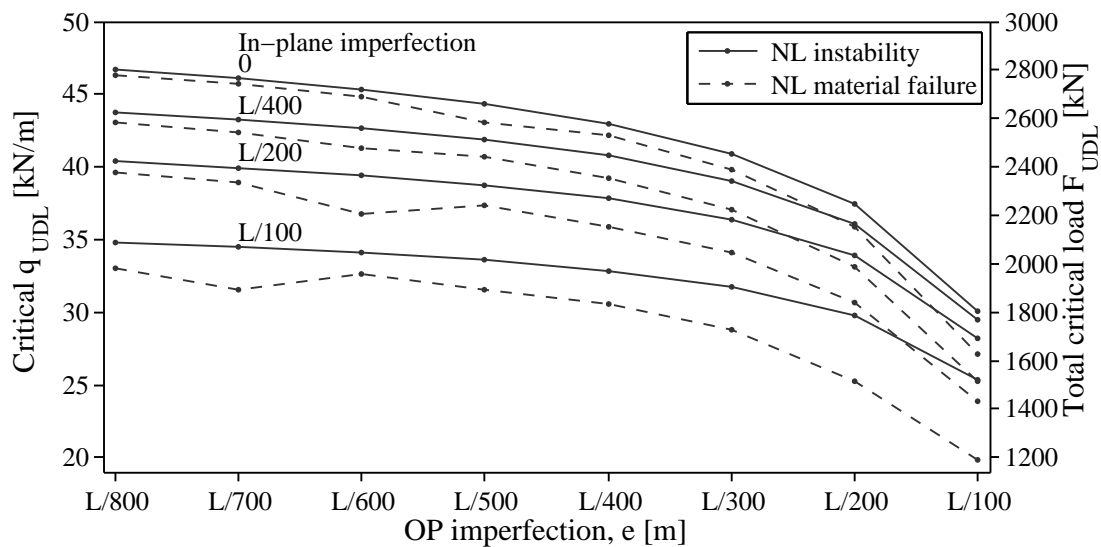


Figure 9.19: Linear combination of imperfections on arch subjected to uniformly distributed load and increasing out-of-plane imperfections. Each line represents an in-plane imperfection based on the first in-plane buckling mode.

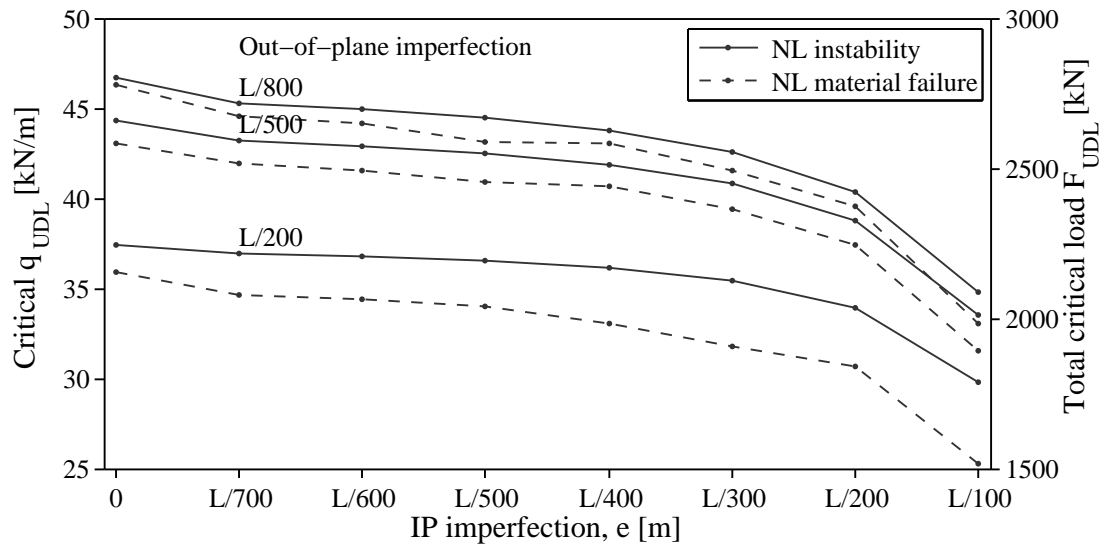


Figure 9.20: Same as above but for increasing in-plane imperfections.

### 9.3.4 Imperfections Conclusions

The general expectation of reduced critical load for larger imperfections is hereby verified for the reference arch. Since imperfections are introduced the non-linear buckling loads are considerably lower than the corresponding linear buckling load.

The analysis concludes that the arch is more sensitive to imperfections when subjected to a uniformly distributed load rather than a triangular distribution. The asymmetrical load case forces the arch into a specific deformation mode causing the influence of imperfection to be small. Furthermore does the triangular load case cause material failure prior to geometrical instability in comparison to the load case with uniform distribution.

The analysis further indicates that the reference arch is more sensitive to out-of-plane imperfections than in-plane, which can be seen in Table 9.1. However, further analysis of different arch geometries is needed to determine whether this is a general phenomenon. For our reference arch, this is possibly due to the fact that the first buckling mode is out-of-plane. In Table 9.1 a comparison can further be seen for the initial imperfections stated by Eurocode.

Table 9.1: Linear combination effect of imperfections in- and out-of-plane for uniformly distributed load and asymmetrical triangular load.

Imperfection	UDL <sup>1)</sup> [kN/m]	%	Triangular load <sup>1)</sup> [kN/m]	%
Reference ( $OP \approx 0, IP = 0$ )	53.2	100	49.5	100
IP ( $L/400$ )	80.9	152	49.6	100
OP ( $L/500$ )	43.7	82	44.6	90
Combination	40.7	77	44.5	90

1) Non-linear analysis at material failure

The increasing difference between the non-linear buckling load and material failure found in several of the presented plots can be explained by visualising the load-deflection curve. An increasing imperfection size will cause the curve to flatten thus making the geometrical instability less prominent, see Figure 9.21.

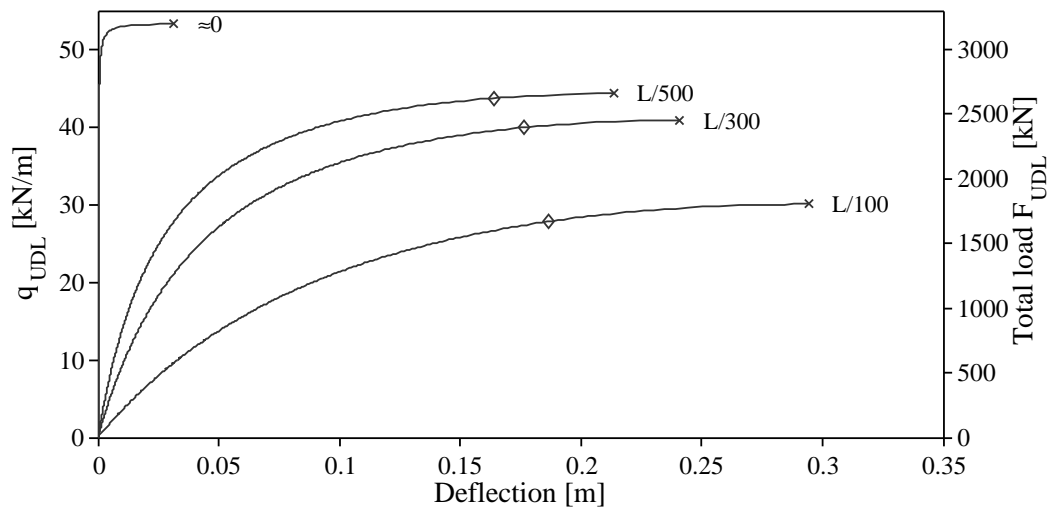


Figure 9.21: Load-deflection curve for out-of-plane movement of parabolic arch. Comparison between increasing initial deformation using out-of-plane buckling mode. Material failure marked with diamonds while geometrical failure is marked with x.

Since the model already has deformations in accordance with the desired mode, no distinctive point exists at which it falls into the mode in comparison to the analysis with negligible imperfections. However, large deformations arise thus the material failure will occur increasingly prior to instability.

## 9.4 Long Term Deformations

### 9.4.1 Reduction of MOE

There are many methods to analyse the creep behaviour of timber including moisture variation to simulate mechano-sorptive creep or load variation with accumulated damage. Similarly to Eurocode, long term deformations are here analysed by a simplified method with a reduction of the modulus of elasticity, c.f. Section 6.2.2, in which no climate or load variations occur. Both instantaneous and slow paced buckling (creep buckling) can occur at which the material responds with original or reduced MOE respectively. In this thesis only instantaneous buckling is analysed since the collapse is sudden, while collapse due to creep buckling is slow paced [Becker and Rautenstrauch, 2001]. In order to determine the parameter sensitivity the critical load is plotted versus the creep coefficient  $\varphi_c$  in Figure 9.22.

The analysis was conducted by non-linearly deforming the structure with initial imperfections using the quasi-permanent load model stipulated in Eurocode 1 [SS-EN 1990-1-1 eqn 6.16b]. The initial imperfections were both in- and out-of-plane with a magnitude of  $L/400$  and  $L/500$  respectively. The MOE used during deformation was changed with respect to  $\varphi_c$  in accordance to Equation 9.1.

$$E_{mean,fin} = \frac{E_{mean}}{1 + \varphi_c} \quad (9.1)$$

The simulated long term deformations obtained were then used as input to a non-linear buckling analysis in order to achieve the critical uniform load. Both elastic and creep deformations were transferred to the buckling analysis while stresses were not, i.e. the material was considered being fully relaxed. Short term MOE was used in the buckling analysis to simulate a fast paced instability phenomenon.

Creep deformation increases the initial imperfections and may alter the stress distribution in the loadbearing members in comparison with the initial configuration. The first order analysis of the arch performed does not consider any changes in stress distribution due to deformations. Instead an analysis of the load bearing capacity is made for increasing creep deformations, see Table 9.2 below.

Table 9.2: Reduction of load bearing capacity due to long term deformations.

Creep coefficient $\varphi_c$	FEM $q_{crit}$ reduction
0.60	0.95
0.80	0.93
2.00	0.79

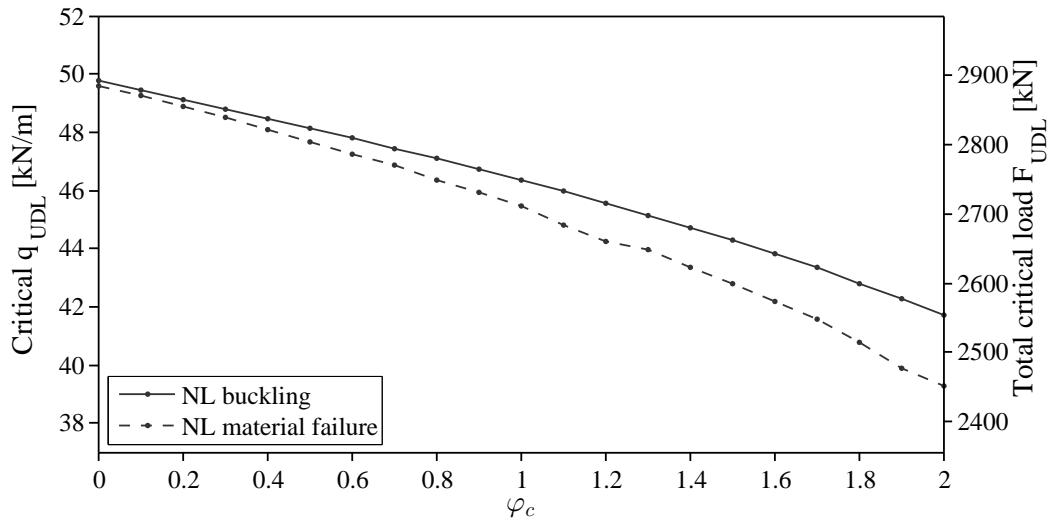


Figure 9.22: Non-linear critical UDL plotted for increasing creep coefficient according to Equation 9.1. Long term deformations simulated using quasi-permanent loading.

The amount of reduction is calculated using a reference value  $q_{crit,0}$  for which material failure occur without any creep deformations ( $\varphi_c = 0$ ) according to:

$$red_i = \frac{q_{crit,i}}{1 + q_{crit,0}} \quad (9.2)$$

For the parabolic arch the reduction of critical load found due to long term deformations are considered moderate, ranging from 5% up to approximately 20% depending on climate condition.

The analysis indicates an almost linear degrade of buckling load. Material failure do occur increasingly prior to geometrical instability which has been previously discussed in Section 9.3.4.

The creep coefficient is however specific for a given material product. In Figure 2.5.2 it can be found that for glulam  $\varphi_c = 0.6$  which reduces the critical load capacity by 5%. Hence it can be concluded that creep does not seriously affect the instantaneous buckling capacity.

### 9.4.2 Reduction of Failure Strength

In addition to the creep behaviour, time also affects the failure strength. As presented in Section 2.4.6, the Madison curve indicates a logarithmic degradation to about 55% after 50 years. An analysis of the effect on the critical load is presented in Figure 9.23.



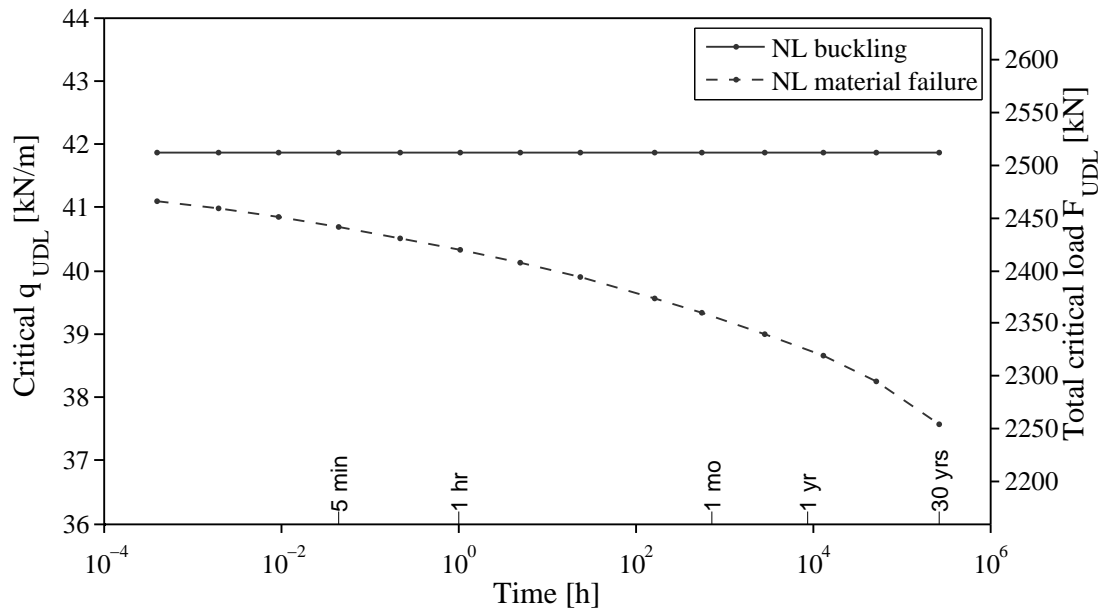


Figure 9.23: Non-linear analysis of critical load reduction over time by reducing the material failure strength according to the Madison curve.

The found reduction of critical load is surprisingly low. The failure strength has indeed been reduced to 56% of the original value for the 30 year simulation, but the critical load is only a decreased by 8%. The very definition of instability does however state that a small increase of load causes a large increase in deflection. Thus a small increase of load does significantly increase stresses in the arch, which in turn causes the MSTRS-critical load curve being flat (c.f. example in Section 8.8.2). The flat curve does imply a small critical load decrease for a significant reduction in failure strength.

## 9.5 Moisture

Stiffness and strength of timber is affected by moisture content for which a simplified analysis has been conducted. The property variations used is described in Section 2.4.3 which are assigned to the entire cross-section, i.e. a steady-state equilibrium is reached between the glulam and its surroundings thus no cross-sectional moisture gradient due to flow exists. Since no volume change nor moisture gradient is present in the analysis, moisture induced stresses are not considered. Hence an over prediction of the material failure load is expected.

In order to assign the variations on the material model certain modifications and assumptions were needed which are noted in Table 9.3, please compare to Table 2.2.

Table 9.3: Material properties of glulam quality GL32h complemented by Norway spruce characteristics. Stiffnesses in MPa.

$E_L$	$E_R, E_T$	$\nu_{LR}, \nu_{LT}$	$\nu_{RT}, \nu_{TR}$	$\nu_{RL}, \nu_{TL}$	$G_{RL}, G_{LT}$	$G_{RT}$
$E_1$	$E_2, E_3$	$\nu_{12}$	$\nu_{13}$	$\nu_{23}$	$G_{12}, G_{13}$	$G_{23}$
-0.9%	-2.7%	2.1% <sup>1)</sup>	2.1%	0.2% <sup>2)</sup>	-1.3%	-2.0%

- 1) Assumed equal to  $\nu_{13}$
- 2) Average of  $\nu_{RL}, \nu_{TL}$

Not only is the stiffness of the material changed, but also the failure strength which is varied according to Section 2.4.3. The results are found in Figure 9.24.

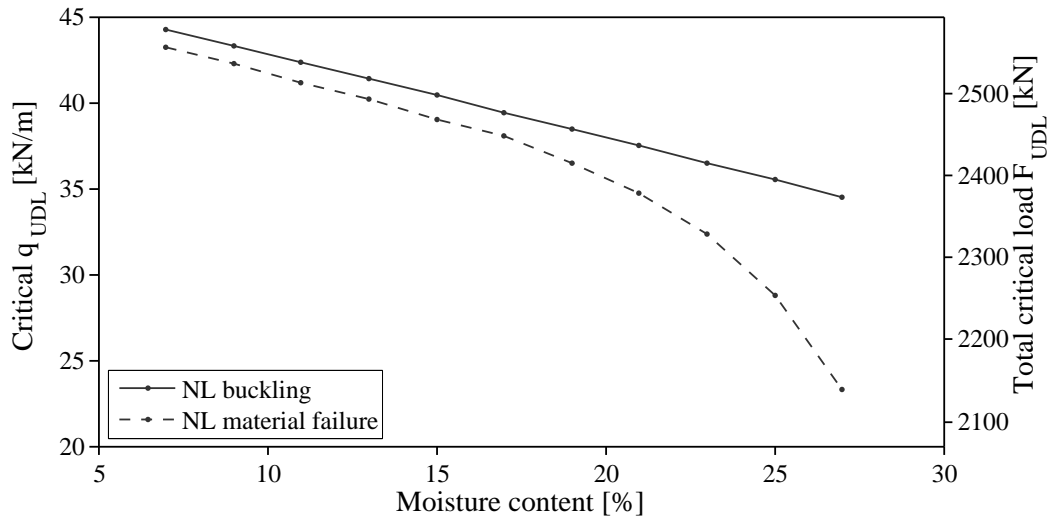


Figure 9.24: Moisture influence on critical load. Clear wood property variations used.

The geometrical instability indicates a linear degradation which is reasonable for a linear degradation of the stiffness properties. However, the material failure is non-linear which is possibly due to the combined result of linear degradation of both stiffness and strength.

The geometrical instability decreases by -1.1% for an increase in moisture content of 1%. The reduction of critical load is between the reduction of  $E_L$  and  $G_{RL}$ . It has previously been found by Persson [2010] that  $E_L$  and  $G_{RL}$  are the most important variables for this type of analysis, and our findings concur.

In comparison to the strength reduction analysis using the Madison curve a considerably larger decrease in load bearing capacity is obtained in the analysis of moisture content. The strength reduction due to loading time reaches approximately 55% while the corresponding reduction due to increased moisture content is approximately 65% (from MC<sub>12</sub> to MC<sub>25</sub> with 5% decrease of  $f_c$  per 1% increase in MC, see Section 2.4.3). Despite the relatively similar reduction of strength the decrease in load bearing capacity is large, approximately 8% and 30% for time and moisture analysis respectively. The reason for this effect is due to the simultaneous reduction of MOE with increasing MC while a constant elasticity were used in the analysis with Madison curve.



# Chapter 10

## Comparison between FE Analysis and Eurocode

The analyses presented in the previous chapter can to some extent be compared with Eurocode. The ambition of this comparison is to find that the design standard is consequently conservative and possibly explain the difference.

### 10.1 Parametric Comparison

In order to obtain an effective design workflow reduction coefficients are in Eurocode used to consider the natural and model characteristics of timber. These coefficients are often the result of several included variables of only which some are studied in this thesis. In such cases the Eurocode reductions are expected to be higher than the findings of the finite element model.

#### 10.1.1 Influence of Initial Imperfections

Instead of calculating buckling loads with formulas for perfect members Eurocode adopts certain buckling curves. These are used in order to take into account the effect of increase in relative slenderness and member imperfections [Porteous and Kermani, 2013].

When conducting FE analysis certain imperfections can be introduced to the model. The imperfections used in the Eurocode buckling curve is  $L/500$  [SS-EN 1995-1-1, 10.2], which is included in the calculation of the buckling reduction factor  $k_c$  using the factor  $\beta_c$ , c.f. Appendix C.7.1.

In Table 10.1 below a comparison shows that an initial imperfection to the arch structure corresponds fairly well to the Eurocode reduction. The FE reduction is based upon a combination of in- and out-of-plane imperfections according to EC.

Table 10.1: Comparison of initial imperfection effect on critical load.

EC reduction <sup>1)</sup>	FEM $q_{crit}$ reduction
$\frac{k_c(\beta_c=0.1)}{k_c(\beta_c=0)} = 0.80$	0.77 <sup>2)</sup>

1) SS-EN 1995-1-1, 6.3.2

2) From Table 9.1 using UDL with combined imperfections.

The size of the initial imperfections stipulated in Eurocode appears reasonable for a parabolic arch. However, the code focuses on in-plane geometrical imperfection modes which is not always the limiting mode. A linear combination of both in and out-of-plane imperfection modes are recommended.

### 10.1.2 Influence of Cross-section Dimensions

In-plane and out-of-plane buckling is verified separately in Eurocode using a reduction factor  $k_c$  which is applied to the normal force capacity, according to Equation 10.1.

$$N_{c,Rd} = f_{cd} A k_c \quad (10.1)$$

The reduction is highly dependent on the slenderness of the cross-section. In order to determine the accuracy of this reduction factor for parabolic arches a comparison has been made with the results presented in Section 9.2.1, in which the critical load for an increasing slenderness was plotted.

In the Eurocode calculations in Section 6.4, the out-of-plane buckling mode was presented as the limiting for the reference arch model. An analogy with a cruciform strut was used in order to estimate the effect of lateral support provided by the load bearing profiled sheets. However, for increasingly bulky cross-sections the in-plane buckling mode will occur and the reduction factor  $k_c$  does modify accordingly, see Figure 10.1.

To compare with the analysis results a comparable reduction factor  $k_{c,FEM}$  was determined according to Equation 10.2.

$$k_{c,FEM} = \frac{N_{q_{crit}}^{1st}}{f_{ck}A} \quad (10.2)$$

The factor  $N_{q_{crit}}^{1st}$  is the maximum normal force obtained by a first order analysis of the critical load of the FE analysis, c.f. Appendix B.1. For the non-linear FE analysis material failure is taken into account and the results are plotted in Figure 10.1.

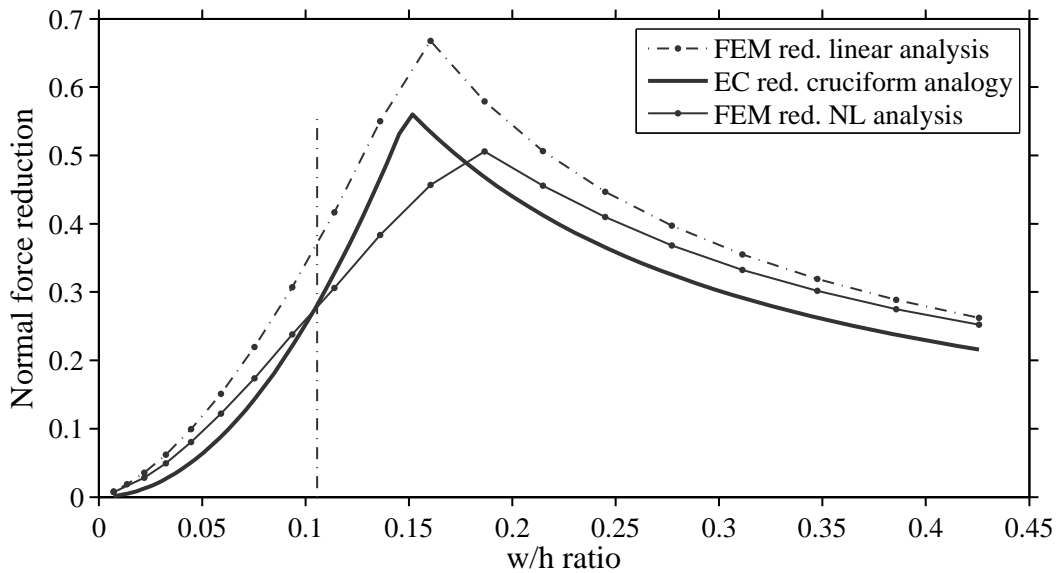


Figure 10.1: First order normal force reduction regarding risk of instability plotted for UDL. Reduction used in the Eurocode calculations,  $k_c$ , is compared to reductions found in linear and non-linear FE analysis.

Similar to Figure 9.5, for low width-height ratios out-of-plane buckling occur while in-plane for large ratios hence the cruciform strut analogy is represented on the left hand side of the plot. A clear resemblance can be seen by the analogy used in the EC calculations to the linear FE analysis. This can most probably be explained by the fact that both members act in pure compression, since UDL load model is applied. The curvature of the reference arch does not seem to affect the lateral torsional buckling behaviour considerably.

However, in comparison to the non-linear analysis, in which bending and shear stresses will arise even for UDL, the analogy is not consistently conservative. By sheer coincidence the reference arch, represented by a vertical line in Figure 9.5, happens to be well corresponded by the analogy.

To obtain an effective slender cross-section additional intrados bracing is needed. The buckling length will then become increasingly straight for which the analogy should become even more accurate.

### 10.1.3 Influence of Time Effects

With the duration of load both deformation and material strength change for timber, c.f. Section 2.4.6. Eurocode uses two coefficients in order to consider these changes over time:  $k_{mod}$  and  $k_{def}$ . The coefficients do not only consider time effects but also climate variations which makes a direct comparison difficult. By evaluating the coefficients with a constant climate class some of the long term effects are sought to be isolated.

The reduction of failure strength over time according to the Madison curve is found in Eurocode using the coefficient  $k_{mod}$ .  $k_{mod}$  also considers moisture content but using service class 1, for which the average moisture content is 12%, i.e. the reference value, moisture variation is here neglected. The load duration factor is traditionally determined empirically by experience on timber structures, but probabilistic methods connected with damage accumulation models are used to estimate the factor  $k_{mod}$ . However, no damage accumulation is treated in this thesis.

In comparison to the Madison curve, the  $k_{mod}$  reduction may initially appear not sufficient. The Madison curve indicates a reduction to 0.55 after 30 years, which by itself is a greater reduction than the  $k_{mod} = 0.60$  used for permanent loading which is usually designed for 50 years of service life. However, it should be kept in mind that the Madison curve is not only based on small specimens of clear wood but the curve is also extrapolated over time. The comparison is presented in Table 10.2 below.

Table 10.2: Duration of load effect comparison with Eurocode.

Load duration	DOL <sup>1)</sup>	EC red. <sup>2)</sup>	Madison red.	FEM $q_{crit}$ red.
Short	< 1 week	0.82	0.76 (1 w)	0.97
Medium	1 week - 6 months	0.73	0.69 (4 mo)	0.96
Long	6 months - 10 years	0.64	0.61 (6 yrs)	0.94
Permanent	> 10 years	0.55	0.56 (30 yrs)	0.92

1) SS-EN 1995-1-1, 2.3.1.2

2) For service class 1 [SS-EN 1995-1-1, 3.1.3]  $k_{mod,i} / k_{mod,Instanteous}$



The reduction is calculated from the results presented in Section 9.4.1. The reduction is calculated using a reference value  $q_{crit,5}$  for which material failure occurs after 5 minutes duration of load.

$$Red_{DOL,i} = \frac{q_{crit,i}}{q_{crit,5}} \quad (10.3)$$

The reference value is chosen in accordance with standardised testing methods in which the specimen is subjected to load during 5 minutes. It is the same reference the Madison curve uses for calibration.

Even though the Eurocode reduction  $k_{mod}$  initially may appear not sufficient, the influence on the critical load is negligible.

#### 10.1.4 Influence of Moisture Content

In order to determine design strength values Eurocode uses a system of service classes for three well defined climate conditions with a corresponding average moisture content of the timber. Similarly to the time effect on failure strength, the moisture effect is within Eurocode included in the reduction factor  $k_{mod}$ . Keep in mind that  $k_{mod}$  also considers climate variations over time. In order to obtain comparable results the duration of load is kept constant in Table 10.3.

Table 10.3: Moisture effect comparison with Eurocode.

Service class	Moisture content	EC reduction <sup>1)</sup>	FEM $q_{crit}$ reduction
1	12%	0.90	1.00
2	20%	0.90	0.96
3	>20%	0.70	0.71 (25% MC)

1) For short load duration [SS-EN 1995-1-1, 3.1.3]

The reduction is calculated using the same method as presented in the DOL analysis above. The results used are presented in Section 9.5 and the reduction is calculated using a reference value  $q_{crit,12}$  for which material failure occur at 12% moisture content.

$$Red_{MC,i} = \frac{q_{crit,i}}{q_{crit,12}} \quad (10.4)$$

It can be seen that Eurocode is consequently on the safe side in comparison to the moisture analysis of the arch. For service class 3, i.e. structures directly exposed to the elements, combination effects should be considered.

Please note that swelling and shrinkage of the timber is not considered. This type of deformation can be vital for the capacity of timber connections reducing the load bearing capacity of the entire structure.

## 10.2 Critical FE Load versus Design Load

With the parametric study conducted, a full load sequence of self-weight and snow load is to be applied to the arch structure in order to compare with the hand calculations according to Eurocode, see Chapter 6.

Since the structure is designed for a lifetime of 50 years, long term effects are modelled by a reduction of the MOE in accordance with Eurocode 5 [SS-EN 1995-1-1, 2.3.2.2]:

$$E_{mean,fin} = \frac{E}{1 + \psi_2 k_{def}} = \frac{E}{1 + 0.2 \cdot 0.8} \quad (10.5)$$

All material strengths are reduced to consider time and moisture effects as well as statistical variation of specimen quality according to [SS-EN 1995-1-1 eqn 2.14]

$$f_d = k_{mod} \frac{f_k}{\gamma_M} = 0.8 \frac{f_k}{1.25} \quad (10.6)$$

The analysis is conducted in two steps representing permanent and variable load respectively, see Figure 10.2. Imperfections according to Eurocode are applied in the first step which is then followed by a non-linear buckling analysis. We recall the load model used in the Eurocode calculations while considering the partial coefficients:

$$X_d = \gamma_d \{1.2X_G + 1.5X_Q\} \quad (10.7)$$

in which the permanent load is represented by  $X_G$  while  $X_Q$  is the variable load. In order to obtain comparable results the partial coefficients must be considered thus the permanent loads were increased by a factor of 1.2. Furthermore, the result of the non-linear buckling analysis must be divided by a factor 1.5 to finally be compared to the variable load which the parabolic arch originally was designed for. The result of the symmetrical and asymmetrical snow load model is presented in Figure 10.3 and Figure 10.4.

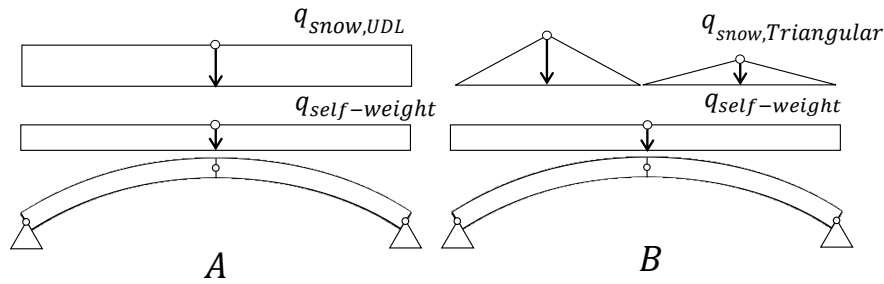


Figure 10.2: Symmetrical and asymmetrical load models used for comparison analysis.

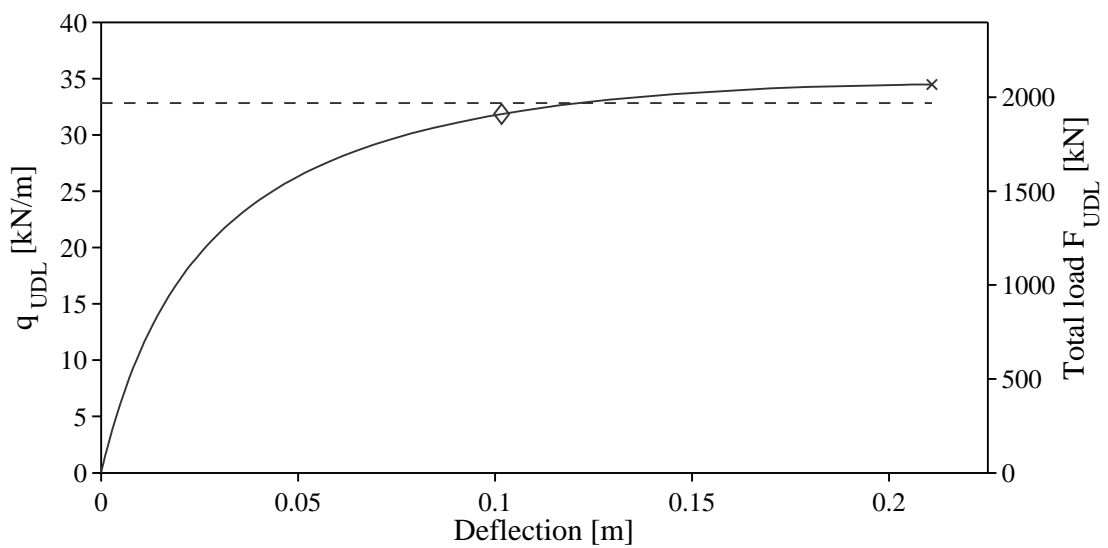


Figure 10.3: Load-displacement for non-linear simulation with UDL. Material failure marked with diamond and hand calculations according to Eurocode is marked with dashed line.

The load-deflection curves continue above the critical load according to Eurocode using first order analysis and beam analogy. The analysis is aborted as the maximum is reached, at which geometrical instability occurs. However, the material has failed prior to the Eurocode buckling load, i.e. Eurocode did not result in a conservative load bearing capacity.

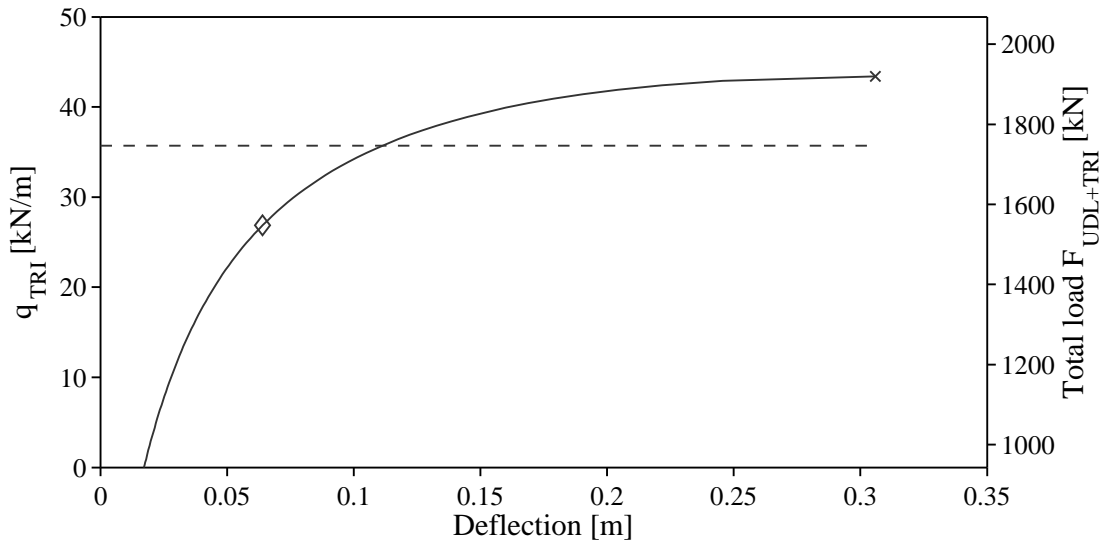


Figure 10.4: Load-displacement for non-linear simulation with triangular load. Material failure marked with diamond and hand calculations according to Eurocode is marked with dashed line.

The reason is probably a combination of the cruciform strut analogy used to determine the first order critical normal force, c.f. Section 6.4 and higher order effects. Even though the normal force reduction using the cruciform analogy was rather accurate according to Section 10.1.2, the internal forces of the arch section comprise of more than only a normal force. Shear force and bending moment of the section will be higher in the non-linear analysis than in a first order analysis the Eurocode calculations are based upon. Please note that the analogy is not supported by the Eurocode but the results of the authors' aim to keep the design according to Eurocode totally separated from FE calculations. This study however clearly indicates that FEM analysis should be used alongside Eurocode for instability analysis of advanced geometries such as curved beams.

# Chapter 11

## Conclusion

The funicular shape to a uniformly distributed load is a compelling structural design concept for large span structures. Environmental awareness and the possibility of curvature makes glulam a good material of choice. However, asymmetrical load models which causes bending moment must be considered in arch design, thus a more slender parabolic arch is commonly preferred.

Slenderness do however imply the risk of instability phenomenon at a critical load. Lateral support of the arch is crucial to obtain an effective slender structure, for which not only extrados but also intrados lateral support is needed.

Structural design according to Eurocode using first order analysis of straight beam analogy is not recommended on curved elements, but a finite element model is required. The arch structure is however sensitive to non-linear effects regarding second and third order of theory. Consequently, a linear buckling analysis using a FE software overestimate the buckling load and thus a non-linear analysis is more suitable.

The parametric studies conducted using non-linear analysis shows good resemblance with Eurocode. An effective design workflow would however be to conduct a non-linear buckling analysis to implement in Eurocode calculations. It is possible to use linear buckling analysis in early design phases in order to evaluate the lateral support setup. The aim of this should be to find an effective combination of cross-section dimensions and lateral support setup, for which the first buckling mode is in-plane.



# Chapter 12

## Suggestions for Further Research

Due to the natural characteristics of timber, fairly advanced models are needed to capture its true behaviour. It is not only a question of a linear or non-linear material model, but also the stochastic nature of local defects and influence of moisture can, among other things, also be considered. Several assumptions have been made in this thesis but the effect of all have not been thoroughly analysed. For example the influence an orthotropic material model with polar coordinates using random pith locations could be analysed using Monte Carlo simulations.

Regarding the influence of moisture only a simplified analysis method has been used with a constant moisture content over the entire cross-sectional area. The influence of moisture gradients over the cross-section may induce local swelling and thus internal stresses, which possibly can affect the load bearing capacity.

Some effort has in this report been put into identifying an optimal arch geometry, i.e. cross-section, arch span and rise. However, by applying some findings of this thesis on a variety of arch geometries one could be able to identify a somewhat general optimum and evaluate its practical use. It would also be interesting if the same geometrical rules applies to circular arches.

A comparison between different lateral bracing setups could be conducted, e.g. roof sheathing, purlins and extent of intrados support. Experimental testing of common lateral supports to obtain a more realistic interaction between arch member and support can be conducted. The lateral support combines structural elements which makes a global analysis of the entire structure interesting, especially considering instability failure and progressive collapse.





# Bibliography

- American Forest and Paper Association. *Designing for lateral-torsional stability in wood members*. American Wood Council, 2003.
- Erik Andersson. Details of fasteners used for profiled roofs. Personal communication, 2014.
- L.D Armstrong and G.N Christensen. Influence of moisture changes on deformation of wood under stress. *Nature*, pages 869–870, 1961.
- P. Becker and K. Rautenstrauch. Time-dependent material behavior applied to timber columns under combined loading. part ii: Creep buckling. *Holz als Roh- und Werkstoff*, pages 491–495, 2001.
- Kristian Berbom Dahl. *Mechanical properties of clear wood from Norway spruce*. PhD thesis, NTNU Trondheim, 2009.
- Jozsef Bodig and Benjamin A. Jayne. *Mechanics of wood and wood composites*. Van Nostrand Reinhold Publishing, 1982.
- Boverket. *Erfarenheter från takras i Sverige vintern 2009/2010*. Boverket, 2010.
- Olle Carling. *Limträ Handbok*. Print & Media Center i Sundsvall AB, 2nd edition edition, 2008.
- Roberto Crocetti. Bridge history - a short introduction. Lecture, 2013.
- Roberto Crocetti and Annika Mårtensson. *Design of structural timber elements in ULS. Ch.3 in Design of timber structures by Swedish Wood*. Swedish Forest Industries Federation, 2011.
- Isaac M. Daniel and Ori Ishai. *Engineering Mechanics of Composite Materials*. Oxford University Press, Inc., 2nd edition edition, 2005.
- Dassault Systèmes Simulia Corp. *Abaqus 6.10 Analysis User's Manual Volume IV: Elements*. Dassault Systemes Simulia Corp., 2010.
- Philipp Dietsch and Stefan Winter. Robustness of secondary structures in wide-span timber structures. In *World Conference on Timber Engineering (WCTE)*, 2010.

- J.M. Dinwoodie. *Timber - Its nature and behaviour*. E&FN Spon, 2nd edition edition, 2000.
- P. J. Gustafsson. *Fracture Perpendicular to Grain - Strutural Applications. Ch.7 in Timber Engineering ed. by Thelandersson,S., Larsen, H.* Chichester West Sussex, 2003.
- Per-Johan Gustafsson. *Balkteori - Course material*. Studentlitteratur, 2012.
- Preben Hoffmeyer. *Strength Under Long-Term Loading. Ch.8 in Timber Engineering ed. by Thelandersson,S., Larsen, H.* Chichester West Sussex, 2003.
- W.M. Hudson. The effect of initial bending on the strength of curved laminated timber beams. *Wood*, pages 234–236, 1960.
- Marie Johansson. *Structural properties of sawn timber and engineered wood products. Ch.2 in Design of timber structures by Swedish Wood.* Swedish Forest Industries Federation, 2011.
- Steen Krenk. *Non-linear modeling and analysis of solids and structures*. Cambridge University Press, 2009.
- H. J. Larsen and H. Riberholt. *Traekonstruktioner - Beregning*. Statens Byggeforskningsinstitut, 4th edition edition, 1999.
- Hans J. Larsen. *Introduction: Fasteners, Joints and Composite Structures. Ch.16 in Timber Engineering ed. by Thelandersson,S., Larsen, H.* Chichester West Sussex, 2003.
- S. Lekhnitskii. *Anisotropic Plates*. Gordon & Breach, 1968.
- Lindab. Lindab lhp 130 and 115. Product catalog, 2014.
- Annika Mårtensson. *Short- and Long-term Deformations of Timber Structures. Ch.13 in Timber Engineering ed. by Thelandersson,S., Larsen, H.* Chichester West Sussex, 2003.
- N. Saabye Ottosen and H. Petersson. *Introduction to the Finite Element Method*. Pearson Prentice Hall, 1992.
- N. Saabye Ottosen and Matti Ristinmaa. *The Mechanics of Constitutive Modeling*. Elsevier, 2005.
- David Persson. Sidostabilitet för limträbågar. Master's thesis, Lund University, 2010.
- Jack Porteous and Adby Kermani. *Structural Timber Design to Eurocode 5*. Wiley, 2nd edition edition, 2013.

- A. Ranta-Maunus and M. Korttesmaa. Creep of timber during eighth years in natural environments. In *WCTE2000 Conference*, 2000.
- J. N. Reddy. *Mechanics of Laminated Composites Plates: Theory and Analysis*. CRC Press, 1997.
- Kenneth Runesson, Alf Samuelsson, and Nils-Erik Wiberg. *Byggnadsmekanik Knäckning*. Studentlitteratur, 1992.
- Erik Serrano. *Mechanical Performance and modelling of glulam. Ch.5 in Timber Engineering ed. by Thelandersson, S., Larsen, H.* Chichester West Sussex, 2003.
- Stephen P Timoshenko and James M Gere. *Theory of elastic stability*. McGraw-Hill Book Company, 2nd edition edition, 1961.
- Unite. Fästteknik med fördelar; unite produktkatalog. Product catalog, 2014.
- Vasilij Zacharovic Vlasov. *Thin-walled Elastic Beams*. Isreal Program for Scientific Translations, 1961.
- L.W. Wood. *Relation of Strength of Wood to Duration of Stress, Report nr. 1916*. U.S. Forest Products Laboratory, 1951.
- Yeong-Bin Yang and Shyh-Rong Kuo. *Theory & Analysis of Nonlinear Framed Structures*. Prentice Hall, 1994.
- Yeong-Bin Yang, Shyh-Rong Kuo, and Jong-Dar Yau. Use of straight-beam approach to study buckling of curved beams. *Journal of Structural Engineering*, pages 1963–1978, 1991.
- Warren C. Young and Richard G. Budynas. *Roark's Formulas for Stress and Strain*. McGraw-Hill, 7th edition edition, 2002.



# Appendix A

## Loads

### A.1 Permanent Load

#### A.1.1 Self-weight of Arch Member

The total mass of the arch member is considered to be distributed uniformly along the horizontal axis.

$$q_{arch} = \frac{\rho g A s}{L} = 1.53 \text{ kN/m} \quad (\text{A.1})$$

where

$\rho$  density of the timber. 430 kg/m<sup>3</sup> (SS-EN 1194)

$g$  gravitational constant. 9.81 m/s<sup>2</sup>

$A$  cross-sectional area.  $A = h \cdot w = 1.8 \cdot 0.19 = 0.342 \text{ m}^2$

$L$  horizontal length or span of the arch. 60 m

$s$  arch length along the system line. According to Carling [2008]  
the arch length can be calculated according to Equation A.2.

$$s = 2f \sqrt{1 + \left(\frac{L}{4f}\right)^2} + 2f \left(\frac{L}{4f}\right)^2 \ln \left[ \frac{4f}{L} \left( 1 + \sqrt{1 + \left(\frac{L}{4f}\right)^2} \right) \right] = 63.4 \text{ m} \quad (\text{A.2})$$

With  $L = 60 \text{ m}$ ,  $f = 9 \text{ m}$

### A.1.2 Roofing and Installations

An estimation of self-weight for steel profiled sheet with insulation and light weight roofing material can span between 0.30-0.65 kN/m<sup>2</sup>. The weight of installations such as ventilation and electricity is estimated to approximately 1 kN/m<sup>2</sup>.

With an arch member spacing of 7 m the distributed load is:

$$q_{roof} = (0.65 + 1) \cdot 7 = 11.6 \text{ kN/m} \quad (\text{A.3})$$

### A.1.3 Combined Load

The combined load of self-weight of arch member and roofing:

$$q_{G,k} = q_{roof} + q_{arch} = 13.1 \text{ kN/m hor} \quad (\text{A.4})$$

## A.2 Snow Load

The snow load is calculated according to Eurocode SS-EN1991-1-3: Actions on structures - Snow loads.

$$s = \mu_i C_e C_t s_k \quad (\text{A.5})$$

where

- $C_e$  exposure factor according to SS-EN1991-1-3 table 5.1 (normal topography): 1.0.
- $C_t$  thermal coefficient, here assumed 1.
- characteristic value of ground snow load. For a building placed in Växjö
- $s_k$  the characteristic ground snow load is 2 kN/m<sup>2</sup> [SS-EN1991-1-3 table NB:1 (Växjö)].

### A.2.1 Roof Shape Coefficient

The roof shape coefficient for a circular roof is calculated according to SS-EN 1991-1-3 figure 5.6. Without influence of snowdrift the loading is uniformly distributed with a shape coefficient of:  $\mu_1 = 0.8$ . With the influence of snowdrift:  $\mu_3 = 1.7$  [SS-EN1991-1-3 figure 5.5,  $h=9\text{m}$ ,  $b=60\text{m}$ ].

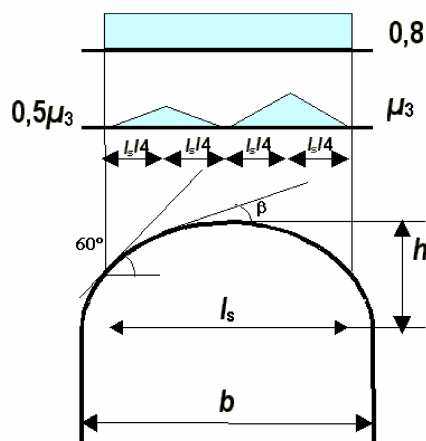


Figure A.1: Roof shape coefficient for an arch-shaped roof. Source: SS-EN1991-1-3 fig 5.6.

### A.2.2 Snow Load on Roof

Uniform distribution:  $s_1 = 0.8 \cdot 1.0 \cdot 1.0 \cdot 2 = 1.6 \text{ kN/m}^2$   
 Triangular distribution:  $s_1 = 1.7 \cdot 1.0 \cdot 1.0 \cdot 2 = 3.4 \text{ kN/m}^2$

## A.3 Wind Load

The wind loads are calculated according to Eurocode SS-EN1991-1-4:2005 General actions - Wind actions and the Swedish national annex EKS 9.

### A.3.1 External Load

The external wind load is dependent on the surrounding terrain, geographical location and shape of the building.

$$w_{e,i} = q_p(z_e) \cdot c_{pe,10} \tag{A.6}$$

where

$q_p(z_e)$  is the peak velocity pressure at the reference height  $z$  with respect to exposure factor  $c_e$  and basic wind velocity  $v_{b,0}$ .

$c_{pe,10}$  is the external pressure coefficient for loaded areas larger than  $10 \text{ m}^2$ .

In order to determine the peak velocity pressure,  $q_p(z_e)$ , the reference wind velocity is determined:

$$v_{b,0} = 24 \text{ m/s [EKS 9 table C-10, City: Växjö]}$$

With a building height of 9 m and an assumed site location within urban area (terrain type III) the peak velocity pressure is:

$$q_p(z_e) = 0.53 \text{ kN/m}^2 \text{ [EKS 9 table C-10a]}$$

The external pressure coefficient for a circular shaped roof is determined with respect to the height-span-ratio according to EKS9 1.1.4 10§.

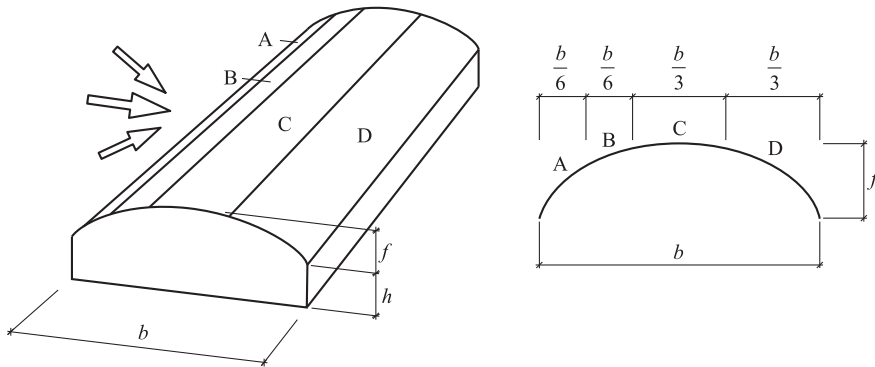


Figure A.2: External pressure coefficients of arch roof with rectangular base. Source: EKS9 figure C-6.

With  $f/b = 0.15$  and  $h/b = 0$  the different pressure coefficients for A,B,C and D is [EKS9 figure C-6]:

$$c_{pe,10,A} = 0.38$$

$$c_{pe,10,B} = -0.15$$

$$c_{pe,10,C} = -0.50$$

$$c_{pe,10,D} = -0.20$$

Which results in an external wind load of:

$$w_{e,A} = 0.53 \cdot 0.38 = 0.20 \text{ kN/m}^2$$

$$w_{e,B} = 0.53 \cdot (-0.15) = -0.08 \text{ kN/m}^2$$

$$w_{e,C} = 0.53 \cdot (-0.50) = -0.27 \text{ kN/m}^2$$

$$w_{e,D} = 0.53 \cdot (-0.20) = -0.11 \text{ kN/m}^2$$



### A.3.2 Internal Load

The external wind load should be supplemented by an internal wind load due to internal negative or positive pressure.

$$w_i = q_p(z_i) \cdot c_{pi} \tag{A.7}$$

The internal pressure coefficient,  $c_{pi}$ , is dependent on the openings in the structure and when the relative opening area is unknown the coefficient should be chosen as +0.2 or -0.3, whichever is more onerous [SS-EN1991-1-4 7.2.9].

Combined with the external wind load either the internal negative or positive pressure can be most unfavourable.

$$w_{i,pos} = 0.11 \text{ kN/m}^2 \quad w_{i,neg} = -0.16 \text{ kN/m}^2$$

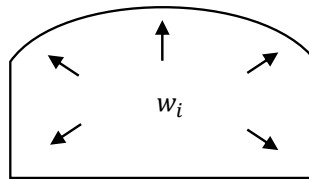


Figure A.3: Definition of positive internal wind load.

## A.4 Load Combination

All different kinds of loads applied to a structure is probably not at its maximum simultaneously, i.e. for strong winds the snow may blow of the roof. Eurocode adopts load combination factors in order to reduce the combined effect of variable loads. This factor is multiplied with any load other than the current main load.

Table A.1: Recommended load combination factor for buildings [SS-EN1990 table A1.1].

	$\psi_0$
Snow	0.7
Wind	0.3

In order to determine the worst load combination with snow and wind as variable loads eight different load cases are considered as seen in Table A.2 and Figure A.4. The wind and snow load is placed in order to obtain the most onerous load combination. Self-weight and partial coefficients are introduced to the internal forces in Section C.4.

Table A.2: Linear combination effect of imperfections in- and out-of-plane for uniformly distributed load and asymmetrical triangular load.

Main load	Snow	Internal pressure	Relative location														
			0,00	0,17	0,17	0,25	0,33	0,33	0,50	0,67	0,67	0,75	1,00	m/m			
Snow	UDL	positive	1,63	1,63	1,54	1,54	1,54	1,49	1,49	1,49	1,49	1,54	1,54	1,54	1,54	1,54	kN/m <sup>2</sup>
Snow	UDL	negative	1,71	1,71	1,62	1,62	1,62	1,57	1,57	1,57	1,57	1,62	1,62	1,62	1,62	1,62	kN/m <sup>2</sup>
Snow	Triangular	positive	0,03	2,30	2,21	3,34	2,21	2,15	-0,11	1,02	1,07	1,07	1,64	-0,06	1,64	-0,06	kN/m <sup>2</sup>
Snow	Triangular	negative	0,11	2,38	2,29	3,42	2,29	2,23	-0,03	1,10	1,15	1,15	1,72	0,02	1,72	0,02	kN/m <sup>2</sup>
Wind	UDL	positive	1,22	1,22	0,93	0,93	0,93	0,75	0,75	0,75	0,75	0,91	0,91	0,91	0,91	0,91	kN/m <sup>2</sup>
Wind	Triangular	positive	0,10	1,68	1,40	2,19	1,40	1,21	-0,37	0,42	0,58	0,58	0,98	-0,21	0,98	-0,21	kN/m <sup>2</sup>
Wind	UDL	negative	1,48	1,48	1,20	1,20	1,20	1,01	1,01	1,01	1,17	1,17	1,17	1,17	1,17	1,17	kN/m <sup>2</sup>
Wind	Triangular	negative	0,36	1,95	1,67	2,46	1,67	1,48	-0,11	0,69	0,85	0,85	1,24	0,05	1,24	0,05	kN/m <sup>2</sup>
Snow	UDL	No wind	1,60	1,60	1,60	1,60	1,60	1,60	1,60	1,60	1,60	1,60	1,60	1,60	1,60	1,60	kN/m <sup>2</sup>
Snow	Triangular	No wind	0,00	2,27	2,27	3,40	2,27	2,27	0,00	1,13	1,13	1,13	1,70	0,00	1,70	0,00	kN/m <sup>2</sup>

Example: Snow main load, triangular distribution with internal negative pressure.

$$x = 0 \rightarrow s(x) + \psi_0(w_{e,A} + w_{i,neg}) = 0 + 0.3(0.13 + 0.16) = 0.03 \text{ kN/m}^2$$

$$x = 0.25 \rightarrow s(x) + \psi_0(w_{e,B} + w_{i,neg}) = 3.4 + 0.3(-0.08 + 0.16) = 3.42 \text{ kN/m}^2$$

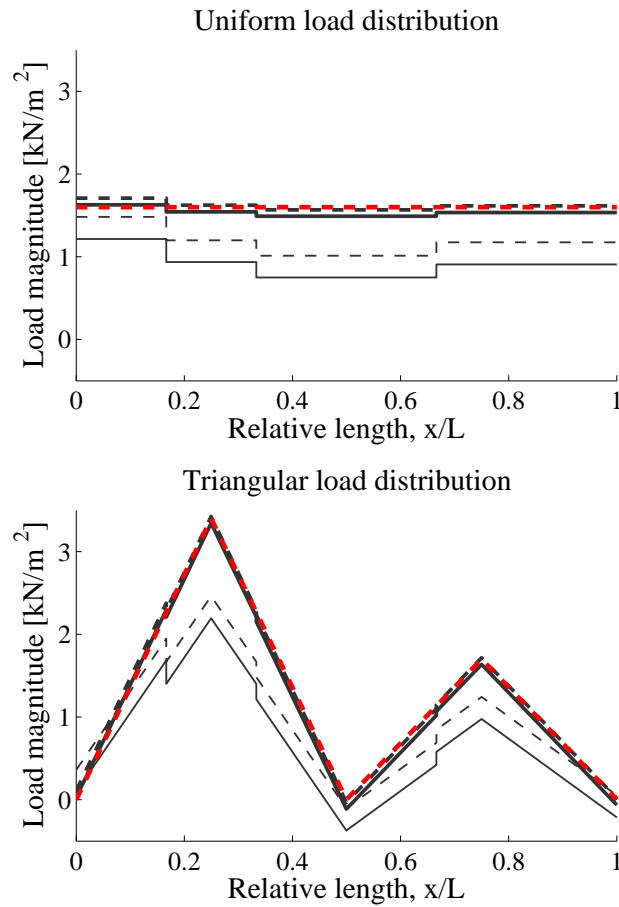
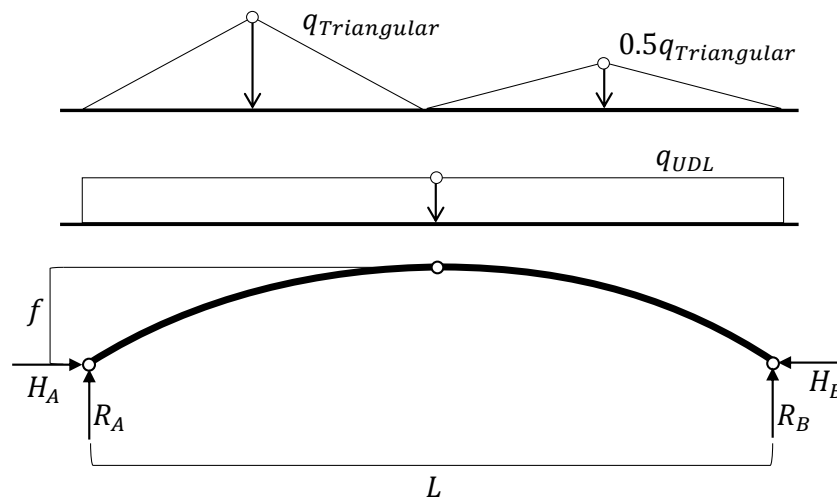


Figure A.4: Magnitude of load for uniform and triangular distribution including wind effect. Main load: Snow (bold), Wind (regular); Internal wind pressure: Positive (solid line), Negative (dashed line). Used load combination in red.

The influence of the wind in the dominating load combination is low and is hereafter neglected in the calculations. Load used henceforth is marked with a dashed red line in Figure A.4.

# Appendix B

## Internal Forces and Reactions



### B.1 Uniformly Distributed Load

The following equations were used to calculate internal and reaction forces caused by UDL:

$$\text{Vertical reaction force: } R = \frac{qL}{2}$$

$$\text{Horizontal reaction force: } H = \frac{qL^2}{8f}$$

$$\text{Maximal normal force: } N = \sqrt{R^2 + H^2}$$

$$\text{Normal force in arbitrary section: } N(x) = \sqrt{(R - qx)^2 + H^2}$$

With the reference geometry presented in Section 5.1 and characteristic loads calculated in Appendix A the internal forces for the uniformly distributed load is:

Characteristic self-weight load,  $q_{G,k}$   $q_{G,k} = 13.1 \text{ kN/m}$   
 Characteristic snow load without snowdrift,  $q_{s1,k}$   $q_{s1,k} = s_1 \cdot 7 = 11.2 \text{ kN/m}$

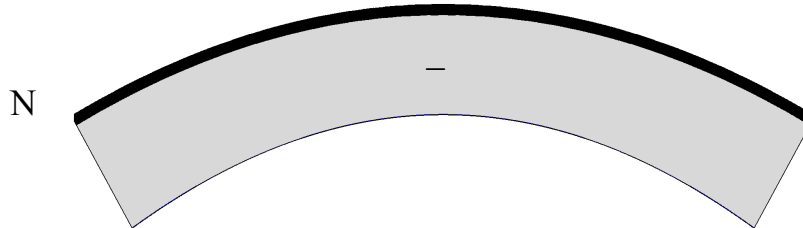


Figure B.1: Normal force distribution for a parabolic arch subjected to UDL.

Table B.1: Characteristic internal forces in a parabolic arch subjected to UDL.

	Self-weight	Snow pressure
Normal force, $N_{max}$	762 kN	682 kN
Shear force, $V$	$\approx 0 \text{ kN}$	$\approx 0 \text{ kN}$
Bending moment, $M$	$\approx 0 \text{ kN}$	$\approx 0 \text{ kN}$

## B.2 Triangular Distributed Load

Characteristic snow load without snowdrift,  $q_{s3,k}$   $q_{s3,k} = s_3 \cdot 7 = 3.7 \cdot 7 = 23.8 \text{ kN/m}$

In order to calculate the internal forces for a triangular distributed load a free body diagram is sketched and equilibrium equations are set up.

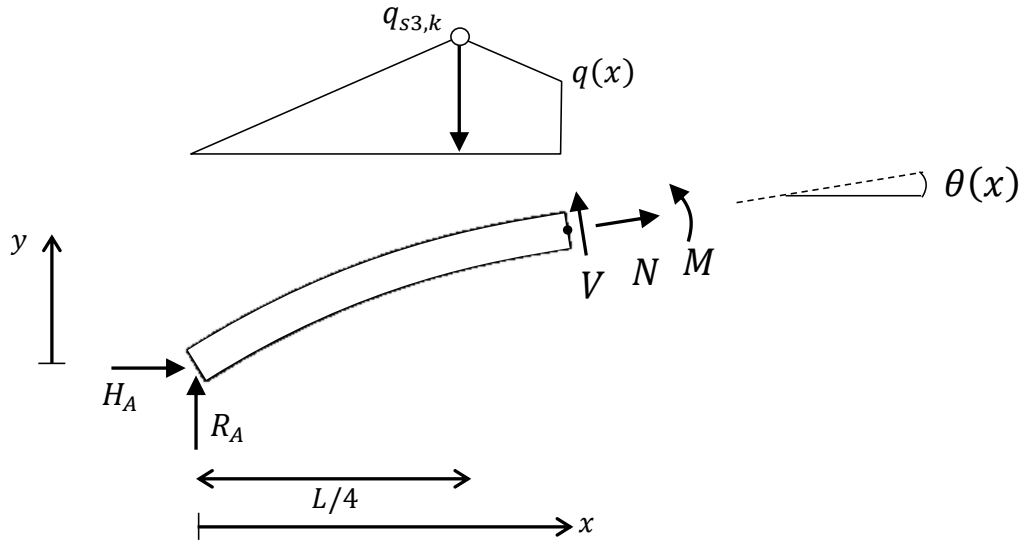


Figure B.2: Free body diagram over arch subjected to non-symmetrical triangular load. Figure is valid in region  $\frac{L}{4} < x \leq \frac{L}{2}$ .

**Example.**  $\frac{L}{4} < x \leq \frac{L}{2}$

$$q_{s3,k} = 23.8 \text{ kN/m}$$

$$q(x) = q_{s3,k} \left(2 - \frac{4}{L}x\right)$$

$$y(x) = y(x) = 0.01 (Lx - x^2)$$

$$\theta(x) = \tan^{-1} \left( \frac{dy(x)}{dx} \right) = \tan^{-1} (0.01 (L - 2x))$$

$$(\searrow) \quad V + R_A \cos(\theta) - H \sin(\theta) - \left( \frac{1}{2} q_{s3,k} \frac{4}{L} + \frac{1}{2} (q_{s3,k} + q(x)) \left(x - \frac{4}{L}\right) \right) \cos(\theta) = 0$$

$$(\swarrow) \quad N - H \cos(\theta) - R_A \sin(\theta) + \left( \frac{1}{2} q_{s3,k} \frac{4}{L} + \frac{1}{2} (q_{s3,k} + q(x)) \left(x - \frac{4}{L}\right) \right) \sin(\theta) = 0$$

$$(\curvearrowright) \quad M + Hy(x) - R_A x + \frac{q_{s3,k} L}{8} \left(x - \frac{2}{3} \frac{4}{L}\right) + q(x) \frac{1}{2} \left(x - \frac{4}{L}\right)^2 + (q_{s3,k} - q(x)) \frac{1}{3} \left(x - \frac{4}{L}\right)^2 = 0$$

Corresponding equilibriums are set up throughout the whole region  $0 < x < L$  to obtain the internal forces and their distribution.

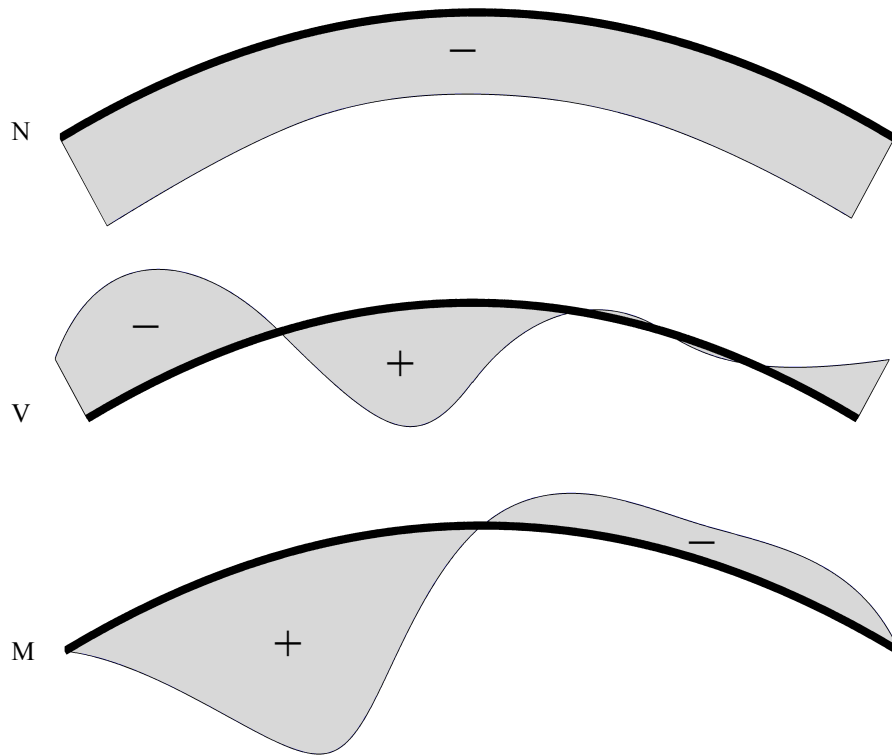


Figure B.3: Internal forces for triangular load case. Normal force, radial shear force and bending moment distribution respectively.

Table B.2: Maximum characteristic internal force with corresponding internal forces at same location.

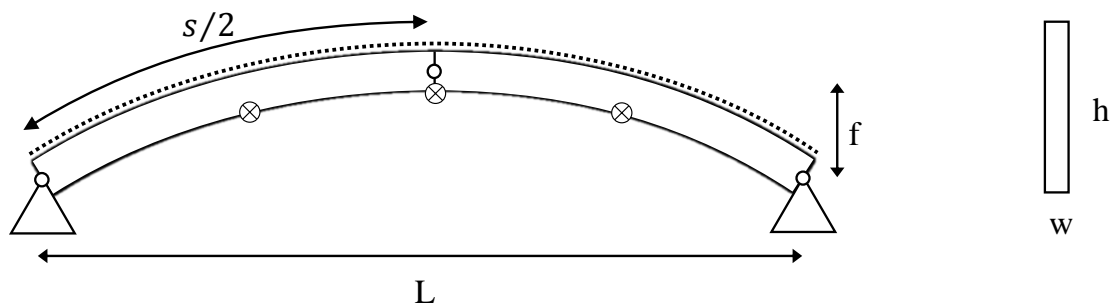
Internal force	Max value	Position	Simultaneously		
			N	V	M
$N_{max}$	550 kN	0		41 kN	0 kNm
$V_{max}$	72 kN	$\approx L/2$	445 kN		348 kNm
$M_{max}$	811 kNm	$L/4$	470 kN	0 kN	
$M_{min}$	-157 kNm	$\approx 3L/5$	456 kN	0 kN	



# Appendix C

## Design According to Eurocode 5

### C.1 Geometric Properties



Width of member,  $w$   $w = 190$  mm

Height of member,  $h$   $h = 1800$  mm

Cross-sectional area,  $A$   $A = w \cdot h = 3.42 \cdot 10^5$  mm<sup>2</sup>

Arch length,  $s$  (see Section A.1.1)  $s = 63.4$  m

Effective length with respect to IP buckling,  $L_{e,y}$  (see Section 6.4)  $L_{e,y} = \beta \frac{s}{2} = 1.25 \cdot \frac{63.4}{2} = 39.6$  m

Effective length with respect to OP buckling,  $L_{e,z}$   $L_{e,z} = \frac{s}{4} \approx 15$  m

Moment of inertia about the y-y axis,  $I_y$   $I_y = \frac{wh^3}{12} = 9.23 \cdot 10^{10}$  mm<sup>4</sup>

Moment of inertia about the z-z axis,  $I_z$   $I_z = \frac{hw^3}{12} = 1.03 \cdot 10^9$  mm<sup>4</sup>

Elastic section modulus about the y-y axis, $W_y$	$W_y = \frac{wh^2}{6} = 1.03 \text{ m}^3$
Elastic section modulus about the z-z axis, $W_z$	$W_z = \frac{hw^2}{6} = 0.011 \text{ m}^3$
Radius of gyration about the y-y axis, $i_y$	$i_y = \sqrt{\frac{I_y}{A}} = 0.52 \text{ m}$
Slenderness ratio about the y-y axis, $\lambda_y$	$\lambda_y = \frac{L_{e,y}}{i_y} = 76$
Torsional constant for the section, $J$ [Young and Budynas, 2002] p. 410 using $a = h/2, b = w/2$	$J = ab^3 \left( \frac{16}{3} - 3.36 \frac{b}{a} \left( 1 - \frac{b^4}{12a^4} \right) \right) =$ $= 0.0038$

## C.2 Material Properties

Glulam strength class GL32h [SS-EN 1194]. Characteristic values:

Bending stress, $f_{m,k}$	$f_{m,k} = 32 \text{ MPa}$
Compression strength parallel to grain, $f_{c,k}$	$f_{c,k} = 29 \text{ MPa}$
Shear strength, $f_{v,k}$	$f_{v,k} = 3.8 \text{ MPa}$
Tension strength perpendicular to grain, $f_{t,90,k}$	$f_{t,90,k} = 0.5 \text{ MPa}$
Modulus of elasticity parallel to grain, $E_{0.05}$	$E_{0.05} = 13700 \text{ MPa}$
Shear modulus, $G_k$	$G_k = 850 \text{ MPa}$

## C.3 Partial Factors

The partial coefficients address the uncertainty in load, material and variations in cross-section measures.

Partial safety factor, $\gamma_d$ [EKS 9]	$\gamma_d = 1.0$
Partial safety factor, $\gamma_G$ [EKS 9 table B-3]	$\gamma_G = 0.89 \cdot 1.35 = 1.2$
Variable actions, $\gamma_Q$	$\gamma_Q = 1.5$
Material factor for glulam at ULS, $\gamma_M$	$\gamma_M = 1.25$

## C.4 Actions

Two load cases are evaluated, uniform and triangular distribution, see Figure C.1. All design loads are calculated according to STR-B [EKS9 table B-3, eqn 6.10b] with snow as main variable load.

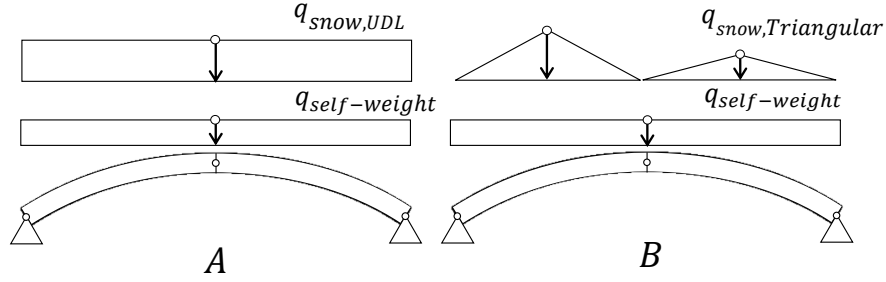


Figure C.1: Load cases considered in the model studied. A: Uniformly distributed load. B: Triangular distribution of snow.

Since the structure is statically determinate the partial safety factors are applied to the internal forces, presented in Section 5.4, in order to obtain the design forces.

$$X_d = \gamma_d \{1.2G + 1.5Q_k + 1.5\psi_{0,i}Q_{k,i}\} \quad (\text{C.1})$$

With safety class 3 and snow as the only variable load the design loads are calculated as follows:

$$X_d = 1.0 \{1.2G + 1.5Q_k\} \quad (\text{C.2})$$

### C.4.1 Load Case A

Load case A represent the maximum normal force in the arch.

$$1.0 \{1.2 \cdot 762 + 1.5 \cdot 682\} = 1938 \text{ kN at } x = 0$$

$$M_{max,A} \approx 0 \text{ kNm}$$

$$V_{max,A} \approx 0 \text{ kN}$$

### C.4.2 Load Case B

Load case B introduces bending moment in the arch while the normal force still is large.

Table C.1: Summary of maximum internal forces for load case B.

Internal force	Max value	Position	Simultaneously		
			N	V	M
$N_{max,B}$	$1.0 \{1.2 \cdot 762 + 1.5 \cdot 550\}$ =1740 kN	0		62 kN	0 kNm
$V_{max,B}$	$1.0 \{1.2 \cdot 0 + 1.5 \cdot 72\}$ =108 kN	$\approx L/2$	1582 kN		522 kNm
$M_{max,B}$	$1.0 \{1.2 \cdot 0 + 1.5 \cdot 811\}$ =1217 kNm	$L/4$	1620 kN	0 kN	
$M_{min,B}$	$1.0 \{1.2 \cdot 0 + 1.5 \cdot (-157)\}$ = -236 kN	$\approx 3L/5$	1600 kN	0 kN	

### C.4.3 Design Load

The design load in Table C.2 is found by the most onerous load combination for each internal force.

Table C.2: Design internal forces.

Internal force	Max value	Load case	Position	Simultaneously		
				N	V	M
$N_{Ed}$	1 938 kN	A	0		0 kN	0 kNm
$V_{Ed}$	108 kN	B	$\approx L/2$	1582 kN		522 kNm
$M_{Ed}^+$	1 217 kNm	B	$L/4$	1620 kN	0 kN	
$M_{Ed}^-$	-236 kNm	B	$\approx 3L/5$	1600 kN	0 kN	

## C.5 Modification Factors

### C.5.1 General Modification Factors

Factor for medium-duration loading and service class 2,  $k_{mod}$  [SS-EN1995-1-1 table 3.1]  $k_{mod} = 0.80$

Size factor based on maximum depth = 1800 mm,  $k_h$  [SS-EN1995-1-1 eqn 3.2]  $k_h = 1.0$

Deformation factor for service class 2,  $k_{def}$  [SS-EN1995-1-1 table 3.2]  $k_{def} = 0.80$

Reduction of cross-sectional width due to,  $k_{cr}$  [EKS 9]  $k_{cr} = \min \left\{ \begin{array}{l} \frac{3.0}{f_{vk}} = 0.79 \\ 1.0 \end{array} \right. = 0.79$

### C.5.2 Reduction due to Bent Lamellas

Reduction due to initial stress in bent lamellas is defined in SS-EN1995-1-1 equation 6.49 as:

$$k_r = \min \left\{ \begin{array}{ll} 1 & \text{for } \frac{r_{in}}{t} \geq 240 \\ 0.76 + 0.001 \frac{r_{in}}{t} & \text{for } \frac{r_{in}}{t} < 240 \end{array} \right. \quad (\text{C.3})$$

where

$r$  inner radius  $\approx 54$  m

$t$  thickness of lamellas, usually 45 mm [Carling, 2008]

$$k_r = 1$$

No reduction is needed with respect to bent lamellas.

### C.5.3 Reduction due to Curved Beam

Stress distribution factor for the apex zone,  $k_{dis}$ , according to SS-EN 1995-1-1 equation 6.52:

$$k_{dis} = 1.4$$

Factor applied to obtain bending stress in the apex zone, see Section 3.3.4,  $k_l$  [SS-EN1995-1-1 eqn 6.43]:

$$k_l = k_1 + k_2 \left( \frac{h_{ap}}{r} \right) + k_3 \left( \frac{h_{ap}}{r} \right)^2 + k_4 \left( \frac{h_{ap}}{r} \right)^3 = 1.01 \quad (\text{C.4})$$

where

$$\begin{aligned} k_1 &= 1 + 1.4 \tan(\alpha_{ap}) + 5.4 \tan^2(\alpha_{ap}) = 1 \\ k_2 &= 0.35 - 8 \tan(\alpha_{ap}) = 0.35 \\ k_3 &= 0.6 + 8.3 \tan(\alpha_{ap}) - 7.8 \tan^2(\alpha_{ap}) = 0.6 \\ k_4 &= 6 \tan^2(\alpha_{ap}) = 0 \\ \alpha_{ap} &= 0 \text{ for curved beams} \\ h_{ap} &= h = 1800 \text{ mm} \\ r &\approx 54 \text{ m} \end{aligned}$$

Factor applied to obtain the tensile stress perpendicular to grain,  $k_p$  [SS-EN1995-1-1 eqn 6.56]:

$$k_p = k_5 + k_6 \left( \frac{h_{ap}}{r} \right) + k_7 \left( \frac{h_{ap}}{r} \right)^2 = 0.008 \quad (\text{C.5})$$

where

$$\begin{aligned} k_5 &= 0.2 \tan(\alpha_{ap}) = 0 \\ k_6 &= 0.25 - 1.5 \tan(\alpha_{ap}) + 2.6 \tan^2(\alpha_{ap}) = 0.25 \\ k_7 &= 2.1 \tan(\alpha_{ap}) - 4 \tan^2(\alpha_{ap}) = 0 \end{aligned}$$

Volume factor,  $k_{vol}$  [SS-EN1995-1-1 eqn 6.51]:

$$k_{vol} = \left( \frac{V_0}{V} \right)^{0.2} = 0.23 \quad (\text{C.6})$$

where

$$V_0 = 0.2 \tan(\alpha_{ap}) = 0$$

stressed volume in the apex zone, max of  $2/3 V_{beam}$ , where  $V_{beam}$  is the volume of the member.  $V$  is assumed to be greater than the maximum, hence  $2/3 V_{beam} = 2/3 A s_{arch} = 2/3 \cdot 1.8 \cdot 0.19 \cdot 63.4 = 14.5 \text{ m}^3$

## C.6 Stresses in Apex

### C.6.1 Bending Stresses

The bending stresses in apex zone should be limited by [SS-EN1995-1-1 eqn 6.41]:

$$\sigma_{m,d} \leq k_r f_{f,d} = 20.5 \text{ MPa} \quad (\text{C.7})$$

where

$$\begin{aligned} k_r &= 1 \\ f_{f,d} &= \frac{k_{mod} k_h f_{m,k}}{\gamma_M} = 20.5 \text{ MPa} \end{aligned}$$

Stresses in apex zone should be calculated according to EC5 [SS-EN1995-1-1 eqn 6.42]:

$$\sigma_{m,d} \leq k_l \frac{6M_{ap,d}}{bh_{ap}^2} = 12 \text{ MPa} \quad (\text{C.8})$$

where

$$\begin{aligned} k_l &= 1.01 \\ M_{ap,d} &= M_{Ed}^+ = 1217 \text{ kNm} \end{aligned}$$

Bending strength in the apex zone is satisfactory.

### C.6.2 Radial Stresses

Radial stress in the apex zone should be limited by [SS-EN1995-1-1 eqn 6.50]:

$$\sigma_{t,90,d} = k_{dis} k_{vol} f_{t,90,d} = 0.69 \text{ MPa} \quad (\text{C.9})$$

where

$$\begin{aligned} k_{dis} &= 1.4 \\ k_{vol} &= 0.23 \\ f_{t,90,d} &= \frac{k_{mod} k_h f_{t,90,k}}{\gamma_M} = 2.1 \text{ MPa} \end{aligned}$$

Largest tensile stress perpendicular to grain is calculated according to EC5 [SS-EN1995-1-1 eqn 6.54]:

$$\sigma_{t,90,d} = k_p \frac{6M_{ap,d}}{bh_{ap}^2} = 0.1 \text{ MPa} \quad (\text{C.10})$$

where

$$\begin{aligned} k_p &= 0.008 \\ M_{ap,d} &= M_{ED}^+ = 1217 \text{ kNm} \end{aligned}$$

Tensile strength perpendicular to grain in the apex zone is satisfactory.

## C.7 Compression Strength

$$\text{Design compression strength, } f_{c,0,d} \quad f_{c,0,d} = \frac{k_{mod} k_h f_{c,0,k}}{\gamma_M} = 18.6 \text{ MPa}$$

### C.7.1 In-plane Buckling

Buckling resistance condition [SS-EN1995-1-1 6.3.2]:

$$\begin{aligned} \text{Relative slenderness ratio about the y-y} \\ \text{axis [SS-EN 1995-1-1 eqn 6.21]} \quad \lambda_{rel,y} = \frac{\lambda_y}{\pi} \cdot \sqrt{\frac{f_{c,0,k}}{E_{0.05}}} = 1.12 \end{aligned}$$

Since the relative slenderness ratio is greater than 0.3, consideration of buckling is needed. The conditions in SS-EN1995-1-1 6.3.2 are used:

$$\begin{aligned} \text{Factor } \beta_c \text{ for glulam. Considers demand for} \\ \text{straightness. [SS-EN 1995-1-1 eqn 6.29]} \quad \beta_c = 0.1 \end{aligned}$$

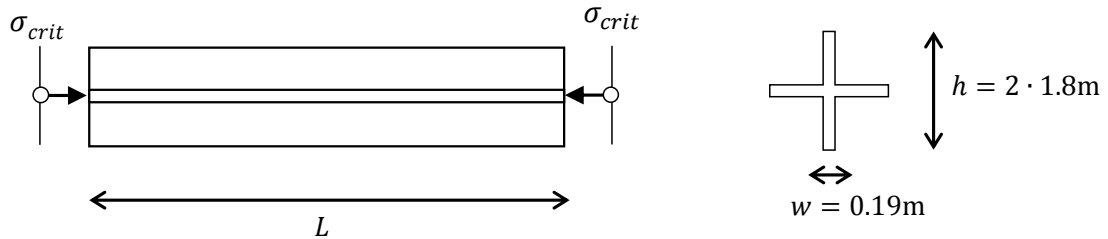
$$\text{Factor } k_y \text{ [SS-EN 1995-1-1 eqn 6.28]} \quad k_y = 0.5 (1 + \beta_c (\lambda_{rel} - 0.3) + \lambda_{rel}^2) = 1.17$$

$$\begin{aligned} \text{Reduction factor with respect to} \\ \text{buckling, } k_c. \text{ [SS-EN 1995-1-1 eqn 6.26]} \quad k_c = \frac{1}{k_y + \sqrt{k_y^2 - \lambda_{rel}^2}} = 0.67 \end{aligned}$$



### C.7.2 Out-of-plane Buckling

Since the extrados of the arch is restricted from lateral displacement the out-of-plane buckling will be due to torsional buckling, see Section 6.4. An analogy to a cruciform strut subjected to compressive force is used to estimate the buckling load of the arch.



$$\text{Moment of inertia, } I \quad I = I_y = I_z \approx \frac{wh^3}{12} + \frac{hw^3}{12} = 0.74 \text{ m}^4$$

$$\text{Polar moment of inertia, } I_0 \quad I_0 = I_y + I_z = 2I = 1.48 \text{ m}^4$$

$$\text{Warping constant, } I_w \quad I_w \approx 0 \text{ for open cross-sections}$$

$$\text{Torsional constant for the open cross-section, } J \text{ [Gustafsson, 2012]} \quad J = \sum \frac{bt^3}{3} = 4 \frac{1.8 \cdot 0.19^3}{3} = 0.016 \text{ m}^4$$

$$\text{MOE reduced for ULS, } E_{mean,fin} \text{ [SS-EN 1995-1-1 2.3.2.2]} \quad E_{mean,fin} = \frac{E_{mean}}{(1+\psi_2 k_{def})} = 11\,810 \text{ MPa}$$

$$\text{Shear modulus reduced for ULS, } G_{mean,fin} \text{ [SS-EN 1995-1-1 2.3.2.2]} \quad G_{mean,fin} = \frac{G_{mean}}{(1+\psi_2 k_{def})} = 733 \text{ MPa}$$

$$\begin{aligned} \text{Critical stress for torsional buckling, } \sigma_{Rd,cruciform} &= \frac{1}{I_0} \left( E_{mean,fin} I_w \frac{\pi^2}{L^2} + G_{mean,fin} J \right) = \\ &= 8.14 \text{ MPa} \end{aligned}$$

## C.8 Bending Strength

$$\text{Design bending strength, } f_{m,d} \quad f_{m,d} = \frac{k_{mod} k_h f_{m,k}}{\gamma_M} = 20.5 \text{ MPa}$$

Design bending strength taking lateral torsional buckling into account [SS-EN 1995-1-1 6.3.3],  $k_{crit}$ :

Effective length of the beam, $l_{ef}$ , including effect of loading on the compressed face. [SS-EN 1995-1-1 table 6.1]	$l_{ef} = L_{e,z} \cdot 1.0 + 2h = 19.5 \text{ m}$
Critical bending stress, $\sigma_{m,crit}$ [SS-EN 1995-1-1 eqn 6.31]	$\sigma_{m,crit} = \frac{M_{y,crit}}{W_y} = \frac{\pi \sqrt{E_{0.05} I_z G_{0.05} J}}{l_{ef} W_y} = 10.7 \text{ MPa}$
Relative slenderness for bending, $\lambda_{rel,m}$ [SS-EN 1995-1-1 eqn 6.30]	$\lambda_{rel,m} = \sqrt{\frac{f_{m,k}}{\sigma_{m,crit}}} = 1.73$
Lateral stability factor, $k_{crit}$ [SS-EN 1995-1-1 eqn 6.34]	$k_{crit} = \begin{cases} 1 & \text{for } \lambda_{rel,m} \leq 0.75 \\ 1.56 - 0.75\lambda_{rel,m} & \text{for } 0.75 < \lambda_{rel,m} \leq 1.4 \\ \lambda_{rel,m}^{-2} & \text{otherwise} \end{cases}$ $k_{crit} = 0.33$

## C.9 Shear Strength

Design value for shear force, $V_d$	$V_d = 108 \text{ kN}$
Design shear strength, $f_{V,d}$	$f_{V,d} = \frac{k_{mod} k_h f_{V,k}}{\gamma_M} = 2.4 \text{ MPa}$
Effective width, $w_{eff}$ [EKS 9 7.b§]	$w_{eff} = k_{cr} w = 0.79 \cdot 190 = 150 \text{ mm}$
Design shear strength, $V_{Rd}$	$V_{Rd} = \frac{2}{3} w_{eff} h f_{V,d} = 437.7 \text{ kN}$

Since  $V_{Rd} = 438 > V_{Ed} = 108$  shear forces are within limits.

## C.10 Combined Stress Condition

In order to evaluate the combined stress condition of the whole arch specific sections where bending moment and axial forces act simultaneously are verified, see Figure C.2.

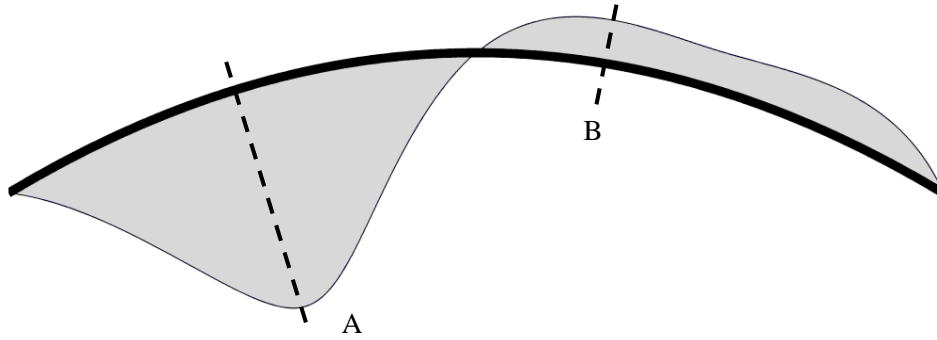


Figure C.2: Sections where combined stress condition is verified.

### C.10.1 Section A

Compressed edge is restrained from lateral buckling.

$$\begin{aligned} \text{Design compression stress, } \sigma_{c,0,d} & \quad \sigma_{c,0,d} = \frac{N_{Ed}}{A} = \frac{1620}{0.34} = 4.7 \text{ MPa} \\ \text{Design bending stress, } \sigma_{m,y,d} & \quad \sigma_{m,y,d} = \frac{M_{y,d}}{W_y} = \frac{M_{Ed}^+}{W_y} = \frac{1217}{0.103} = 11.9 \text{ MPa} \\ \text{Design bending stress, } \sigma_{m,z,d} & \quad \sigma_{m,z,d} = \frac{M_{z,d}}{W_y} = 0 \text{ MPa} \end{aligned}$$

Simultaneous bending and axial force [SS-EN 1995-1-1 eqn 6.23-24]:

$$\frac{\sigma_{c,0,d}}{\sigma_{Rd,cruciform}} + k_m \frac{\sigma_{m,y,d}}{f_{m,y,d}} + \frac{\sigma_{m,z,d}}{f_{m,z,d}} = \frac{4.7}{9.4} + 0.7 \frac{11.9}{20.5} + \frac{0}{20.5} = 0.99 < 1.0 \quad (\text{C.11})$$

$$\frac{\sigma_{c,0,d}}{k_{c,y} f_{c,0,d}} + \frac{\sigma_{m,y,d}}{f_{m,y,d}} + k_m \frac{\sigma_{m,z,d}}{f_{m,z,d}} = \frac{4.7}{0.67 \cdot 18.6} + \frac{11.9}{20.5} + 0.7 \frac{0}{20.5} = 0.96 < 1.0 \quad (\text{C.12})$$

### C.10.2 Section B

Compressed edge is free to buckle laterally and the risk of lateral torsional buckling needs to be considered. Stress condition since risk of lateral torsional buckling,  $\lambda_{rel,m} > 0.75$  [SS-EN 1995-1-1 eqn 6.35]:

$$\begin{aligned} \text{Design compression stress, } \sigma_{c,0,d} & \quad \sigma_{c,0,d} = \frac{N_{Ed}}{A} = \frac{1600}{0.34} = 4.7 \text{ MPa} \\ \text{Design bending stress, } \sigma_{m,d} & \quad \sigma_{m,d} = \frac{M_{y,d}}{W_y} = \frac{M_{Ed}^-}{W_y} = \frac{236}{0.103} = 2.3 \text{ MPa} \end{aligned}$$

$$\left( \frac{\sigma_{m,d}}{k_{crit} f_{m,d}} \right)^2 + \frac{\sigma_{c,0,d}}{k_{c,z} f_{c,0,d}} = \left( \frac{2.3}{0.33 \cdot 20.5} \right)^2 + \frac{4.7}{0.67 \cdot 18.6} = 0.49 \leq 1.0 \quad (\text{C.13})$$



# Appendix D

## FE Analysis Support Calculations

### D.1 Stiffness of Extrados Lateral Support

#### D.1.1 Characteristic Maximum Force

Calculated according to Eurocode 5 [SS-EN 1995-1-1 8.2.3]. The strength of the timber to metal connection is dependent on the thickness of the steel plate. Depending on the thickness different failure modes will occur, see Figure D.1.

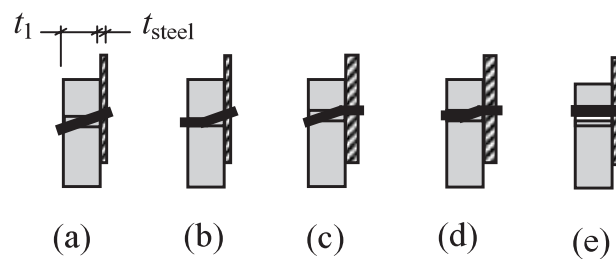


Figure D.1: Failure modes for steel-timber connections. Source: [SS-EN 1995-1-1 figure 8.3].

Thin steel plates will fail according to mode a or b whereas a thick steel plate will have a failure mode according to c-e. A steel plate is considered thin if the thickness is less than or equal to  $0.5d$ , where  $d$  is the diameter of the fastener.

### D.1.2 Geometric and Material Properties of the Connection

Thickness of steel plate [Lindab, 2014]	$t_{steel} = 1.04$ mm
Diameter of fastener. Screw, Unifast A21 6.5x51 [Unite, 2014]	$d = 6.5$ mm
Penetration depth of screw, Unifast A21 6.5x51	$t_1 = 51 - 1.04 = 50$ mm
Type of steel-timber connection [SS-EN 1995-1-1 8.2.3 (1)]	$\text{type} = \begin{cases} t_{steel} = 1.04 < 0.5d = 3.25 & \text{thin} \\ t_{steel} = 1.04 \not< d = 6.5 & \text{thick} \end{cases}$ type = thin
Characteristic density of glulam GL32h [SS-EN 1194]	$\rho_k = 430$ kg/m <sup>3</sup>
Tensile strength for each screw, Unifast A21 - AISI 1018-1022 [Unite, 2014]	$f_{u,k} = 1022$ MPa

### D.1.3 Strength Properties of Glulam and Screw

The lateral support will apply a shear force perpendicular to the fibre direction.

Characteristic embedment strength parallel to grain [SS-EN 1995-1-1 eqn 8.32]	$f_{h,0,k} = 0.082(1 - 0.01d)\rho_m = 33$ N/mm <sup>2</sup>
Angle between force and fibre direction	$\alpha = 90^\circ$
Embedment factor for softwood [SS-EN 1995-1-1 eqn 8.33]	$k_{90} = 1.35 + 0.015d = 1.45$
Characteristic embedment strength with an angle to fibre direction [SS-EN 1995-1-1 eqn 8.31]	$f_{h,90,k} = \frac{f_{h,0,k}}{k_{90}\sin^2(\alpha) + \cos^2(\alpha)} = 22.8$ N/mm <sup>2</sup>
Characteristic yield moment of the screw [SS-EN 1995-1-1 eqn 8.30]	$M_{y,Rk} = 0.3f_{u,k}d^{2.6} = 39 \cdot 10^3$ Nmm

### D.1.4 Load Carrying Capacity

Since a thin steel-timber connection is used only failure modes a-b in Figure D.1 will be verified.

$$F_{v,Rk} = \min \begin{cases} 0.4f_{h,k}t_1d & = 4286 \text{ N (a)} \\ 1.15\sqrt{2M_{y,Rk}f_{h,k}d} & = 3949 \text{ N (b)} \end{cases} \quad (\text{D.1})$$

$$F_{v,Rk} = 3950 \text{ N}$$

## D.2 Stiffness of Intrados Lateral Support

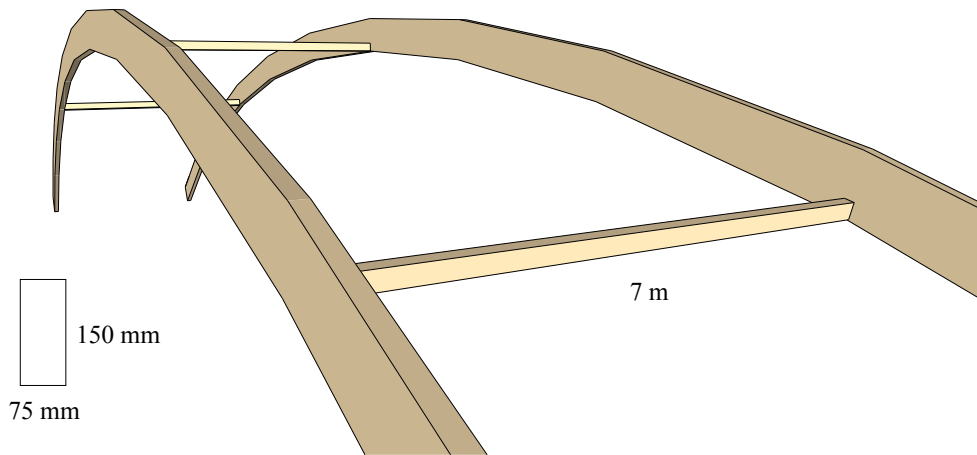


Figure D.2: Principle view of lateral support at intrados with cross-section constants.

With assumption of tension action and linear increase in supporting force:

$$k = \frac{EA}{L} = \frac{13700 \cdot \frac{150 \cdot 75}{10^6}}{7} \approx 18\,000 \text{ kN/m} \quad (\text{D.2})$$